


2015

STABILIZATION OF IRON MINE TAILINGS THROUGH MICROBIALLY INDUCED CALCITE PRECIPITATION

Noah D. Buikema
Michigan Technological University

Follow this and additional works at: <https://digitalcommons.mtu.edu/etds>


 Part of the [Civil Engineering Commons](#), and the [Environmental Engineering Commons](#)

Copyright 2015 Noah D. Buikema

Recommended Citation

Buikema, Noah D., "STABILIZATION OF IRON MINE TAILINGS THROUGH MICROBIALLY INDUCED CALCITE PRECIPITATION", Master's Thesis, Michigan Technological University, 2015.
<https://digitalcommons.mtu.edu/etds/981>

Follow this and additional works at: <https://digitalcommons.mtu.edu/etds>

 Part of the [Civil Engineering Commons](#), and the [Environmental Engineering Commons](#)

STABILIZATION OF IRON MINE TAILINGS THROUGH MICROBIALLY
INDUCED CALCITE PRECIPITATION

By
Noah D. Buikema

A THESIS
Submitted in partial fulfillment of the requirements for the degree of
MASTER OF SCIENCE
In Environmental Engineering

MICHIGAN TECHNOLOGICAL UNIVERSITY
2015

© 2015 Noah D. Buikema

This thesis has been approved in partial fulfillment of the requirements for the Degree of
MASTER OF SCIENCE in Environmental Engineering.

Department of Civil and Environmental Engineering

Thesis Advisor: *Eric A. Seagren*

Committee Member: *Stanley Vitton*

Committee Member: *Thomas Oommen*

Committee Member: *Timothy Eisele*

Department Chair: *David Hand*

Table of Contents

List of Figures	6
List of Tables	9
Abstract	10
Chapter 1 Introduction	11
1.1 Background	11
1.2 Scope and Objectives of Study.....	12
Chapter 2 Literature Review	14
2.1 <i>Sporosarcina pasteurii</i>	14
2.2 Urease.....	15
2.2.1 Soil Urease	16
2.3 Urea Utilization in <i>S. pasteurii</i> and Calcium Carbonate Precipitation	17
2.4 Taconite and Magnetite Mine Tailings	21
2.5 Dusting	22
2.5.1 Associated Risks	22
2.5.2 Seasonal Processes.....	22
2.5.3 Traditional Methods of Dust Mitigation.....	23
2.6 Summary and Conclusions.....	24
Chapter 3 Materials and Methods	25
3.1 Magnetite Mine Tailings	25
3.1.1 Raw Soil Sample Collection.....	25
3.1.2 Mine Tailing Particle Size Characterization.....	25
3.1.3 Preparation of Soil Samples for Geotechnical and Biological Testing.....	26
3.2 Microbial Culture	27
3.2.1 Rehydration of <i>S. pasteruii</i> Culture	27
3.2.2 Cell Growth Curve.....	30
3.3 Syringe Barrel Bioreactor Experimental Methodologies	32
3.3.1 Syringe Barrel Reactor Setup.....	33
3.3.2 Monitoring and Analysis of the Syringe Barrel Reactors.....	35
3.4 Soil Box Experimental Methodology.....	36

3.4.1	Soil Box Reactor Setup.....	37
3.4.2	Monitoring and Analysis of the Soil Box Reactors	40
3.5	Analytical Methods	40
3.5.1	pH.....	40
3.5.2	Soil Cell Counts	41
3.5.3	Urea Agar Slants	41
3.6	Specific Gravity Determination	42
3.7	Calcium Carbonate by CO ₂ Pressure Determination	46
3.7.1	Apparatus	47
3.7.2	Method Development.....	47
3.7.3	Length of Reaction Time	51
3.7.4	Sample Preparation	52
3.7.5	Calibration Curve.....	52
3.8	Strength Measurement – Steel Bearing Drop Test.....	53
3.8.1	Calibration Curve.....	54
3.9	SEM Analysis.....	55
Chapter 4	– Syringe Barrel Results and Discussion	57
4.1	pH of Bioreactors	57
4.2	Viable Cell Plate Counts	60
4.3	Specific Gravity Measurements	61
4.4	Calcium Carbonate Measurements.....	64
4.5	ESEM Analysis	66
4.6	EDS Analysis	70
4.7	Summary and Conclusions.....	71
Chapter 5	– Soil Box Bioreactors Results and Discussion	72
5.1	pH of Effluent.....	75
5.2	Percolation.....	76
5.3	Urea Agar Slants	79
5.4	Cell Counts.....	81
5.5	Specific Gravity.....	85

5.6	Calcium Carbonate.....	88
5.7	ESEM Results	91
5.8	EDS Analysis	96
5.9	Ball Bearing Drop Test	97
5.10	Summary and Conclusions.....	99
Chapter 6	– Summary and Conclusions.....	100
Chapter 7	– Recommendations for Further Research.....	102
	Bibliography	104
	Acknowledgements.....	109
	APPENDIX A - Syringe Barrel Bioreactors.....	110
	APPENDIX B - Soil Box Bioreactors	120
	APPENDIX C - Calibration Curves.....	131

List of Figures

Figure 2.1: Intracellular degradation and metabolism of urea in <i>S. pasteurii</i> as proposed by Dejong <i>et al.</i> , 2010.	20
Figure 3.1: Hydrometer method grain size analysis for iron mine tailing samples.	26
Figure 3.2: Dilution scheme for cell plating.	31
Figure 3.3: Cell density related with absorbance units.	32
Figure 3.4: Experimental setup for syringe barrel bioreactors.	35
Figure 3.5: Soil packing pluviation method setup.	38
Figure 3.6: Dilution scheme for viable plate counts of <i>S. pasteurii</i> in the soil layers.	42
Figure 3.7: Specific gravity convergence after five measurements in the pycnometer.	43
Figure 3.8: Soil washing step and associated pH of supernatant.	44
Figure 3.9: Pycnometer calibration curve for acid treated and non-acid treated iron mine tailings.	46
Figure 3.10: Experimental setup for the pressure-calculator method.	48
Figure 3.11: Pressure measured from both the analog and digital pressure gauges.	49
Figure 3.12: Pressure increases in the pressure vessel due to injection of fluid.	50
Figure 3.13: Pressure generated over time in the pressure vessel.	51
Figure 3.14: Calibration curve for the pressure-calculator method. The 80% and 100% by wt. CaCO ₃ measurements exceeded the pressure transducer sensitivity range, and were not reported.	53
Figure 3.15: Calibration curve for the ball drop test with the average crater diameter of five drops as a function of moisture content. (error bars = ± 1 standard deviation).	54
Figure 3.16: Untreated iron mine tailings at 1000x magnification.	56
Figure 4.1: pH of the effluent from syringe bioreactors, (A) inoculated with <i>S. pasteurii</i> , (B) with native microorganisms, and (C), using autoclaved iron mine tailings. Symbols represent individual sample measurements, and lines represent the two day moving average of the experimental data.	59
Figure 4.2: Viable cell plate counts (CFU/g wet soil) in the syringe bioreactors, (A) inoculated with <i>S. pasteurii</i> , (B) with native microorganisms, and (C) using autoclaved iron mine tailings. For samples that did not produce any countable plates (30-300 CFU), the result is reported as the lower detection limit, 10 ³ CFU/g wet soil.	62
Figure 4.3: Specific gravity measurements in the syringe bioreactors, (A) inoculated with <i>S. pasteurii</i> , (B) native microorganisms, and (C) using autoclaved iron mine tailings.	63

Figure 4.4: Calcium carbonate content based on the measured pressure in the syringe bioreactors, (A) inoculated with <i>S. pasteurii</i> , (B) native microorganisms, and (C) using autoclaved iron mine tailings.	65
Figure 4.5: Surface crust layer at 3500x magnification in R1 (A), and crust layer with iron mine tailings in R1 crushed into powder at 1000x magnification (B).	67
Figure 4.6: Surface crust layer at 1500x magnification of R2 (A). Crust layer with iron mine tailings in R2 crushed into powder at 1200x magnification (B).	68
Figure 4.7: Surface crust layer at 2500x magnification of R3 (A) and crust layer with iron mine tailings in R3 crushed into powder at 500x magnification (B).	69
Figure 5.1: Surfaces of bioreactors after the conclusion of the treatment phase for R1 (A), R1* (B), R2 (C), R2* (D), R3 (E), and R3* (F).	73
Figure 5.2: Solid white precipitate crust from R1. Note the iron mine tailings directly beneath the crust.	74
Figure 5.3: pH of the effluent from the soil box bioreactors, (A) inoculated with <i>S. pasteurii</i> , (B) with native microorganisms, and (C) using autoclaved iron mine tailings. Symbols represent individual sample measurements, and lines represent the three day moving average of the experimental data.	77
Figure 5.4: The percolation effluent flow rate through the soil box bioreactors, (A) inoculated with <i>S. pasteurii</i> , (B) with native microorganisms, and (C) using autoclaved iron mine tailings. Symbols represent individual measurements, and lines represent the three day moving average of the experimental data.	78
Figure 5.5: Urea - Agar slants after 6 hours of incubation time (A and C) and after 24 hours of incubation time (B and D). All reactors tested positive for urea-degraders. From left to right (in duplicates), R1,R1*, R2,R2*,R3,R3*.	80
Figure 5.6: Viable cell plate counts (CFU/g wet soil) with depth in the soil box bioreactors, (A) inoculated with <i>S. pasteurii</i> , (B) with native microorganisms, and (C) using autoclaved mine tailings. For samples that did not produce countable plate counts (30-300 CFU), the result is reported as the lower detection limit, 10 ³ CFU/g wet soil.	83
Figure 5.7: Bacterial colony morphology for (Left) R1,R1*, (Middle) R2,R2*, (Right) R3,R3*.	84
Figure 5.8: Specific gravity measurements in the soil box bioreactors, (A) inoculated with <i>S. pasteurii</i> , (B) with native microorganisms, and (C) using autoclaved iron mine tailings.	89

Figure 5.9: Cell density plotted against specific gravity demonstrating a general correlation between cellular density and specific gravity changes.	90
Figure 5.10: Calcium carbonate content (based on the pressure calcimeter) in soil box bioreactors, (A) inoculated with <i>S. pasteurii</i> , (B) with native microorganisms, and (C) using autoclaved iron mine tailings.	89
Figure 5.11: Pressure measurements plotted against measured specific gravity for all layers of all bioreactors. The specific gravity of calcite (2.71) is plotted along with the background pressure due to naturally present carbonates in the iron mine tailings)..	90
Figure 5.12: Surface crust layer in R1 at 1000x magnification (A), and iron mine tailings underneath the surface crust in R1 at 1000x magnification (B).	93
Figure 5.13: Surface crust layer in R2 at 2000x magnification (A), and iron mine tailings underneath the surface crust in R2 at 1500x magnification (B).	94
Figure 5.14: Surface crust layer in R3 at 1500x magnification (A), and iron mine tailings underneath surface crust in R3 at 1500x magnification (B).	95
Figure 5.15: Results for the crater diameter from the ball drop test on biotreated and untreated iron tailings, as a function of the sample moisture content. Each symbol represents the average of 5 measurements, and the error bars represent \pm one standard deviation. Note that a high standard deviation was calculated at a moisture content of 0%, due to some ball drops not creating a crater.	98
Figure A.1: EDS Spectra of R1 for the white surface crust precipitate (Plot A) and surface mine tailing powder (Plot B).....	116
Figure A.2: EDS Spectra of R2 for the white surface crust precipitate (Plot A) and surface mine tailing powder (Plot B).....	117
Figure A.3: EDS Spectra of R3 for the white surface crust precipitate (Plot A) and surface mine tailing powder (Plot B).....	118
Figure B.1: EDS Spectra of R1 for the white surface crust precipitate (Plot A) and surface mine tailing powder (Plot B).....	127
Figure B.2: EDS Spectra of R2 for the white surface crust precipitate (Plot A) and surface mine tailing powder (Plot B).....	128
Figure B.3: EDS Spectra of R3 for the white surface crust precipitate (Plot A) and surface mine tailing powder (Plot B).....	129

List of Tables

Table 3.1: Media and buffer solutions used for <i>S. pasteurii</i> experiments.....	29
Table 3.2: Average specific gravity of riffler bins with ten measurements per sample.....	45
Table 4.1: Percent by weight of calcium carbonate in syringe barrel layers.	61
Table 4.2: Summary of crystal formation morphology in biologically treated iron mine tailings assessed during ESEM imaging. The tailings powder is iron mine tailings directly beneath the surface crust.....	66
Table 4.3: EDS analysis of syringe barrel soil surface crust layer for R1, R2, and R3. Some elements present at less than 1% (by wt.) were not included in this table. A complete assessment is located in Appendix A. The crust sample refers to the white surface crust; the powder sample refers to the mine tailings directly under the white crust.	70
Table 5.1: Summary of crystal formation morphology in biologically treated iron mine tailings. The tailings powder is iron mine tailings directly beneath the surface crust.	92
Table 5.2: EDS Analysis of surface crust layer from the soil box bioreactor experiment. The crust sample refers to the white surface crust; the powder sample refers to the mine tailings directly under the white crust.	96
Table A.1: pH of syringe barrel bioreactor effluent.	111
Table A.2: Raw data for viable plate counts in the syringe barrel bioreactors. “TMC” denotes “Too Many to Counts”.	112
Table A.3: Raw data for specific gravity measurements of the syringe barrel bioreactors R2*, R3, and R3*. Grayed data indicates a non-composite sample.	113
Table A.4: Raw data for specific gravity measurements of the syringe barrel bioreactors R2*, R3, and R3*.	114
Table A.5: Raw data for the pressure-calcimeter method in the syringe barrel bioreactors.	115
Table A.6: Complete EDS analysis of syringe barrel surface crust layers for R1, R2, and R3.	119
Table B.1: pH of bioreactor effluent in the soil box bioreactors. Day 6, R1* is an interpolated value.	121
Table B.2: Percolation and flow data for soil box bioreactors.	122
Table B.3: Raw data for viable plate counts in the soil box bioreactors. “TMC” denotes “Too Many to Count”.	123
Table B.4: Raw data for specific gravity measurements of the soil box bioreactors R1, R1*, and R2.	124
Table B.5: Raw data for specific gravity measurements of the soil box bioreactors R2*, R3, and R3*.	125
Table B.6: Raw data for the pressure-calcimeter method in the soil box bioreactors.	126
Table B.7: Raw data for the ball drop strength test.	130
Table C.1: Raw data for the acid treated and non-acid treated pycnometer calibration curve	132
Table C.2: Raw data for the mine tailing and calcium carbonate calibration curve.	132

Abstract

Mine tailings are deposited into large-scale impoundments. Seasonal temperature fluctuations destabilize particles on the impoundment surface. Wind-induced shear stresses on the destabilized particles can in turn result in suspension of micron-sized particles into the atmosphere, creating dust storms that pose hazards to humans and the environment. Thus, efficient and sustainable methods of dust abatement are needed. One novel method for controlling dust emissions is biomodification. For example, *Sporosarcina pasteurii* can promote biocalcification in soil via ureolysis. However, application of this method to fined grained materials, such as mine tailings, is challenging. The goal of this work was to perform a proof-of-concept demonstration of biocalcification applied to mine tailings, and examine the associated strength increase at the soil surface. Laboratory experiments coupled with multiple analytical methods were used to confirm the formation of the surface crust, and its impact on strength. Crust formation was demonstrated with *S. pasteurii* and native microorganisms.

Chapter 1 Introduction

1.1 Background

Mining operations extract valuable materials from the earth, and supply industrial processes for the production of usable products. Not all of the extracted material is useful, however, resulting in massive volumes of waste materials called tailings, which are finely crushed rock particles that result from ore beneficiation. The tailings are deposited into massive, permanent mine tailing impoundments that can cover several square miles¹. Additionally, the U.S. Environmental Protection Agency estimates that there are thousands of active mine tailing impoundments, and tens of thousands of inactive mine tailing impoundments¹. Due to naturally-occurring processes of cold and warm weather temperature fluxes, fine particles that compose the surface of the tailing impoundments can at times become destabilized. Wind-induced shear stresses at the soil-air interface can suspend these destabilized particles into the atmosphere, creating dust storms. These dusting events can be hazardous to human respiratory health, and also reduce visibility thereby increasing the risk for vehicular accidents in nearby roadways. Accordingly, there is a need for efficient and economical means for controlling dust emissions from tailings impoundments.

Conventional approaches for control of the hazard associated with dust emissions from tailings impoundments include a variety of mechanical (e.g., applying water directly to the tailings), and chemical (e.g., use of adhesives such as emulsified asphalt) techniques^{2,3}. Unfortunately, these techniques have several limitations and potential negative side effects such as runoff into local vegetative and aquatic systems and potential exposure of humans to carcinogens from now defunct petroleum-based methods⁴. Additionally, there are associated costs with controlling dust emissions using those methods; thus a more permanent dust mitigation method is desirable.

An innovative approach for modifying soil properties that has been investigated in recent years is the use of bioengineering techniques to solve common engineering problems⁵. For example, *Sporosarcina pasteurii* has been studied due its ability to promote biocalcification via ureolysis⁶⁻⁸, which is used to increase the shear strength of soils. Research with *S. pasteurii*, however, has generally been focused on treating sand-size particles. The complications and difficulties that exist with the application of biomediated methods to fine-grained materials such as mine tailings have not been addressed. Although some mine tailings are processed into material with grain size diameters similar to 60/40 Ottawa sand, a major obstacle exists with mine tailings that have been crushed into smaller silt particle sizes that on the micron scale. This presents challenges for biomodification techniques due to the small size of the rod-shaped bacteria (< 5 μm in length), which has been observed to be similar to the size of the pore space between tailings particles. In comparison, sandy soils allow for ample substrate (e.g., oxygen) transport into deeper soil horizons, and have a greater capacity to ensure calcite precipitation due to the relatively large bulk pore space. Thus, the lack of available pore space in mine tailings restricts the movement of cells and the effective promotion of cementation by *S. pasteurii*.

1.2 Scope and Objectives of Study

Controlling dust emissions from tailings impoundments is important for human health and safety. Conventional techniques for dust control exist, but have limitations. Biomodification of the tailings properties represents a potential innovative alternative approach for controlling the surface of the tailings and reducing dust emissions. Specifically, in this research it is hypothesized that under controlled environmental conditions, microbially-induced calcite precipitation (MICP) mediated by *S. pasteurii* will result in the stabilization of the upper mine tailings layer at the air-soil interface. Thus, the overall goal of this project is the development of a bio-mediated solution for minimizing fugitive dust emissions originating from tailings impoundments via MICP. To accomplish this goal, the research has two specific objectives:

1. Perform a bench-scale laboratory feasibility study using syringe-barrel bioreactors to determine if MICP mediated by *S. pasteurii* can be stimulated in the fine-grained magnetite (Fe_3O_4) iron mine tailings originating from a North American iron mine.
2. Perform bench-scale laboratory soil box experiments to more conclusively evaluate the use of MICP mediated by *S. pasteurii* with iron mine tailings, and examine resulting improvements to the surface strength of iron mine tailing samples.

In the following chapter (Chapter 2), the background literature is reviewed with respect to the key processes relevant to the stimulation of MICP in porous media. Subsequent chapters review the experimental materials and methods (Chapter 3), and the experimental results and discussion for objectives 1 (Chapter 4), and 2 (Chapter 5). Finally the conclusions drawn from this research are presented in Chapter 6, along with recommendations for future work in Chapter 7.

Chapter 2 Literature Review

A variety of microbially remediated processes have been reviewed for their potential to influence the geomechanical properties of earth materials⁵. Much of the work to date on biomediated geomechanical processes has been on the in situ formation of mineral precipitates. In particular, MICP has been studied extensively, primarily via the process of the urea hydrolysis, or ureolysis. Successful application of MICP in earth materials requires knowledge of the microbes and the biochemical processes they mediate, as well as the physical-chemical processes of carbonate precipitation. In this chapter, therefore, background information is reviewed on *S. pasteurii*, one of the most studied organisms for MICP via ureolysis. The enzyme urease that catalyzes urea hydrolysis, urea utilization in *S. pasteurii*, and calcium carbonate precipitation and its influence on geomechanical properties of soils is reviewed in this chapter. Because this research is focused on the application of MICP to mine tailings, the chapter reviews the properties of iron mine tailings, the problem of dust emissions from tailings impoundments, and conventional techniques for dust mitigation and their limitations.

2.1 *Sporosarcina pasteurii*

Sporosarcina pasteurii is a gram positive, endospore forming⁹, aerobic, alkaliphilic bacterium¹⁰ that is part of the genus *Sporosarcina*. Endospore formation occurs when nutrients in the local environment are unavailable or if environmental conditions become too harsh for bacterial reproduction. The bacteria in this genus produce extracellular enzymes that hydrolyze complex molecules. For example, *S. pasteurii* is able to hydrolyze urea (NH₂CONH₂) via the catalytic action of the enzyme urease. Hydrolysis of urea allows this bacterium to use urea as a nitrogen source¹¹ and there is some evidence that the urea hydrolysis contributes to creation of a proton gradient and adenosine triphosphate (ATP) synthesis¹².

The primary interest in *S. pasteurii* with respect to biocementation is the ability of this bacterium to initiate and promote calcium carbonate precipitation in the crystalline form

of calcite^{8,13} under certain environmental conditions, via the induction of the intracellular urease. As discussed in more detail below, the degradation of urea by the intracellular urease in *S. pasteurii* results in the creation of favorable conditions for calcium carbonate precipitation when calcium ions are present in the local extracellular microenvironment. In addition, as discussed further below, the bacterial cell surfaces and associated exopolysaccharides (EPS) are hypothesized to function as a nucleation site for calcite formation^{8,14}. The significance of this microbially-mediated biocementation process has been used in various applications. For instance, one novel application is for concrete crack remediation^{15,16}. Other studies have found that MICP catalyzed by *S. pasteurii* is a feasible option for increasing soil stability¹⁷, reducing permeability via bioclogging^{7,18}, and suppressing dust emissions¹³. Although *S. pasteurii* is considered an obligate aerobe^{10,19}, it has been suggested that *S. pasteurii* can still induce ureolysis under both anoxic and aerobic conditions in the subsurface due to the presence of intracellular urease produced during growth under aerobic conditions¹⁹. However, it appears that ureolytic activity may eventually decline under anoxic conditions due to the inhibition and degradation of urease¹⁹.

Based on recent research, it is known that *S. pasteurii* (and the associated urease activity) is an effective agent for promoting MICP in controlled environments where a high pH can be maintained, competition and inhibition by indigenous bacteria are minimal, and a high urease activity can be sustained. Nevertheless, much remains to be learned regarding the physical/chemical/biological factors that may limit application of *S. pasteurii* for MICP, as well as the feasibility of full-scale implementation of *S. pasteurii* for influencing geomechanical properties in the field.

2.2 Urease

The key enzyme required for promoting MICP via ureolysis is urease. Urease enzymes (urea amidohydrolases, Enzyme Commission Number 3.5.1.5) are abundantly present in plants, fungi, and bacteria in the terrestrial environment²⁰, and serve to catalyze the hydrolysis of urea into ammonia and carbonic acid. The catalysis achieved with urease is

significant, with the rates of urea degradation projected to be on the order of 10^{14} - 10^{15} faster with this enzyme²⁰⁻²² compared to the uncatalyzed reaction.

The urease enzyme contains an active site consisting of two nickel ions²¹⁻²³ that catalyzes the hydrolysis of urea in a two-step process. The process is initiated when urease first attacks a urea molecule in the presence of water. Although different mechanisms have been proposed (e.g., Karplus *et al.* 1997, vs. Benini *et al.*, 1999), the general mechanism can be attributed to the active site of the enzyme. Urease contains a flap, which when open, allows for urea and water molecules to proceed into the active site. It is hypothesized that the first nickel ion serves to bind with the urea, while an acid either bound to the second nickel ion²³ or integrated into the urease flap²² facilitates the transfer of protons to the exiting NH_3 molecules. A nearby carboxylate serves to stabilize the resonance structure of urea²². When the urea and hydroxyl molecules are bound to the active site, the flap proceeds to close, allowing a nucleophilic attack on the urea carbon atom. After the completion of the reaction, the flap opens to allow the resulting ammonia and carbamate products to exit the enzyme active site²³

2.2.1 Soil Urease

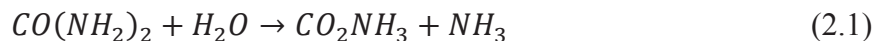
Soil urease is derived from microorganisms and dead plant material, when free extracellular urease is released and immobilized onto clay particles^{20,24,25}, and can persist in the soil even after the source urease-producing bacterial population has declined. Although less efficient at catalyzing urea degradation than the intracellular urease, immobilized urease still has the ability to contribute to the precipitation of calcium carbonate²⁶. In fact, immobilized urease has the advantage of being less susceptible to inhibitors, temperature, and pH sensitivities²⁷. Additionally, when subject to a high temperature environment, immobilized urease has been shown to possess a higher activity than its free counterpart²⁶. This phenomenon may be beneficial in environments where free and immobilized urease can degrade urea, releasing ammonia, which is transformed to nitrate via nitrification, providing nitrate nitrogen for local vegetation. However, high concentrations of urease in soils can result in undesirable changes to the local environment due to an increase in the soil pH, and increased ammonia volatilization

as well as release into surface water bodies, thereby contributing to eutrophication²⁸. Additionally, urease is considered a virulence factor for ureolytic human carcinogens^{20,21} and excessive concentrations are undesirable from a human health perspective. Therefore, in environmental settings sensitive to the conversion of urea to ammonia and carbonic acid via urease, inhibitors of the enzyme may be used to mitigate such effects.

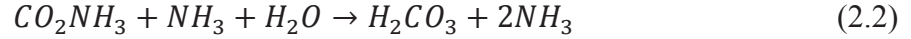
Various methods of urease inhibition have been explored. For example, with compounds such as amides and esters of phosphoric acid, the resulting diamidophosphate group replaces the conglomerate of the four water molecules in the uninhibited urease enzyme²⁰. B-mercaptoethanol inhibits urease activity by displacing the water and hydroxide molecules at the active site²⁰. Heavy metals such as mercury, lead, copper, zinc, and nickel are also inhibitors of urease, although it has been found that while higher concentrations of nickel inhibit urease, addition of low concentrations of Ni²⁺ ions in a system dramatically increases MICP²⁶. In addition, acetohydroxamic acid, which shortens the Ni-Ni distance²⁹, can also be a viable option for urease inhibition. Application of these inhibitors could potentially counteract the widespread negative effects of urease in sensitive soils, but could also, if naturally present, inhibit desirable calcium carbonate precipitation²⁶. Additionally, inhibitors such as these suggest that pollution due to anthropogenic sources could have a negative effect on the potential for calcium carbonate precipitation if the site becomes contaminated. Therefore, control mechanisms must be developed and enforced to ensure urease activity is not retarded if biological treatment via *S. pasteurii* is to be considered a viable method for fugitive dust mitigation.

2.3 Urea Utilization in *S. pasteurii* and Calcium Carbonate Precipitation

The overall proposed process by which *S. pasteurii* catalyzes ureolysis and induces calcium carbonate precipitation is summarized in Figure 2.1. First, under a concentration gradient, urea enters the cell via urea transporters³⁰, which is then hydrolyzed via intracellular urease into ammonia and carbamate:



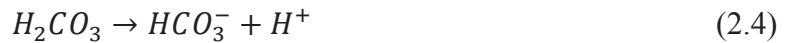
Carbamate is subsequently and spontaneously degraded into additional ammonia and carbonic acid in the presence of water²⁰:



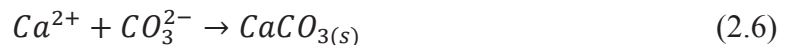
Ammonia molecules are expelled from the cell and subjected to hydrolysis, resulting in ammonium and hydroxide ion products, and raising the external pH to approximately 9^{7,8,19}:



At the same time, the carbonic acid produced in Equation 2.2 also is expelled from the cell and in equilibrium with the carbonate system in the external solution. In the high pH extracellular medium, the carbonate system is shifted toward bicarbonate and carbonate anions.



Carbonate anions in the extracellular medium are able to react with unbound calcium cations, resulting in calcium carbonate solids, which may either precipitate out in solution or form an attached solid on particulate or cellular nucleation sites:



The solubility of calcite is very low ($3.3 \times 10^{-9} \text{ mol L}^{-1}$ at 25° C)³¹, which results in precipitation under very low concentrations. Specifically, for calcium carbonate precipitation to occur, the production of the calcium ion concentration and the carbonate ion concentration must exceed the solubility production, $K_{sp} = 5 \times 10^{-9} \text{ mol}^2/\text{L}^2 = [Ca^{2+}][CO_3^{2-}]$.

Precipitation of calcium carbonate probably occurs via a combination of homogeneous and heterogeneous nucleation. Homogeneous nucleation occurs when the reactions described above lead to oversaturation of calcium and carbonate in the solution (i.e., $[Ca^{2+}][CO_3^{2-}] > K_{sp}$), catalyzing precipitation³². Heterogeneous nucleation occurs when precipitation occurs on porous medium solids, or on the cellular nucleation sites. Cells and EPS serve as nucleation sites via the binding of calcium cations to the negatively charged cell surface and EPS³³. Specifically, when calcium carbonate precipitation occurs via this “passive” mechanism, extracellular calcium ions and carbonate anions react at the nucleation sites of the bacteria due to electrostatic attraction between the positive calcium cations and negatively charged sites on the cell wall³⁴. Most studies have concluded that MICP occurs in the microenvironment at the cell wall/solution interface, and that the thin-watery layer that bacteria are covered with provide the means (as a microenvironment) to allow MICP to occur³⁵. However, cell stagnation or death can occur when the bacterium is completely encapsulated in calcium carbonate³⁴. It has been suggested that a slower reaction of calcite formation results in larger crystals with more cementation potential³⁶, when compared to smaller calcite crystals produced from quicker precipitation rates. (Bodek *et al.*, 1988 cited in Whiffin³⁶).

As outlined in the equations above, calcium carbonate precipitation is driven by four variables: 1) The calcium cation concentration, 2) the carbonate anion concentration, 3) the environmental pH, and 4) the availability of nucleation sites^{34,35,37,38}. With the exception of (1) the calcium cation concentration, these variables are directly affected by the reactions associated with microbially-mediated ureolysis.

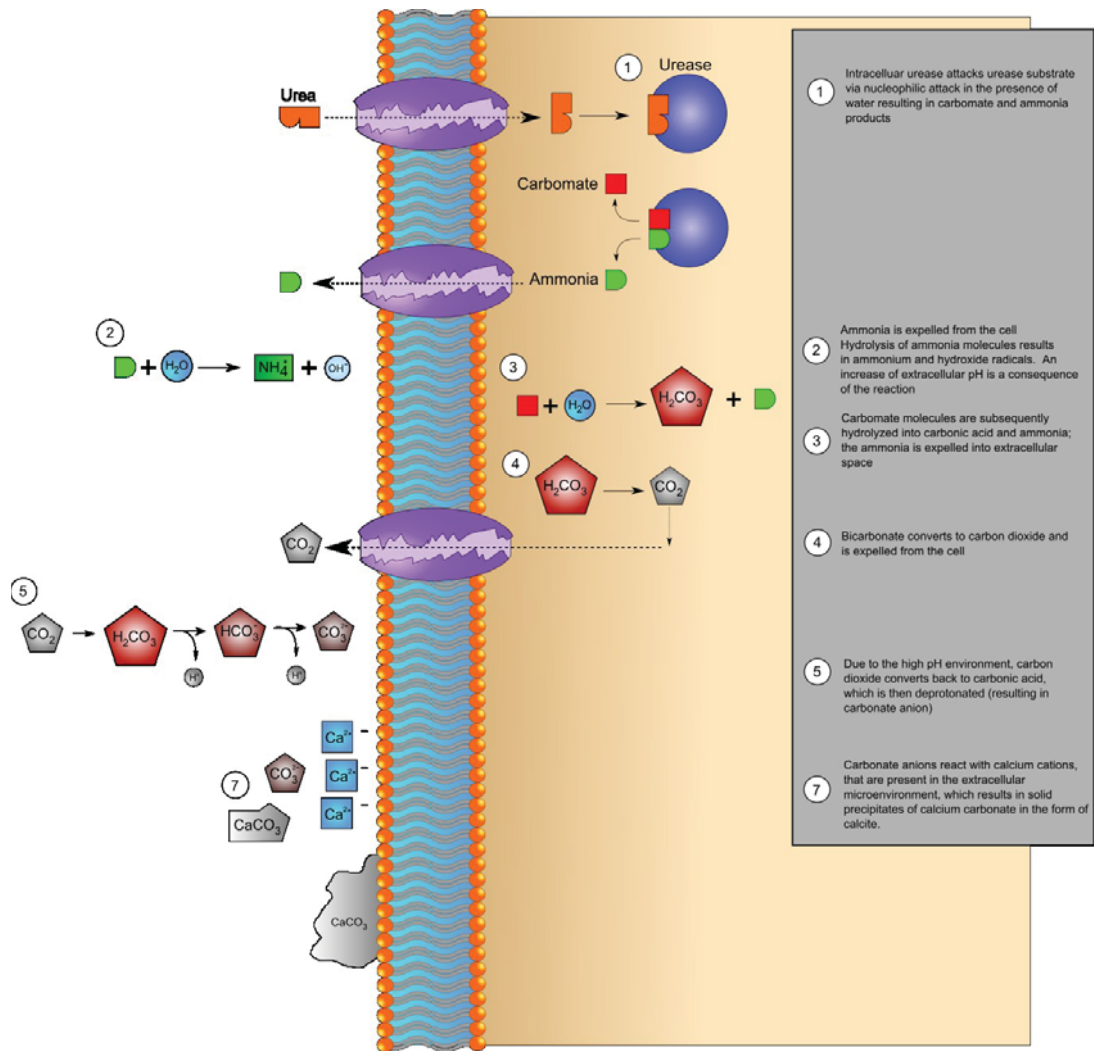


Figure 2.1: Intracellular degradation and metabolism of urea in *S. pasteurii* as proposed by Dejong *et al.*, 2010.

2.4 Taconite and Magnetite Mine Tailings

The mine tailings investigated in this research are from iron mining operations in northern Michigan and Minnesota where the main ore body consists of taconite ore. Taconite is a banded iron formation that contains layers of jasper, chert, hematite, and magnetite minerals, as well as martite and goethite. The taconite ores formed during the middle Precambrian age^{39,40}. The taconite formations resulted by the deposition of the iron and silica on the sea floor along with other sedimentary layers and later subjected it to immense pressure and heat.

In northern Michigan and Minnesota the taconite is extracted using open pit mining methods. The first step in mining is to extract the economically significant material “ore” using drilling and blasting techniques to fragment the ore. The ore/rock mixture is then subject to crushing, grinding, treating, and pelletizing^{40,41}. The end product of this mining and beneficiation process are mine tailings, which generally have an average size of about 40 to 60 microns. The resulting mine tailings are disposed of in large mine tailings impoundments, which can encompass several square miles¹. Tailings are transported to the impoundments in a slurry with a 60% particle/40% water¹ using a piping distribution network. The impoundments are the final destination for the mine tailings. Wastewater effluents from the impoundments are treated before the water is reintroduced into the mining environment. Most iron mining operations reuse the water from the impoundment after it is treated and clarified in a closed system.

The dominant iron ore mineral present in the tailings used in this research is magnetite. Magnetite is the mineral form of iron (III) oxide (Fe_3O_4), and is strongly magnetic. Magnetite mine tailings consist of silt sized particles as noted about in the size range of 40 to 60 micron, although the size-distribution can range from sand size to colloidal size, this is, less than one micron.. These tailings can consist of a variety of minerals such as silica (in the form of chert and jasper), iron carbonates, iron silicates, and sulfides⁴¹. The tailings particles exhibit a wide variation in size, which is a result of the degree of iron removal via the iron extraction processes (crushing of the source rock).

2.5 Dusting

2.5.1 Associated Risks

Mine tailing impoundments, when not vegetated for dust control or final reclamation, are typically free of vegetation and, as a result, the surface area is largely void of any root systems that may stabilize the upper layers of soil. Consequently, the strong wind events can result in dusting events when the shear stresses induced by the wind exceed the shear strength of the tailings. This shearing failure allows soil particles to become suspended in the atmosphere, resulting in fugitive dust emissions. Fugitive dust emissions present a hazard to humans through the reduction of visibility, and the inhalation of dust particles resulting in irritation of the respiratory tract. In particular, damage to the lungs can be expedited by particulate matter with a diameter $\leq 2.5 \mu\text{m}$ ($\text{PM}_{2.5}$)⁴².

2.5.2 Seasonal Processes

The processes that result in fugitive dust emissions occur in both winter and summer seasons. Evaporation of soil moisture in the summer months reduces the shear strength of the upper layer of tailings resulting in potential dusting. The dusting that occurs in the winter months is the result of a more complex process in which ice lenses form in the upper layers of tailings, especially during the fall time of the year. During the fall freezing generally occurs in the evening and can last for a period of time until thawing occurs or the temperature stay below freezing for the winter. As the freezing front moves downward into the tailings water moves vertically upward to the freezing front and results in the formation of ice lenses when the water freezes. Once the ice lenses have formed they are susceptible to rapid sublimation in which the ice sublimates to a gas leaving dry tailings on top of frozen tailings. Many of the large scale dust storms that occur at iron mines in cold climates are generated from this process and are known in the mining industry as “dry-freeze” events, which as noted above, generally occur in the fall time of the year.

2.5.3 Traditional Methods of Dust Mitigation

Many methods have been used to control fugitive dust events, such as from mine tailings impoundments. These methods are categorized as agronomic, surface penetration, admixture, and surface blanket^{33,39}. Agronomic methods consist of establishing vegetative cover and applying mulch layers⁴. Activities associated with agronomic methods include seeding, sprigging, sodding, with the addition of top soil when the mine tailings are not able to support plant growth (e.g., due to the pH, or lack of organic matter)⁴³. Disadvantages associated with agronomic methods include the fact that it is only applicable to impoundments in which equipment can navigate the tailings or after closure. In some cases, irrigation may be required, which presents a challenge in arid and semi-arid locations.

Surface penetration consists of applying a liquid directly to the soil surface by spraying or sprinkling. The most commonly applied liquid for dust suppression is water; however, this is not an effective approach for arid and semi-arid areas⁴³. Additionally, water is only a temporary measure, and thus must be reapplied frequently. Other applied liquids include bituminous materials, emulsified asphalts, road tars, and resinous materials (such as a lignin solution or resin petroleum-water emulsion)². Complications with the use of these chemical suppressants include slow curing times and the overall volume of liquid needed to suppress dusting. In addition, there may be adverse environmental impacts associated with some of the chemicals added as dust suppressants⁴³.

The admix method requires more time and equipment than agronomic and surface penetration methods, but results in the strengthening of the soil. With this technique, the dust palliative is blended with the soil to produce a uniform mixture and subsequently compaction of the surface. Materials used include Portland cement and bituminous materials.

The surface blanket or capping method involves covering the top layer of tailings with prefabricated membranes and mesh, aggregates (e.g., gravel), soil, and bituminous

surface treatments³. Disadvantages associated with such capping techniques include the possibility that appropriate aggregates or soil may not be available nearby, and this approach is really only applicable after closure of the impoundment (Chen *et al.* 2015).

As noted, each dust mitigation technology has its advantages and disadvantages, and application is likely to be site-specific, with some methods inappropriate for some sites. For example, wetting for dust control requires large volumes of water, and is not cost effective, or environmentally friendly, especially in arid and semi-arid areas (Chen *et al.*, 2015). In addition, use of dust suppressing chemicals to susceptible areas is likely to require reapplication, making it an expensive application. Also, some of the chemical methods, such as introducing crusting, binding, or petrol agents, have been banned (e.g., such as PCB-containing oil⁴⁴, dioxin-containing suppressants⁴, and asbestos-containing suppressants⁴) by the U.S. Environmental Protection Agency due to concerns with groundwater contamination, surface water contamination, and overall persistence in the environment. Therefore, there remains a need for permanent, sustainable, cost effective for mine tailing dust control.

2.6 Summary and Conclusions

Relevant background information was reviewed in this chapter. *S. pasteurii* has the potential to promote biocementation of fine grained iron mine tailings due to presence of intracellular urease in the microorganism. Additionally, the resulting calcium carbonate precipitation is viable under certain environmental conditions, and has the potential to alter the geomechanical properties of the mine tailings. Finally, because current dust mitigation technologies are somewhat limited with respect to their application, scope, and costs, a more permanent dust mitigation technology is desirable. Such a technology is potentially achievable through MICP mediated by *S. pasteurii*.

Chapter 3 Materials and Methods

3.1 Magnetite Mine Tailings

3.1.1 Raw Soil Sample Collection

Iron mine tailings, consisting of mostly magnetite tailings were collected from two North American iron mine tailing impoundments. Samples were extracted from the impoundment using a shovel, and placed in five-gallon buckets for storage and transportation. Additional samples were collected at later times, with the sampling date and location recorded.

3.1.2 Mine Tailing Particle Size Characterization

After collection, the tailings were analyzed for key chemical and physical characteristics. The pH was the primary chemical characteristic of the mine tailings that was determined. Each measurement was performed by following ASTM method D4972-01⁴⁵ (Standard Test Method for pH of Soils).

To characterize the tailing's particle size distribution a grain-size analysis was performed. Because of the process by which the tailings are deposited in the impoundment, the particle sizes were expected to vary spatially from location to location, as well as with depth. Therefore, it was necessary to characterize the particles sizes of each individual sample group. Accordingly, each tailing sample had a hydrometer analysis conducted following ASTM method D422⁴⁶ in order to characterize the distribution of particle sizes in the tailings samples. The hydrometer analysis confirmed the spatial variability of the particle sizes. The particle distributions are displayed in Figure 3.1. Two buckets (Coarse A and Coarse B) had less than 10% finer in a particle range of 0.1 mm and smaller, indicating larger sand sized particles. It was also determined that two of the sample buckets (Fine A and Fine B) consisted of mostly silt sized particles; a particle range (0.002 mm to 0.075 mm) that is susceptible to dusting. Therefore, iron mine tailings from bucket Fine A were chosen as the source for all subsequent biological and geotechnical tests.

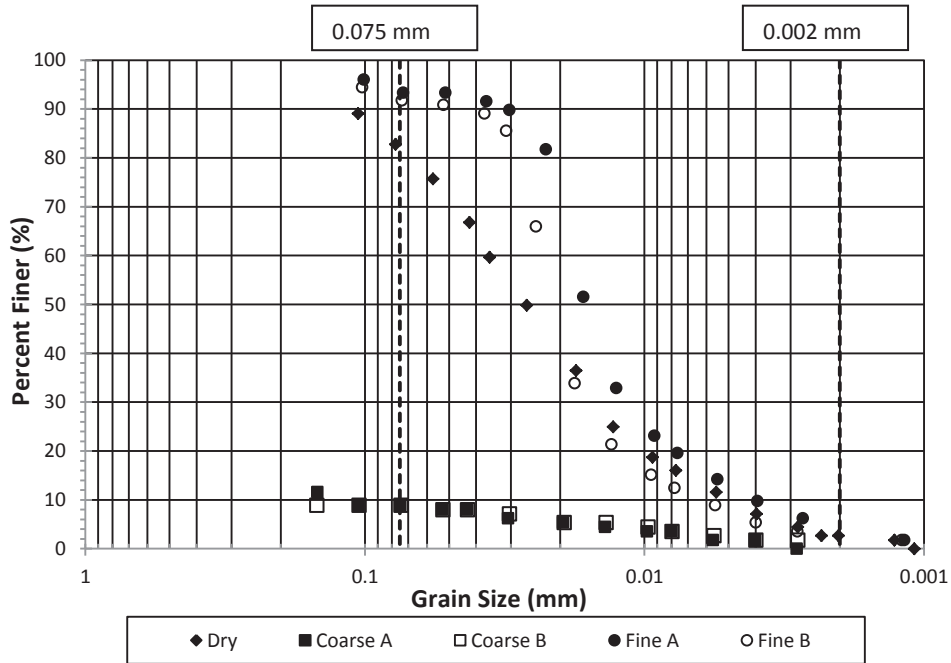


Figure 3.1: Hydrometer method grain size analysis for iron mine tailing samples.

3.1.3 Preparation of Soil Samples for Geotechnical and Biological Testing

Procedures were developed to ensure the reproducible preparation of tailings specimens with consistent properties for the biological and strength testing. First, tailings were transferred from the 5-gallon storage buckets to a large soil bin, and allowed to air dry for a few weeks, after which they were left in the air dry condition until the tailings were tested. The air-dried tailings were crushed using a Micro Deval apparatus. For the crushing process, one-third of the apparatus' soil capsule was filled with tailings, placed on the rollers, and the apparatus ran for seven minutes. After crushing, the tailings were transferred to another soil bin, and the remaining chunks were crushed by hand using a steel cylinder underneath a snorkel ventilation apparatus to control dusting. The crushed tailings were sifted using a flour sifter. Before packing the soil into the syringe barrel reactors or soil boxes, as described below, water was added to the dry tailings to a 5% (by wt.) moisture content to suppress any dust from the packing process. Specifically, 5% (by weight) of distilled water was measured and then mixed into the dried, crushed

tailings using a spoon and trowel. After mixing, the wet tailings were then sifted again to break up any clumping resulting from the addition of water to the soil.

3.2 Microbial Culture

3.2.1 Rehydration of *S. pasteurii* Culture

A dehydrated sample of *S. pasteurii* culture⁴⁷ (American Type Culture Association, ATCC 11859) was obtained and rehydrated using the recommended liquid medium ATCC 1376, *Bacillus pasteurii* NH4-YE medium⁴⁸ (Tris-YE medium) (Table 3.1). Tris-YE medium was prepared as follows. First, Tris-buffer was prepared by mixing Tris Acid (1.976 g) and Tris Base (14.22 g) into 1 L of distilled water. The buffer pH was adjusted to 9 using a pH probe and 6M HCl. Next, yeast extract (20 g) and (NH₄)SO₄ (10 g) were placed in separate 1 L glass bottles, and 500 mL of Tris-buffer was poured into in each bottle. The two bottles were then autoclaved for 15 minutes at 121° C, cooled to 50-55°C after completion of the autoclave cycle, and aseptically combined to avoid precipitation.

The vial containing the pure freeze-dried culture of *S. pasteurii* was opened by following ATCC protocol. First, 0.5 to 1.0 mL of liquid Tris-YE medium was aseptically added to the vial with the freeze-dried material using a sterile Pasteur pipette. The vial contents were then mixed well using a vortex mixer. The mixture was transferred back to a test tube containing 5.0-6.0 mL of Tris-YE medium. Finally, 1.0 mL of the suspension was transferred to a second tube containing 5.0-6.0 mL Tris-Ye medium. The latter step was conducted because the cryoprotectant used in the freeze-drying procedure may inhibit growth in the primary tube. The culture was incubated at 30°C in a shaker bath for 48-72 hours.

After incubation, the bacteria from each tube were then plated onto two *Bacillus pasteurii* urease (BPU) media (Table 3.1) agar streak plates. BPU plates were created by preparing and combining two solutions (A and B). Solution A was prepared by combining trypticase peptone (10 g), yeast extract (5 g), tricine (4.5 g), ammonium sulfate (5 g),

glutamic acid (2 g), urea (10 g), and distilled water (500 mL) into a 1 L glass bottle. This solution was mixed well, and the pH adjusted to 8.6 ± 0.1 using 6M HCl. After pH adjustment, the solution was filter sterilized using a sterile 0.2 μm filter (Nalgene SupormachV fast PES bottle top filter). Solution A was then warmed in a 50°C water bath, such that Solution B would not solidify when combined with Solution A. Solution B was prepared by adding agar (15 g) to 500 mL of distilled water, and autoclaving at 121°C and 21 psi for 15 minutes. When the solution with the agar cooled down to about 50°C, the two solutions were mixed together by gently pouring Solution A into the bottle containing Solution B. The combined solutions were gently swirled and inverted (not shaken) as to not create air bubbles. The solution was then immediately poured into Fisher Scientific 100 mm x 15 mm sterile petri dishes (Cat. No. FB0875712) and allowed to cool and solidify. After cooling, the agar plates were inverted, stacked, and stored at 4° C in a refrigerator. Before use, the BPU plates were dried in the incubator at 30° C for 24 hours.

Table 3.1: Media and buffer solutions used for *S. pasteurii* experiments.

Tris - YE Solution		BPU Plates		Urea-CaCl ₂ Solution		Phosphate Buffer Solution	
Ingredient	Amount	Ingredient	Amount	Ingredient	Amount	Ingredient	Amount
<i>Solution A</i>		<i>Solution A</i>		<i>Solution A</i>		<i>Solution A</i>	
Tris Acid	1.976 g	Trypticase peptone	10 g	Nutrient broth	3 g	Na ₂ HPO ₄	3 g
Tris Base	14.22 g	Yeast extract	5 g	Urea	20 g	NaH ₂ PO ₄ ·H ₂ O	20 g
Distilled Water	1 L	Tricine	4.5 g	NH ₄ Cl	10 g	NaCl	10 g
<i>Solution B</i>		(NH ₄) ₂ SO ₄	5 g	NaHCO ₃	2.12 g	Distilled Water	1 L
Yeast extract	20.0 g	Glutamic acid	2 g	CaCl ₂	2.8 g		
(NH ₄) ₂ SO ₄	10.0 g	Urea	10 g	Distilled Water	500 mL		
0.13 M Tris buffer	1.0 L	Distilled Water	500 mL				
Agar (if needed)	20.0 g	<i>Solution B</i>					
		Agar	15 g				
		Distilled Water	500 mL				

An inoculating loop was used to transfer the original culture from the test tube to the BPU agar plates, using the streak plate method. After streaking, the plates were wrapped in Parafilm, inverted and incubated at 30°C for 2 days, and then stored inverted in a refrigerator. To maintain a high enzymatic activity, approximately every 30 days, the cultures were transferred onto fresh BPU plates. These plates were used as the source of inoculum for the experiments described below.

3.2.2 Cell Growth Curve

A cell density - absorbance relationship was developed, so that the cell density as cell counts (colony forming unit; CFU) could be estimated during the batch growth of the bacteria in a liquid media while monitoring growth via absorbance in a spectrophotometer. This cell density – absorbance curve was conducted in duplicate.

First, a *S. pasteurii* colony from a stored BPU plate was used to inoculate a 300 mL nephelo flask containing 60 mL of Tris-YE medium, with a sterile cotton bung wrapped in gauze enclosure. The inoculated flask was placed in a New Brunswick Scientific Reciprocating Shaker Bath (Model R76) at 30° C. Cell growth was monitored by measuring absorbance in a Fisher Scientific spectrophotometer, with λ set at 600 nm and zeroed using a Tris-YE blank. The solution was allowed to stabilize for 10 seconds before the absorbance measurement was recorded. The solution was considered stabilized when the absorbance stopped varying. Following inoculation, the culture absorbance was checked every hour until the lag phase was complete, after which absorbance measurements were taken every 15 minutes. The culture was monitored until the late exponential phase, at which point 0.6 mL of inoculum was transferred into a second 300 mL nephelo flask containing 60 mL of sterile Tris-YE media. This flask was placed in the shaker bath and grown until the late exponential phase by following the same procedures as for the first flask. The first flask took approximately 24 hours to reach the late exponential phase, while the second flask reached this phase after approximately 17 hours.

To obtain the relationship between absorbance and cell counts, the inoculum was first diluted down to five different absorbance values by preparing varying ratios of inoculum to Tris-YE. The absorbance of each solution was read at 600 nm, and then each initial dilution was diluted further five times as illustrated in Figure 3.2. The last three of the serial dilutions were plated onto Tris-YE medium agar plates to get the spread-plate counts, which were incubated at 30° C for 36 hours. After the incubation period, the colonies growing on the plates were counted, and the colony counts that fell within a

range of 30 to 300 colonies were averaged. The absorbance values were then plotted as a function of the average colony counts, as shown in Figure 3.3. A linear regression through the two data sets gave the following relationship, which was used to relate liquid culture absorbance to colony counts for all experiments:

$$y=0.2511\ln(x)-4.1223 \quad (3.1)$$

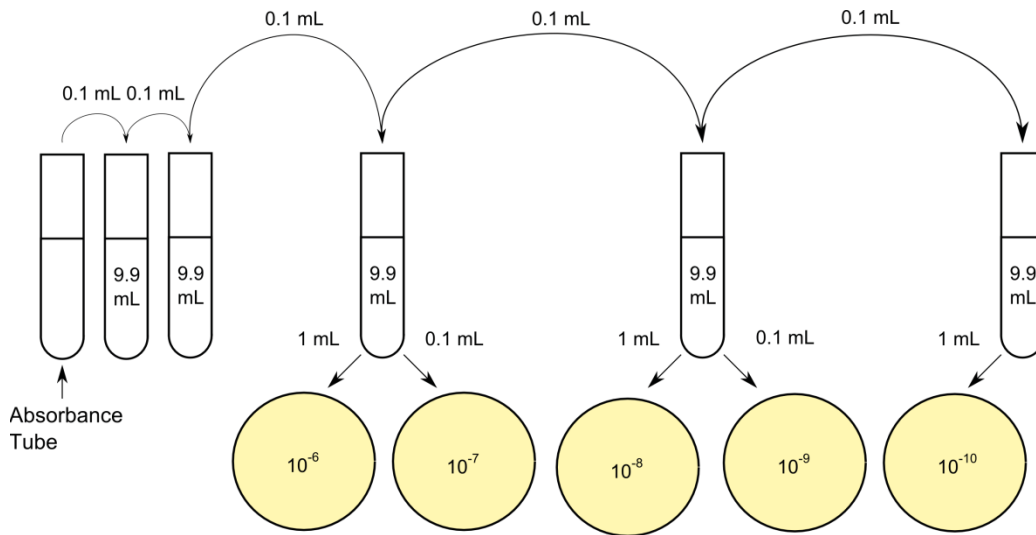


Figure 3.2: Dilution scheme for cell plating.

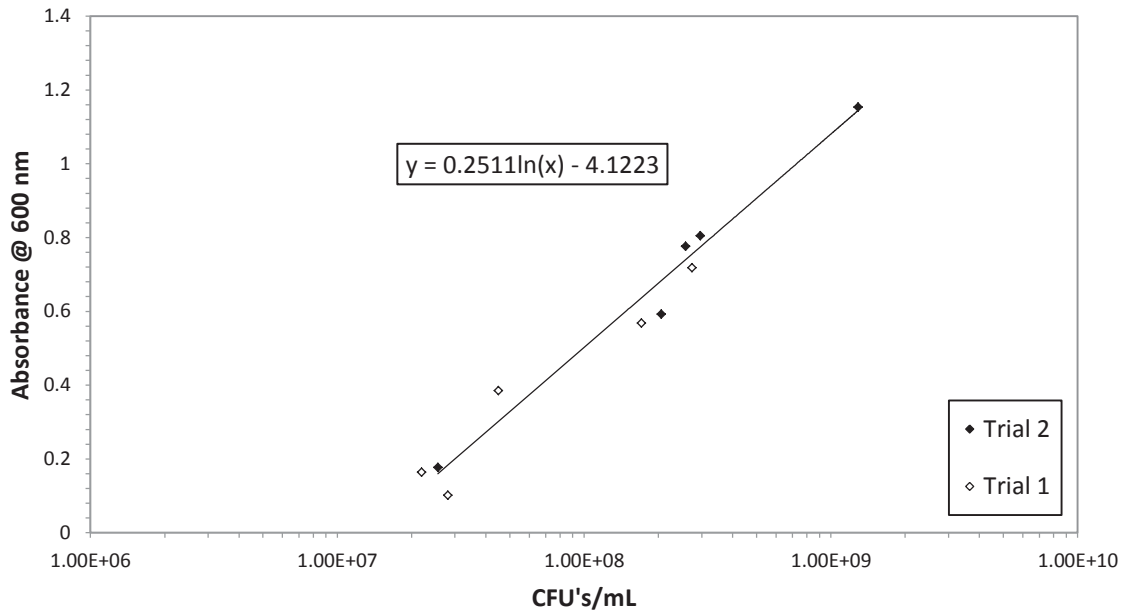


Figure 3.3: Cell density related with absorbance units.

3.3 Syringe Barrel Bioreactor Experimental Methodologies

To demonstrate that *S. pasteurii* can be inoculated, and MICP stimulated, in the iron mine tailings, a series of experiments were developed and conducted on biologically treated iron mine tailings using syringe barrel reactors. After treatment, three major tests were conducted on the specimens obtained from the syringe barrel reactors to evaluate for the occurrence of MICP: (1) cell plate counts via spread plate method, (2) CO₂ pressure measured through the use of a pressure-calculator apparatus, and (3) specific gravity measurements obtained using a pycnometer. In addition, scanning electron imaging was performed using an environmental scanning electron microscope (ESEM) to visually assess the treatment process. Along with the ESEM, energy dispersive spectroscopy (EDS) analysis was obtained to evaluate the relative abundance of calcium in the treated samples.

First, a single, isolated colony of *S. pasteurii* was transferred from a BPU plate to 60 mL of Tris-YE solution in a 300 mL nephelo flask and placed in a reciprocal shaker bath at 30° C. Absorbance measurements were taken in varied intervals until the late exponential phase was reached. 0.6 mL of the inoculum was transferred via sterile 1 mL pipette to another nephelo flask containing 60 mL of Tris-YE. Absorbance measurements were taken every hour until a cell density of approximately 10⁹ CFU/mL was acquired.

3.3.1 Syringe Barrel Reactor Setup

The syringe barrel reactors were constructed using BD 60-mL syringe barrels with Luer-Lok tip (Cat. No. 309653), the plunger removed⁴⁹, and Whatman 41 filter paper (Cat No. 1441-150) placed in the bottom of the barrel (Figure 3.4). Three treatments were conducted in duplicate for a total of six bioreactors. In the first treatment (reactors R1 and R1*), the bioreactor was bioaugmented by inoculating with *S. pasteurii*. The second treatment (bioreactors R2 and R2*) was the live control, and contained only native microbes in the iron mine tailings. Finally, the third treatment (bioreactors R3 and R3*) contained autoclaved iron mine tailings as an inhibited control. The iron mine tailings for treatment 3 was prepared by autoclaving the soil once per day for three days at 115° C for 30 minutes⁵⁰.

Iron mine tailings were packed into the syringe barrel reactors via pluviation using a flour sifter with attached funnel and 0.75” diameter hose to transfer the tailings to the soil box. The hose was initially placed one inch from the bottom of the syringe barrel, and the sifter was turned to distribute the tailings into the syringe barrel. After approximately 1” to 1.5” of tailings were deposited, the tailings were hand tamped. This process was repeated until the syringe barrel was filled with tailings. The goal of packing was to achieve a 0.9-1 void ratio and 5% moisture content. However, the reactors were actually packed consistently to a void ratio of approximately 1.1. After the reactors were packed, they were saturated for 24 hours by connecting the bottom of the reactors to a mariotte tube containing sterile distilled water (Figure 3.4). The reactors were considered

saturated based on a visual assessment of surface of the reactor and color change in the sides of the reactor.

After the saturation period, the tubing was removed from bioreactors R1 and R1*, which were then inoculated with the *S. pasteurii* inoculum. To prepare the inocula, a single, isolated colony of *S. pasteurii* was transferred from a BPU plate to 60 mL of Tris-YE solution in a 300 mL nephelo flask and placed in a reciprocal shaker bath at 30° C. Absorbance was monitored until the late exponential phase was reached, at which point 0.6 mL of the inoculum was transferred via sterile 1 mL pipette to another nephelo flask containing 60 mL of Tris-YE. Absorbance measurements were taken every hour until a cell density of approximately 10^9 CFU/mL was acquired. 15 mL of inoculum from the second flask was pipetted via a sterile 10 mL pipette into the headspace of the bioreactor R1 and R1*. This was allowed to percolate until the volume in the headspace decreased such that another 5 mL could be applied. To maintain saturation, the other reactors remained attached to the mariotte tube while the first reactors were being inoculated. After 24 hours, any remaining liquid on the top of R1 and R1* was removed via sterile 10 mL pipette with care taken to ensure no surface soil was removed with the fluid. The tubing to the mariotte tube was then removed from R2, R2*, R3 and R3*, and 25 mL graduated cylinders were placed below the opening of all reactors. Parafilm was placed loosely on the top of the reactors to prevent contamination from atmospheric deposition.

After set up, the reactors were maintained twice daily for 10 days by feeding with Urea-CaCl₂ media, first at 9:00 AM, and then at 5:00 PM. First, Urea-CaCl₂ media was aseptically transferred from the storage bottle into a sterile beaker. Then, using a sterile 10 mL glass pipette, Urea-CaCl₂ media was transferred from the beaker into the headspace of the reactors by slowly pipetting onto the inside sidewall of the reactor (to prevent scouring of soil surface).

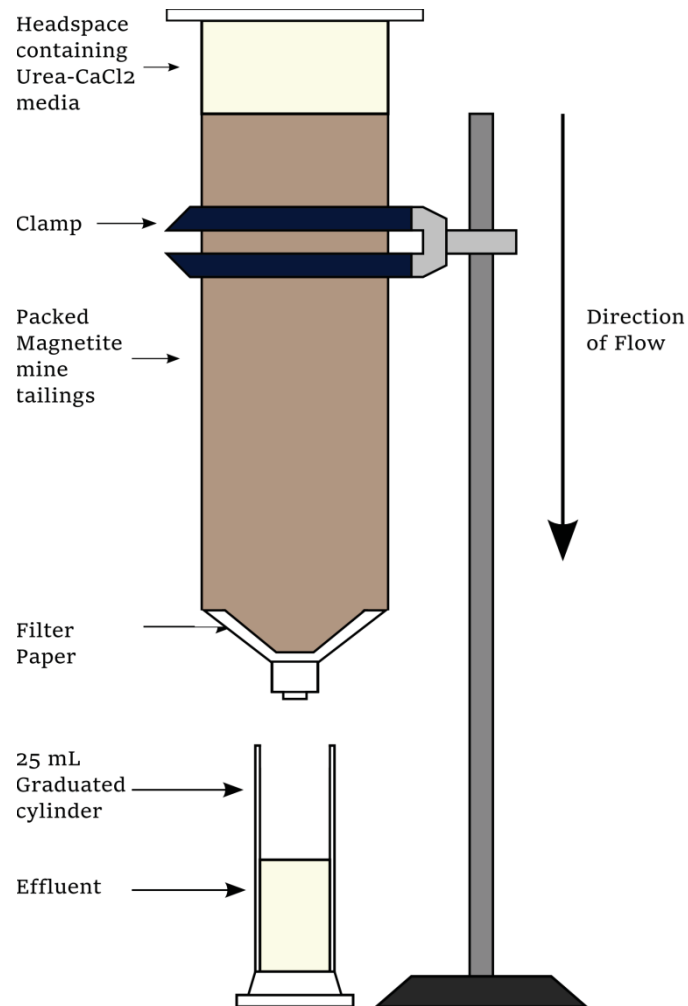


Figure 3.4: Experimental setup for syringe barrel bioreactors.

3.3.2 Monitoring and Analysis of the Syringe Barrel Reactors

As biological treatment progressed, a series of measurements were conducted to monitor the bioreactors for the duration of the test. These measurements included the: (1) volume added to the headspace of each bioreactor, (2) volume of effluent collected in the graduated cylinder for each bioreactor pH of the effluent, (3) pH of the influent, and (4) pH of the effluent. The volume of influent was measured as described above, while the effluent in the graduated cylinder (Figure 3.4) was recorded daily. The pH of the influent and effluent were initially measured by using 1-14 pH range and pH paper, but ultimately the measurements were all made using a pH meter and probe, as described below. pH

measurements using the pH meter and probe were made in the effluent collected in the graduated cylinder (Figure 3.6), whereas the measurements made using pH paper were made on the effluent coming directly out of the bottom of the reactors. The graduated cylinders were washed between measurements following Standard Method 9040 Washing and Sterilization⁵¹.

After the conclusion of the treatment phase of the study, the bioreactors were allowed to air dry for 30 days before analysis. After air drying, each reactor was divided into four volumetric intervals using a hacksaw and flame-sterilized blade: 0-10 mL, 10-20 mL, 20-30 mL, and 30-60 mL. Preliminary tests indicated that the majority of biological activity occurred in the upper 30 mL of the bioreactors and, thus, the fourth layer consisted of a larger volume of tailings (30-60 mL). Plastic shavings from the cutting process were removed using a sterile spatula. Each soil layer was then extracted by pushing the soil plug out of the syringe barrel section and into a sterile soil tin. 1 gram of soil from each layer was set aside to conduct cell plate counts, while the rest of the material was then oven dried for three days at 40° C in a Despatch (Model No. LBB2-27-1) oven. Although ASTM D2216-10⁵² dictates that drying soil for duration of one day at 110° C is appropriate, drying at 40° C was used to ensure that cells were not destroyed during the drying cycle, allowing their observation later using environmental scanning electron microscopy (ESEM)⁶. After drying, the soil tins containing the samples were covered and edges sealed with Parafilm until they were analyzed. This portion of the material was used for measurement of specific gravity, CaCO₃, and ESEM.

3.4 Soil Box Experimental Methodology

The syringe barrel reactors were next scaled up to larger soil box experiments. These larger reactors allowed for measurements of surface strength in addition to the analyses that were used to monitor biological transformations of the tailings in the syringe barrel reactors. Following the same approach as for the syringe barrel reactors, three treatments were conducted in duplicate for a total of six bioreactors: (1) for the first treatment (bioaugmented bioreactors R1 and R1*), the bioreactor was inoculated with *S. pasteurii*;

(2) for the second treatment (live control bioreactors R2 and R2*), only the native microbes were present; and (3) for the third treatment (autoclaved control, bioreactors R3 and R3*), the iron mine tailings were prepared by autoclaving the soil once per day for three days at 115° C for 30 minutes⁵⁰.

3.4.1 Soil Box Reactor Setup

The soil boxes were fabricated using ¼ in. thick polycarbonate, which was cut to construct a box with 3 in. x 3 in. x 3 in. inside dimensions. The polycarbonate sections were glued together using SCIGRIP 16 Acrylic Cement, and allowed to bond overnight. Barbed brass hose fittings (¼ in.) were installed in the bottom of the box (Figure 3.7) via threaded holes tapped into the polycarbonate. After fabrication, Whatman 41 filter paper (Cat No. 1441-150) was placed on the bottom of the soil box, and covered with a thin (<1 mm) layer of well graded sand. The sand was used to facilitate capillary rise from the water inlet/mine tailing soil interface. Subsequently, the soil boxes were then packed with mine tailings via pluviation, which has been demonstrated previously to be an effective technique for evenly distributing soil⁵³ (Figure 3.5). Pluviation was conducted by utilizing a flour sifter with an attached funnel and 0.75” diameter hose. The end of the hose was initially held approximately one inch from the bottom of the soil box. Tailings were then transferred into the flour sifter, and the sifter was turned to distribute the tailings into the soil box. The tailings were first placed into the box along the inside edge, and then moving inwards toward the center in a square pattern. After one surface pass was completed (approximately 1-1.5” of soil height, covering the entire bottom layer of the soil box), the tailings were compacted via hand tamping. First, a large hand tamp with a diameter of 2” was used to pack the loose soil. After one pass of the large hand tamp, a smaller (~ 0.75” diameter) hand tamp was used. Another seven to ten lifts of tailings were then added by following the same procedure for pluviation and compaction, until the soil box was completely full of tailings. A Mariotte tube was then connected to the bottom of the soil box via the brass fitting with hose barb, and the specimen was allowed to saturate overnight.

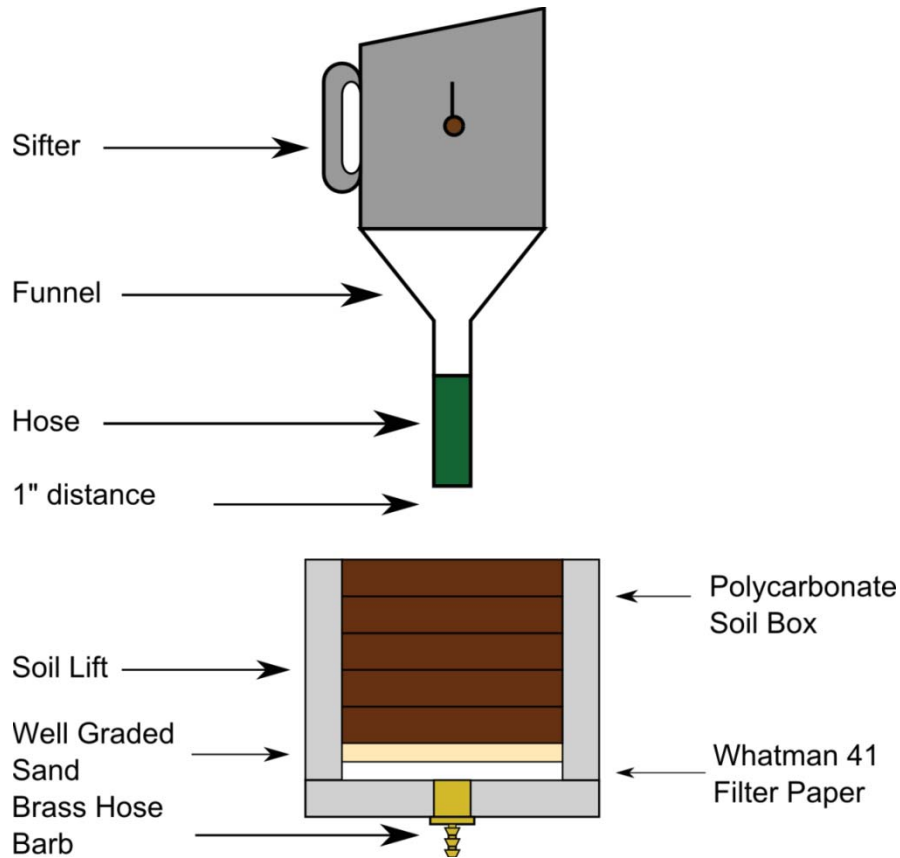


Figure 3.5: Soil packing pluviation method setup.

Three treatments were prepared using the procedure described above. The first treatment was native iron tailings that were inoculated with *S. pasteurii* to demonstrate the effect of bioaugmentation. For this treatment, soil boxes R1, R1* were packed with unmodified iron mine tailings, and then inoculated. The *S. pasteurii* inoculum was prepared using a modified cell growth protocol because of the large volume required for treatment of two soil boxes. The required volume of Tris-YE inoculum with a cell density of 10^9 CFUs/mL was obtained by scaling up from the surface area of the syringe bioreactors. Accordingly, approximately 207 mL of inoculum were required per soil box. To prepare this volume of inoculum, 1.5 L sterile Tris-YE was aseptically placed in a pre-autoclaved 9.5 L glass Pyrex aspirator bottle (1220-2X). The bottle was placed on a stir plate with a stir bar rotating at 350 rpm, and incubated in a temperature control room at 30°C. Growth was monitored periodically by aseptically taking samples and monitoring the

culture absorbance. Because of the different growth conditions (i.e., temperature control room and stir bar instead of a shaker bath), the *S. pasteurii* cells at stationary phase only grew to about 0.8 ABS. This culture was then used to inoculate soil boxes R1 and R1*. This was done in 4 sequential treatments of 50 mL of the 0.8 ABS cell solution, with a final fifth treatment of 7 mL.

For the second treatment soil boxes R2 and R2* were packed with unmodified iron mine tailings to demonstrate the impact of the native microbial population during treatment. Finally, the third treatment and control was prepared in soil boxes R3 and R3* by packing them with autoclaved iron mine tailings, which had been prepared by autoclaving for 1 hour at 15 psi and 121° C once per day for three days. The goal of this treatment was to eliminate or reduce the population of native microbes and demonstrate the role of any non-biologically mediated reactions.

Constant head was maintained in all of the soil reactors with the Urea-CaCl₂ media. The media was applied via a sterile squirt bottle, taking care to ensure that there was no scouring of the soil surface. Wire mesh covered with cotton was placed on top of the reactors to reduce the potential for microbial contamination from atmospheric deposition. The wire mesh provided rigidity to the cotton so that the Urea-CaCl₂ media was not absorbed by the cotton.

3.4.2 Monitoring and Analysis of the Soil Box Reactors

The treatment phase for the soil box experiment lasted for 23 days. Following the same approach as for the syringe barrel reactor experiments, during the biological treatment phase, a series of measurements were conducted twice daily to monitor the bioreactors including: (1) the volume of media added to each bioreactor, (2) the volume of effluent collected from each bioreactor, (3) the pH of the influent and (4) the pH of the effluent. The volume of influent was measured by a mass change. It was assumed the density of the Tris-YE was equivalent to water, and thus the volume of influent was determined by weighing the squirt bottle before and after application. The effluent volume was measured in a 25-mL graduated cylinder. The pH of the effluent (collected in the graduated cylinder) was analyzed using a pH meter and probe, as described below. The graduated cylinders were washed between measurements following standard methods 9040 Washing and Sterilization⁵¹.

After the conclusion of the treatment phase of the study, the bioreactors were allowed to air dry for 22 days before analysis. After air drying, each reactor was cored using a sterile 60 mL syringe barrel with the end cut off. The soil in each layer was pushed out of the cut syringe barrel segment using the plunger, and placed into pre-sterilized soil tins. The samples were then analyzed for cell numbers, specific gravity, CaCO₃, and ESEM, as described below.

3.5 Analytical Methods

3.5.1 pH

The pH of the influent and effluent of the syringe barrel bioreactors was measured using either Hydrion 1-14 pH range pH paper (Cat. No. 19847156), and MColorpHast alkaline pH paper (Cat. No. 1095430001), or a Thermo Scientific Orion Dual Star pH meter (Cat. No. 2115001) with a Ross Orion Ultra refillable pH electrode probe (Cat. No. 8102BNUWP). Influent and effluent samples from the soil box experiments were also analyzed for pH using the pH meter and probe. The pH meter and probe were calibrated by a three point calibration, utilizing pH buffers of 4.01, 7, and 10.01.

3.5.2 Soil Cell Counts

Cell counts on each soil layer were conducted by first making a 1:100 dilution (Figure 3.6). A 1 gram of extracted soil was placed in an autoclaved blender containing 99 mL of phosphate buffer solution⁵⁴ and mixed at a medium to high speed for 2 minutes. This time was selected to minimize damage to the soil bacteria.⁵⁵ After mixing, the soil-buffer slurry was allowed to settle for two minutes⁵⁶. Subsequently, 0.1 mL was aseptically extracted from the middle fraction of the fluid in the blender, and pipetted into a test tube containing 9.9 mL of autoclaved phosphate buffer solution. As illustrated in Figure 3.6, serial dilutions were then conducted to achieve a range of 10^{-3} to 10^{-7} . Each dilution was plated on Tris-YE plates and allowed to sit for 15 minutes to allow the media to soak into the agar. The plates were then inverted and incubated for 36 hours at 30° C. After incubation, plates were counted to determine the cellular density in each soil layer, as CFU/g.

3.5.3 Urea Agar Slants

BD Urea agar slants (Cat. No. 221096) were used to determine the presence of urea degraders in the treated soil specimens. The slants were conducted in triplicate for each soil box. A combination of iron mine tailings and white precipitate was scraped off the surface of each reactor with a flame-sterilized loop, and streaked onto the agar slants. After inoculation, the tubes were incubated at 35° C. Color change was observed at 6 hours, 24 hours, and then every day for 6 days⁵⁷.

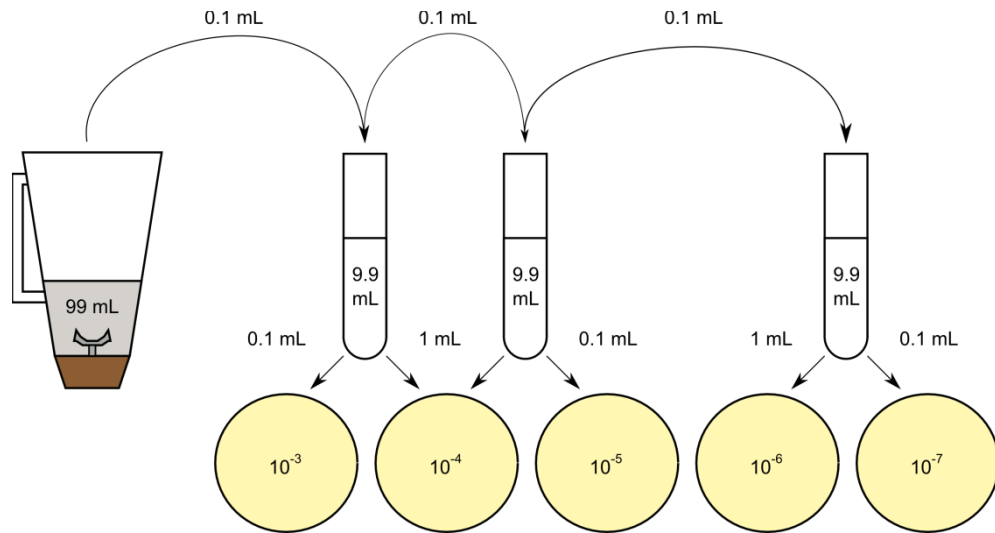


Figure 3.6: Dilution scheme for viable plate counts of *S. pasteurii* in the soil layers.

3.6 Specific Gravity Determination

A Micromeritics AccuPyc 1330 pycnometer was used to determine the specific gravity of treated and untreated soil samples. Because the specific gravity of calcite⁵⁸ (2.71) is lower than iron mine tailings (2.9-3.1 measured), the biologically treated iron mine tailings are expected to have a lower specific gravity than untreated mine tailings. Thus, a comparison of the specific gravity of a treated sample relative to an untreated sample is a novel approach to characterizing the calcium carbonate increases in the treated soil sample.

Before performing the test, the sample was oven dried at 40° C for three days. Then, 10 grams of the oven dried soil were packed in the pycnometer cup. The pycnometer was set to measure the specific gravity five times, with the final value used for analysis. Preliminary analyses comparing the value obtained after five and ten measurements demonstrated that the results were similar. It was concluded that there was no advantage to obtaining more than five measurements per sample (See Figure 3.7). In addition to measuring the specific gravity of the samples from the different layers in the syringe barrel and soil-box experiments, specific gravity measurements were also obtained for each sample bucket of tailings. Importantly, the specific gravity within a given bucket

varied spatially with a range determined to be ± 0.05 . Therefore, the reported specific gravity value for each individual bucket can only be considered an estimate of the overall specific gravity for the entire sample.

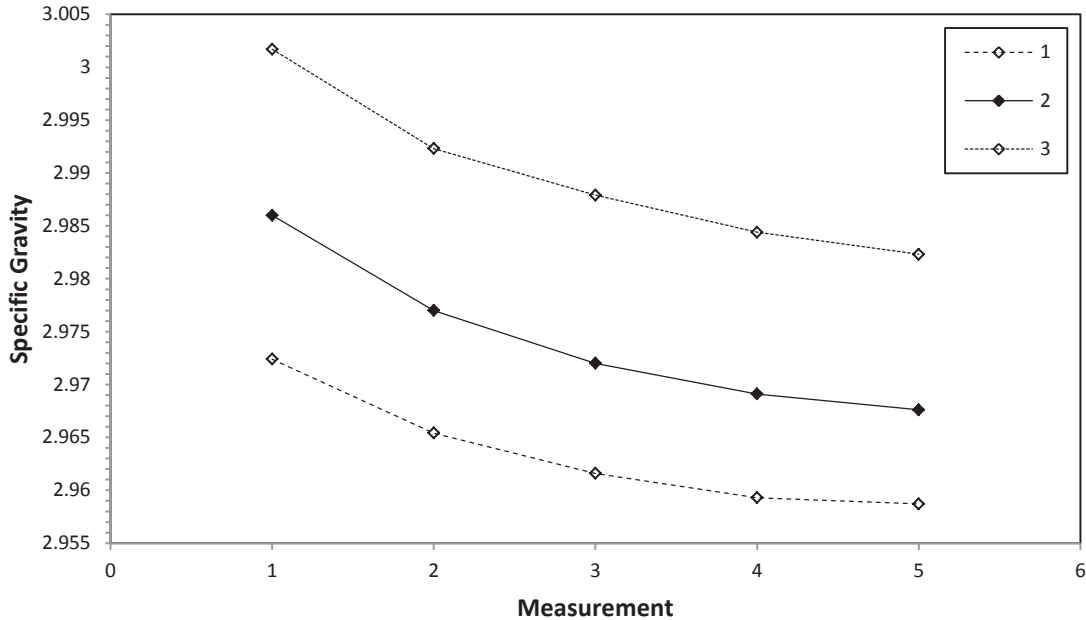


Figure 3.7: Specific gravity convergence after five measurements in the pycnometer.

As part of this procedure, a calibration curve was developed with a goal of being able to relate the specific gravity of treated and untreated iron mine tailings to a relative percentage of calcium carbonate present in the sample. The first step in this calibration process was to remove any naturally occurring carbonate material from the iron mine tailings. This was accomplished by placing 50 grams of air-dried iron mine tailings in a 400 mL glass beaker. Then, 100 mL of 3M HCl was added to the tailings in the beaker under a fume hood. The beaker was swirled, and the contents mixed using a glass stir rod. This resulted in significant effervescence in the iron mine tailings, indicating the presence of carbonate species in the mine tailings. After 20 minutes of mixing, 50 mL of distilled water was added to dilute any remaining acid. The tailings were then washed by first adding 100 mL of distilled water to the beaker. The flask was swirled and mixed

using a glass rod to completely suspend the tailings in the distilled water. The tailings were then allowed to settle for 1.5 hours. After settling, approximately 90 mL of the residual fluid was removed from the beaker using a 10 mL pipette, centrifuged at 10000 rpm for 10 minutes, and the pH of the supernatant determined using a Thermo Scientific Orion Dual Star pH meter (Cat. No. 2115001) with a Ross Orion Ultra refillable pH electrode probe (Cat. No. 8102BNUWP). This washing method was repeated until the pH change in the supernatant began to plateau (Figure 3.8). After all the washing steps were completed, the mine tailing pellets from the centrifuge tubes were recombined with the bulk of the mine tailings.

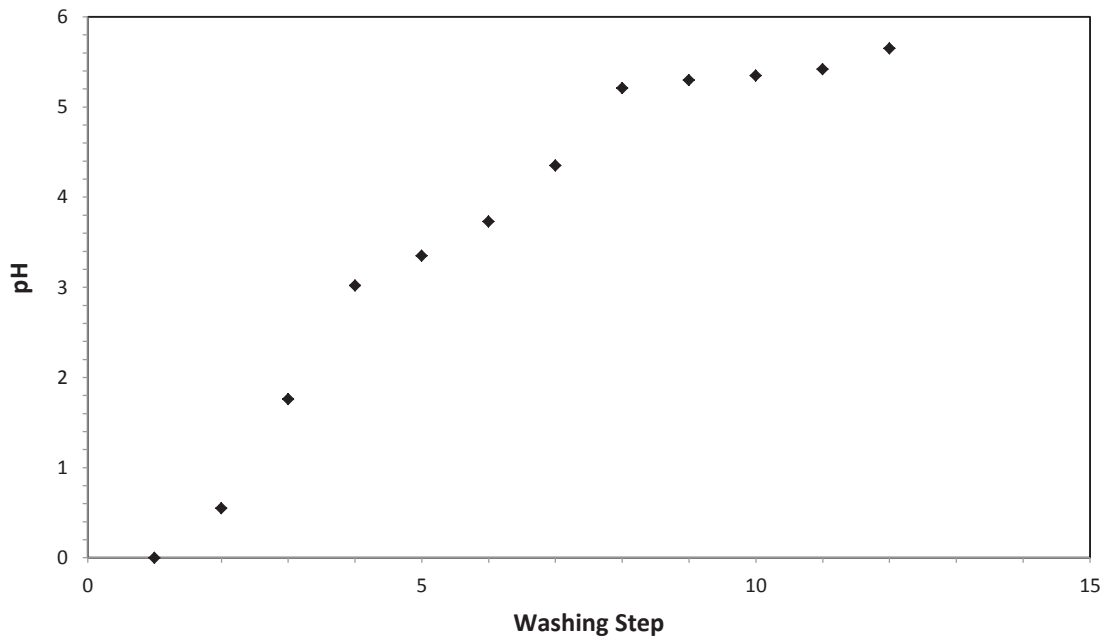


Figure 3.8: Soil washing step and associated pH of supernatant.

After washing, the iron tailings were oven dried at 110° C for 48 hours, along with a sample of powdered calcium carbonate in a small soil tin. After drying, the mine tailings and calcium carbonate were separately run through a micro-vibratory riffler to obtain more homogeneous soil samples. For each material, eight 13 mm x 100 mm test tubes with beaded rims were weighed and placed in each of the riffler bin holders.

Approximately 40 grams of the dried material were placed into the vibratory bin and the apparatus was started using a slow motor speed and a medium vibration setting. After all of the soil partitioned into each bin, the test tube and contents were weighed and then oven dried at 110° C for 24 hours. The contents of each bin were then subjected to pycnometer analysis, to determine the specific gravity. The pycnometer measured the specific gravity ten times per bin, with the final specific gravity being recorded. Specific gravity values were homogenous across the samples (see Table 3.2), indicating that the micro-vibratory riffler successfully produced consistent samples compared to native, in-situ samples. The six bins of each material with the most similar specific gravity values were selected for use in the calibration curve.

Table 3.2: Average specific gravity of riffler bins with ten measurements per sample

Bin	Average Specific Gravity	
	CaCO ₃	Tailings
1	2.717	2.913
2	2.724	2.918
3	2.725	2.918
4	2.731	2.911
5	2.734	2.912
6	2.736	2.909
7	2.735	2.906
8	2.737	2.905

The mine tailings and calcium carbonate were then combined in six different ratios in test tubes. Each test tube was sealed using a rubber stopper and the contents homogenized by using a vortex mixer at a medium-high speed setting for approximately 5 seconds. Then the samples were oven dried at 110° C for 24 hours, and analyzed using the pycnometer. The results are presented in Figure 3.9.

For comparison, a calibration curve was also developed for iron mine tailings without acid treatment by following the same methodology as described above. The resulting calibration curve (Figure 3.9) had specific gravity values that were higher than the acid

treated tailings. Because of the difference between the acid-treated and non-acid treated calibration curves, the non-acid treated calibration curve was used. This was determined to be more appropriate because unaltered iron mine tailings were used in the rest of the experiments. These findings may be explained by the presence of carbonate minerals in the tailings, such as iron carbonate (siderite), which may be common in the taconite material native to the local area⁵⁹, although the relative amounts are unknown.

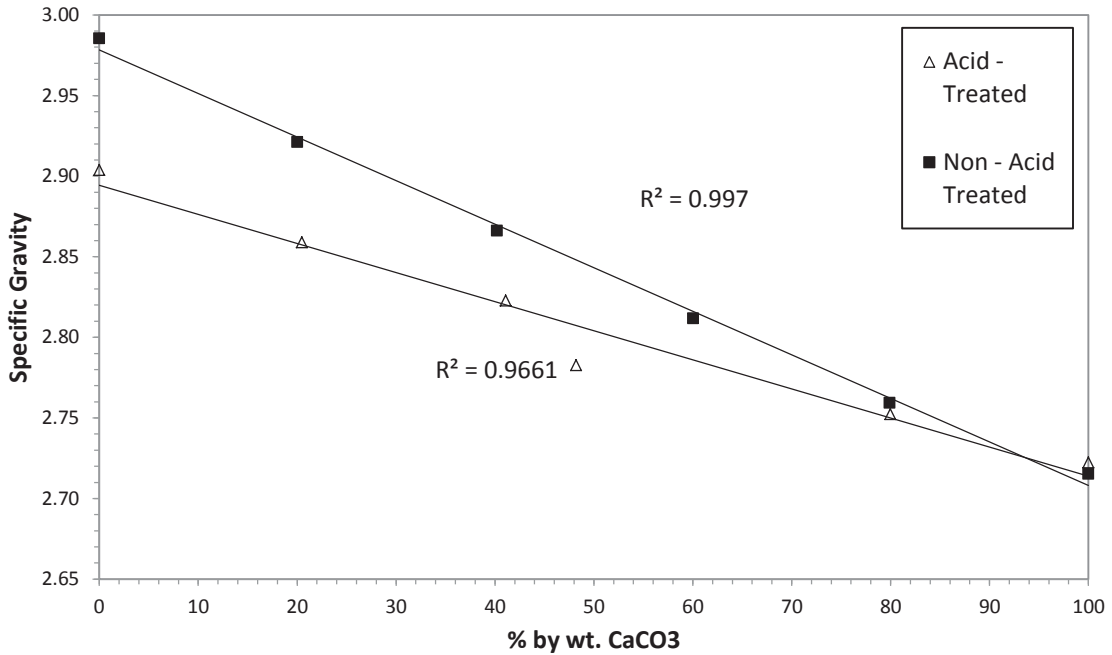


Figure 3.9: Pycnometer calibration curve for acid treated and non-acid treated iron mine tailings.

3.7 Calcium Carbonate by CO₂ Pressure Determination

Calcium carbonate determination by a pressure transducer method was demonstrated successfully by Sherrod *et al.*,⁶⁰ and further improved by Fannesbeck *et al.*,⁶¹. In this study, a method similar to that of Fannesbeck *et al.*,⁶¹ was used for calcium carbonate measurements. Specifically, the treated and untreated mine tailings were subject to a hydrochloric acid treatment to generate a measurable carbon dioxide gas pressure that could then be related to the calcium carbonate mass in the sample as a percent by weight via a calibration curve. To apply the technique in this study, the experimental apparatus

was first fabricated, then method troubleshooting was performed, followed by development of the methods for sample preparation and calibration.

3.7.1 Apparatus

The calcium carbonate pressure apparatus is illustrated in Figure 3.10. This set-up incorporated an Omega PX309-015GV 0-15 psi pressure transducer that was attached to an Omega digital measurement device via 3.13mm (OD) diameter tubing through multiple brass fittings sealed with Teflon tape. A pressure transducer was used rather than an analog pressure gauge due to the relatively low projected pressures that would be generated due to MICP when compared to background carbonate species, and because a pressure transducer had previously been demonstrated to be a viable option for characterizing carbonates in soil samples^{60,61} The pressure transducer was in turn connected to the reaction vessel (a 125-mL glass serum bottle sealed with a rubber septum and aluminum crimp cap) via 3.13mm (OD) diameter tubing. A luer-lock fitting was connected to the end of the tubing, with an attached 18-gauge stainless steel non-coring needle. Acid was injected into the vessel using a 20-mL BD syringe and 22-gauge stainless steel non-coring needle.

3.7.2 Method Development

Four tests were performed as part of the method development: (1) leak testing, (2) pressure validation, (3) injection pressure assessment, and (4) required reaction time. The first test was conducted to ensure that the apparatus was not leaking. To perform the test, 6M HCl was injected into the apparatus containing 0.5 grams of calcium carbonate, and the total pressure in the serum bottle recorded and monitored for loss of pressure over time. After three trials, all leaks were eliminated and after 22 hours there was less than 0.1 psi loss in the bottle.

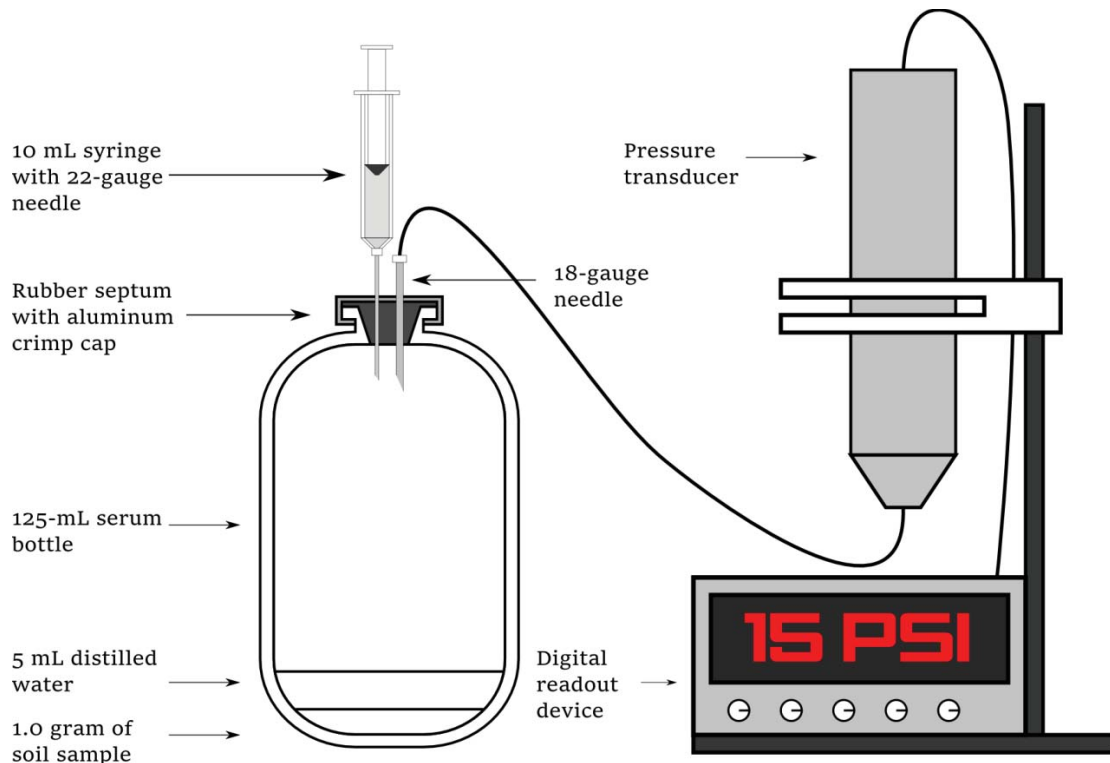


Figure 3.10: Experimental setup for the pressure-calimeter method.

In the second test, the pressure measurement displayed via the digital readout device was validated with an analog pressure gauge. The pressure transducer was attached to the bottle via the 18-gauge needle, while the analog gauge was also attached in the same fashion. Two trials were conducted by pressurizing a serum bottle by making a series of injections of distilled water into the serum bottle. After 10 seconds past each injection, a reading was taken from both the digital readout and the analog gauge (Figure 3.11). The average pressure difference was approximately 0.70 psi for the first trial, while the second trial had a difference of approximately 0.79 psi. It was concluded that the digital readout device was properly calibrated as the difference between the analog and digital gauge remained consistent throughout the injections.

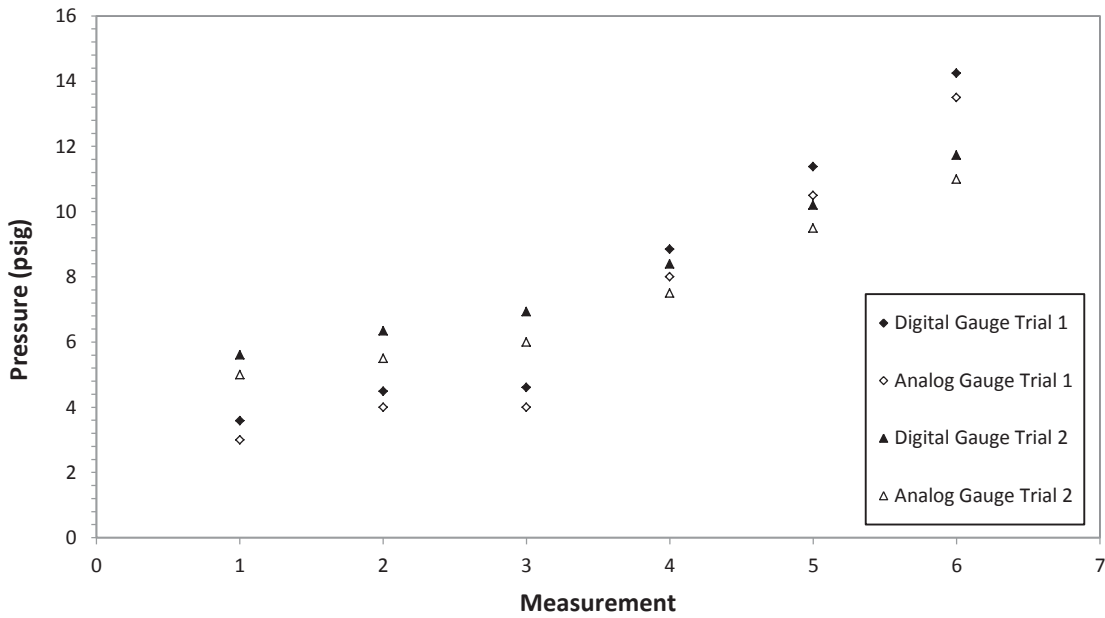


Figure 3.11: Pressure measured from both the analog and digital pressure gauges.

The third test was to determine the pressure generated from injection of solution into the serum bottle. For this assessment, six trials were conducted, each consisting of injecting various incremental volumes of distilled water into the serum bottle: test one had injection increments of 3 mL; test two had injection increments of 5 mL; and the other trials had variable volumes of injected distilled water to obtain a spectrum of data points. Based on the data from the six trials (Figure 3.12), it was determined that the injection volume linearly contributed to the bottle pressure at a rate of approximately 0.11 psi of pressure per 1 mL of fluid added ($R^2 = 0.9835$).

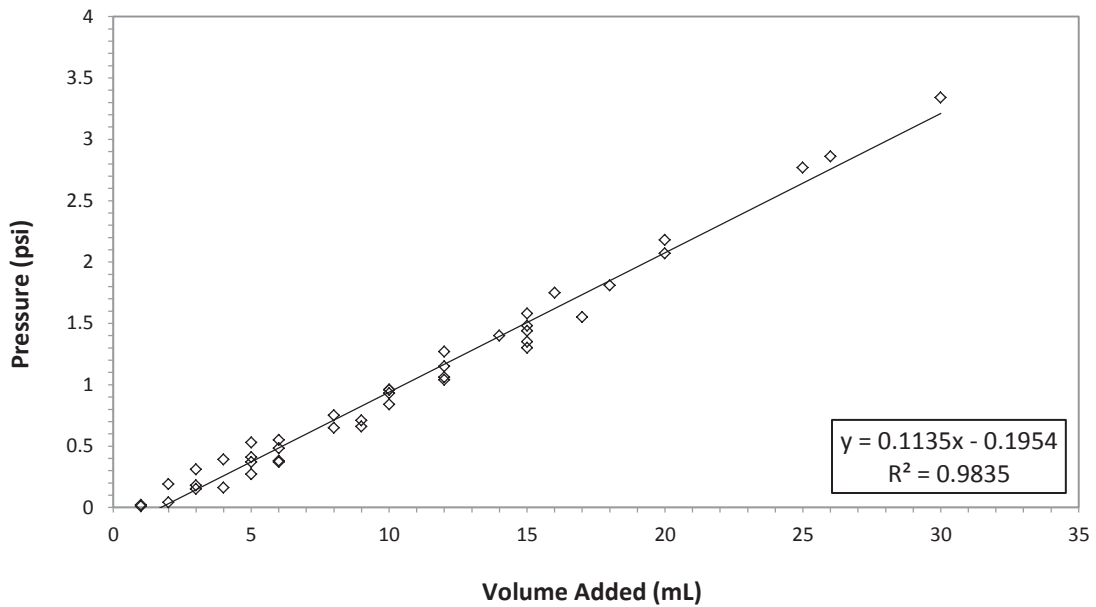


Figure 3.12: Pressure increases in the pressure vessel due to injection of fluid.

3.7.3 Length of Reaction Time

Finally, although Fannesbeck *et al.*, 2013⁶¹ determined that a 6-hour reaction time was sufficient for accurate data with their samples⁶¹, verification of the required reaction time was necessary for the experimental materials in this study. To examine the required reaction time, two trials were conducted in which 1.0 grams of dried iron mine tailings were placed in the 125 mL serum bottle, sealed, and 1 mL of 6M HCl injected into the vessel. In the first trial, the acid was allowed to react with the mine tailings for 4.5 hours, but results were inconclusive as to whether or not that was sufficient for complete reaction of the acid with the carbonates (Figure 3.15). Therefore, in the second trial, the pressure was monitored for 21.5 hours, and after 7 hours, the pressure measurement began to plateau. Thus, it was concluded that 6 hours was a suitable reaction time for any test with the iron mine tailings.

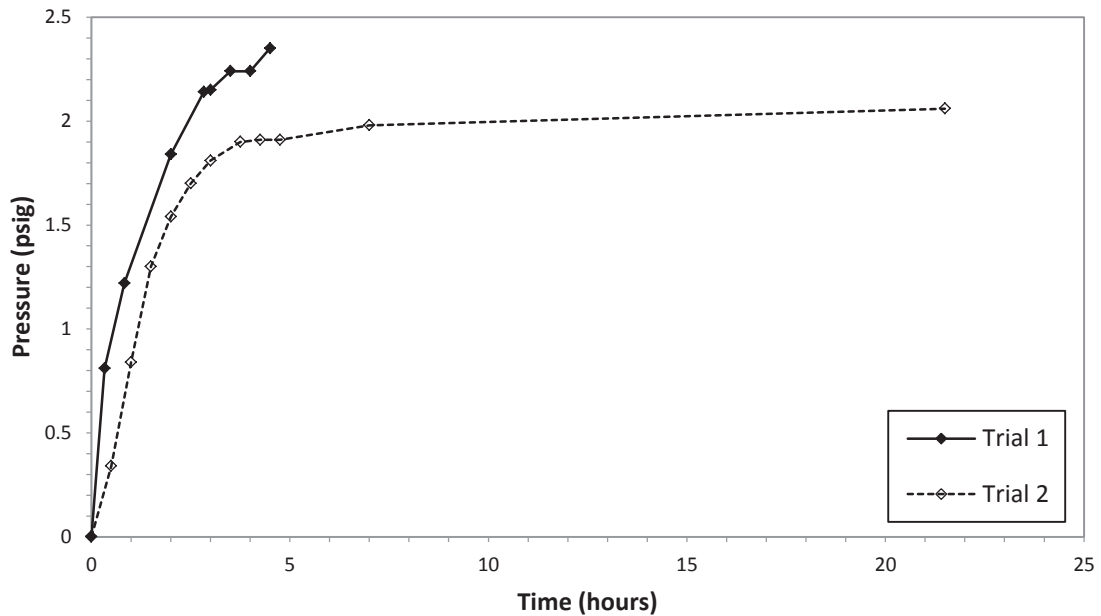


Figure 3.13: Pressure generated over time in the pressure vessel.

3.7.4 Sample Preparation

To prepare samples for analysis in the pressure-calculator system, 1.0 ± 0.01 grams of tailings were placed in a pre-tared 125 mL serum bottle. The tailings addition of 1.0 grams was chosen based on recommendations from Fannesbeck *et al.*, 2013⁶¹ for highly effervescent soils, as previous tests had shown that iron mine tailings were highly effervescent, as with pure calcium carbonate. Next 5 mL of distilled water was pipetted into the serum bottle to help facilitate the reaction between the acid/tailing interface. Next a butyl rubber septum was used to seal the serum bottle mouth, and an aluminum tear off cap was crimped onto the neck of the bottle. Then, 4 mL of 6M HCl with 3% by weight $\text{FeCl}_2 \cdot 4\text{H}_2\text{O}$ was injected into the bottle with a 10 mL syringe and a 22-gauge stainless steel reusable needle. The ferric chloride was added to prevent the release of carbon dioxide from organic matter⁶⁰. After the acid addition, samples were swirled for 15 seconds every half hour to facilitate the acid-carbonate reaction. After six hours, the septum was connected to the pressure transducer via a 22-gauge stainless steel reusable needle attached to 3.13 mm (OD) diameter tubing. The bottle was swirled for 15 seconds and let rest for 10 seconds before a measurement was recorded. Three measurements were recorded 7 to 9 seconds apart, and the average value was used for analysis.

3.7.5 Calibration Curve

To correlate the pressure measurements with the calcium carbonate content of a tailings sample, it was necessary to develop a calibration curve. Accordingly, six 125-mL serum bottles were prepared, each with a different mass ratio of iron mine tailings to calcium carbonate. Subsequently, each bottle was injected with 4 mL of 6M HCl with 3% by weight $\text{FeCl}_2 \cdot 4\text{H}_2\text{O}$, allowed to react, and the gas production recorded, as illustrated in Figure 3.14. Based on a linear regression of the data, the following relationship was developed:

$$y = 0.1847x + 3.2158, R^2 = 0.9984 \quad (3.2)$$

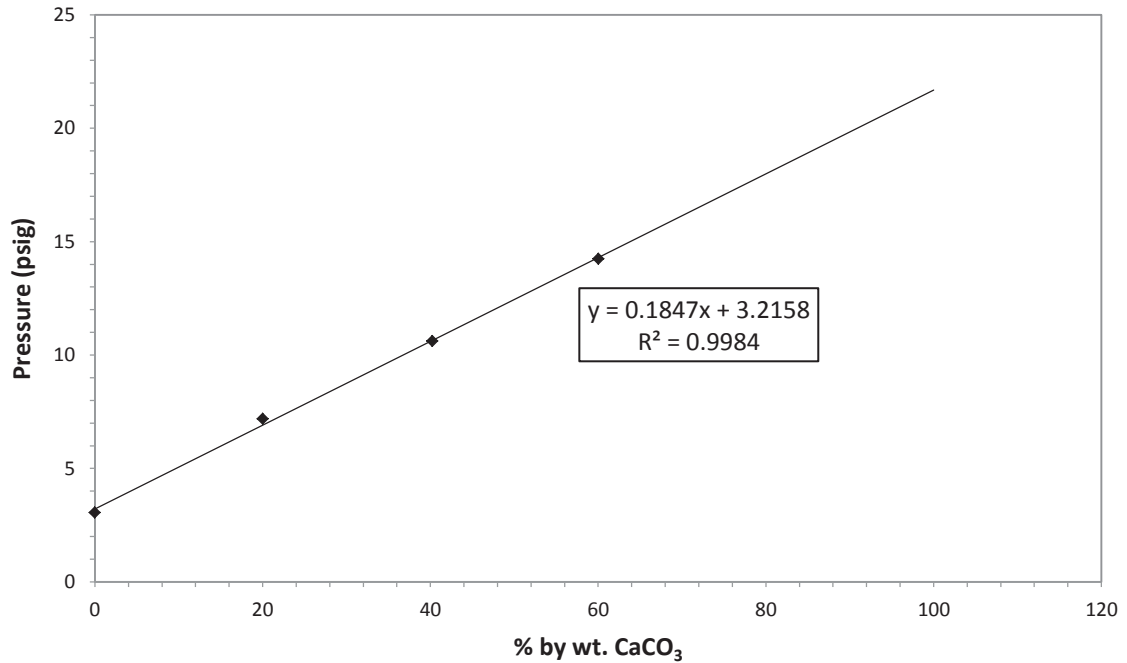


Figure 3.14: Calibration curve for the pressure-calciometer method. The 80% and 100% by. wt. CaCO₃ measurements exceeded the pressure transducer sensitivity range, and were not reported.

3.8 Strength Measurement – Steel Bearing Drop Test

Strength of the mine tailings’ surface was characterized through a ball-drop method that was developed during this study. The test was performed on the 3” x 3” soil boxes used in the soil box experiments. To perform the test, a 3.392 g steel ball bearing with a diameter of 0.372 in was dropped from a height of 5 feet onto the surface of the tailings at different moisture contents. The diameter of the crater was measured in both the y and x direction using a TruePower 6” Digital Caliper, and the values averaged together. Five ball drops were completed for each soil box. The moisture content was also determined to allow use of the calibration curve.

3.8.1 Calibration Curve

A calibration curve of the untreated soils was developed that related the sample moisture content to the diameter of crater from impact. First, a 6" x 6" x 3" soil box was packed to a void ratio of 1.2 following the above mentioned soil packing protocol. Then, the soil box was dried in an oven and monitored so that eight different moisture contents were tested. At each moisture content, five drops were conducted at a height of 5 feet. The results of the calibration curve analyses are presented in Figure 3.15. A large standard deviation was encountered at 0% moisture content, due to the ball bearing bouncing off of the surface and leaving no impact crater.

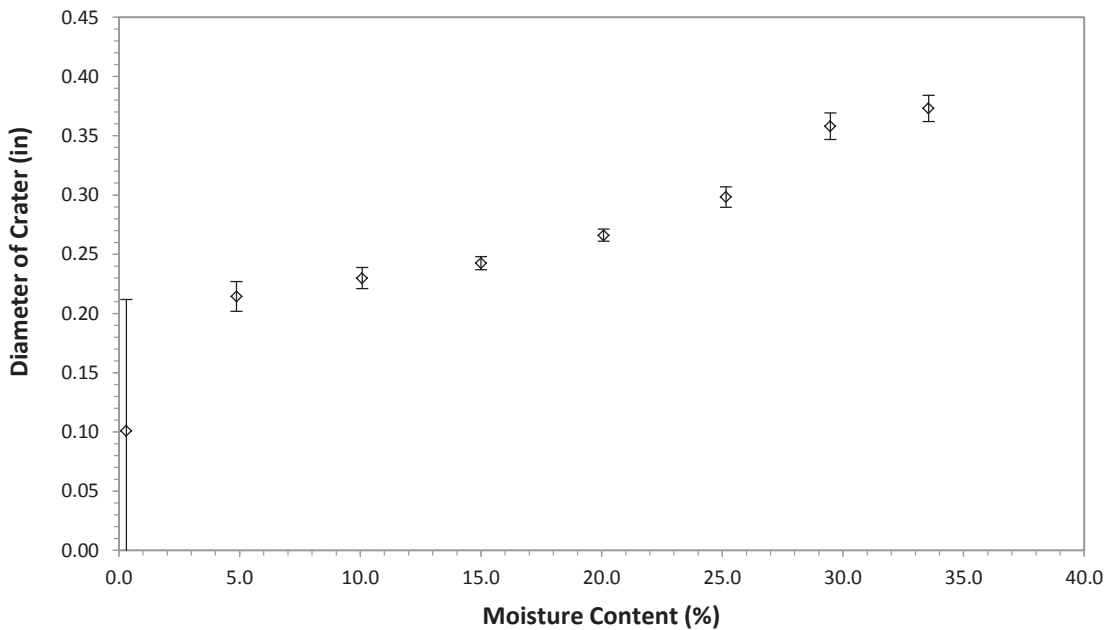


Figure 3.15: Calibration curve for the ball drop test with the average crater diameter of five drops as a function of moisture content. (error bars = ± 1 standard deviation)

3.9 SEM Analysis

Treated and untreated samples were run through an environmental scanning electron microscope (ESEM) to visually assess the occurrence of MICP. Additionally, energy dispersive spectroscopy (EDS) was obtained simultaneously for each SEM image to assess the relative ratio of calcium in the soil samples. All samples were first oven-dried at 40°C for three days. Samples were subsequently prepared for the SEM in two different ways. The first method involved crushing the tailings with a pestle and mortar and spreading them onto carbon tape on a small sample button. Excess, loose soil was dusted off of the top using a hand duster canister. The second method involved extracting the crust layer from the treated samples and placing them directly on the carbon tape, as to not disturb or destroy the crust. With both methods, the sample was then coated with a carbon coating approximately 10 µm thick, and placed in a sample holder. The sample holder was then wrapped in Parafilm and placed into a desiccator until use. These analyses were performed with the assistance of Mick Small in the ESEM laboratory at Michigan Technological University. An example ESEM image for untreated iron mine tailings is presented in Figure 3.16.

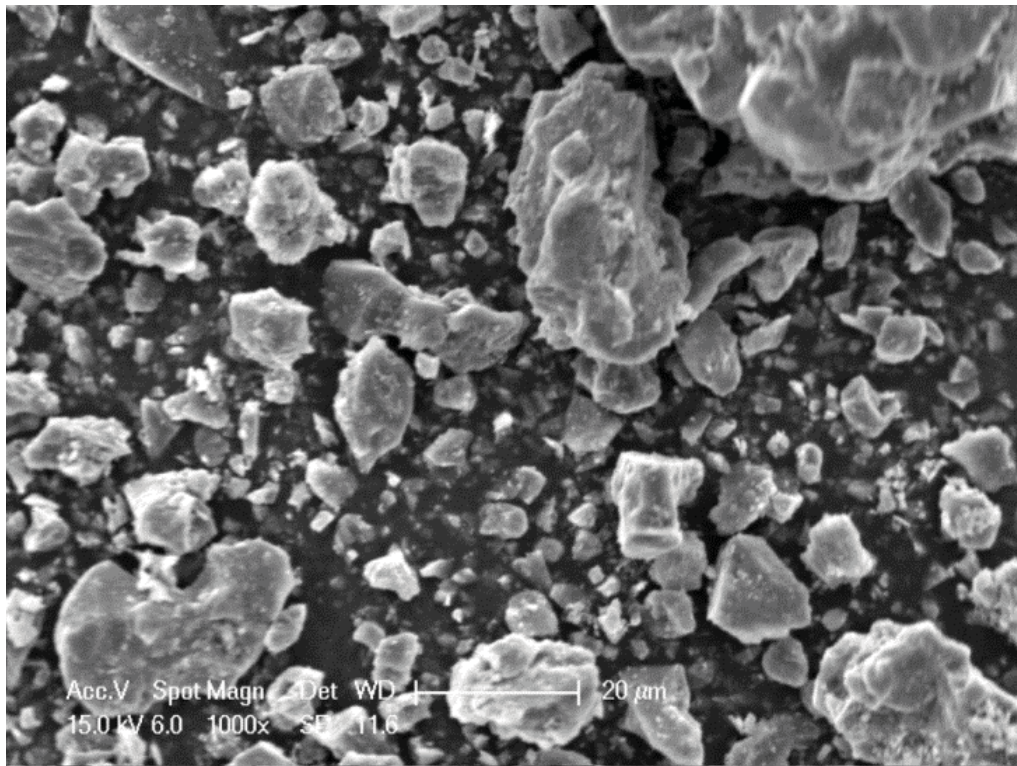


Figure 3.16: Untreated iron mine tailings at 1000x magnification.

Chapter 4 – Syringe Barrel Results and Discussion

The syringe barrel experiments provided a preliminary demonstration of the potential for promoting MICP in fine grained materials. Based on the discussion in Chap. 2, stimulation of MICP is expected to result in an increase in the system pH, as well as increased numbers of urea-degrading bacteria, and calcium carbonate precipitate in the tailings. To examine these trends, the pH of the fluid draining from the syringe barrel reactors was monitored during the treatment phase. Then, after the treatment phase, the overall extent of MICP was evaluated by using the results from a combination of analytical methods including: specific gravity change (analyzed through the use of a pycnometer), ESEM and EDS analysis, and CO₂ pressure measurements (obtained through the calcium carbonate pressure). In addition to evaluating the potential for MICP in the treated bioreactors, the results were also used to examine whether urea-degraders capable of promoting MICP are naturally present in the mine tailings.

4.1 pH of Bioreactors

The pH of the bioreactor effluent was measured twice daily, as summarized in Figure 4.1. Initial pH measurements for all of the reactors ranged from pH 7.5 to pH 8. However, the pH steadily increased in all reactors, ultimately converging to a value of approximately pH 9, which is consistent with the theoretical equilibrium pH of the growth medium with urea hydrolysis⁶², and similar to what has been observed by other researchers in systems promoting ureolysis with the same medium^{8,14}. Interestingly, the lag before the pH reached a value of approximately 9 varied with the treatment. The reactors inoculated with *S. pasteurii* reached a pH of ≈ 9 after about 5 days (Figure 4.1A), but the uninoculated reactors (Figure 4.1B), and autoclaved reactors (Figure 4.1C) reached a pH of ≈ 9 after a lag period of about 7-8 days. These results suggest that native urea-degraders are present in the iron mine tailings, but in smaller numbers than in the inoculated reactor, thereby requiring a lag period before the native microbes increased sufficiently in numbers due to the urea-CaCl₂ treatment to influence the system pH.

Further evidence supporting these conclusions was provided by the analyses performed after the treatment phase, as described in the following sections.

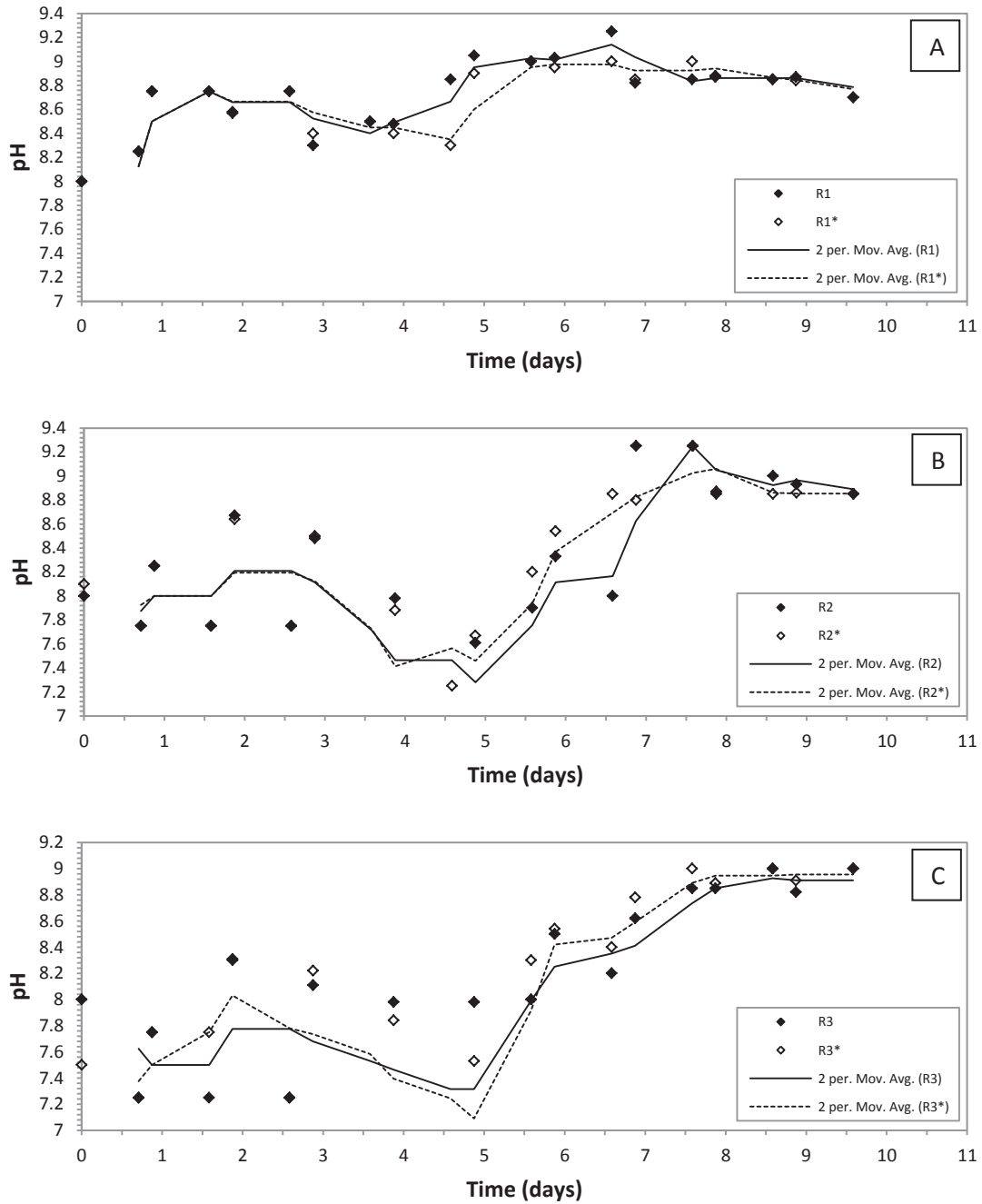


Figure 4.1: pH of the effluent from syringe bioreactors, (A) inoculated with *S. pasteurii*, (B) with native microorganisms, and (C), using autoclaved iron mine tailings. Symbols represent individual sample measurements, and lines represent the two day moving average of the experimental data.

4.2 Viable Cell Plate Counts

Because urea-CaCl₂ growth medium was applied to the syringe bioreactors, it was expected that the cell density would increase in reactors that exhibited evidence of MICP. As illustrated in Figure 4.2A, bioaugmented reactors R1 and R1* had high cell densities in the upper soil layer (10⁵ to 10⁶ CFU/mL), but the cell density decreased in the deeper soil horizons, with no detectable cell counts in the deepest soil layer. This suggests that the inoculated *S. pasteurii* cells, which were added to the surface of the syringe bioreactor, did not readily penetrate deeply into the iron mine tailings, with the iron mine tailings essentially functioning as a filter. The filtering of the bacteria may actually be considered advantageous for this application, because the air-tailings surface interface is the focus of the dusting hazard. A high cellular density in the surface layer may expedite and increase the overall extent of calcium carbonate precipitation, further reducing the potential for dust.

Similarly, the uninoculated reactor R2* had measureable cell counts in the upper three soil layers but no cell counts were measured in the deepest soil layer (Figure 4.2B), while R2 had detectable cell counts within the upper two soil layers. These results indicate that native urea-degraders are present in the iron mine tailings, and that the microorganisms near the surface of the reactors had more favorable conditions for growth. The latter suggests that the nutrient supply and/or oxygen transfer may not be sufficient in the deeper tailings horizons to sustain microbial growth. Presumably most of the urea and oxygen is being metabolized at the surface resulting in reduced substrate availability for the microbes in the deeper soil horizons. However, it was demonstrated that urease activity was not negatively impacted by anoxic or anaerobic conditions⁶². Thus, oxygen may limit bacterial growth, but does not limit ureolytic activity. The fact that some subset of the native microbial community is able to grow on the ATCC 1376 Tris-YE medium agar plates, which is the suggested growth medium for *Bacillus pasteurii*⁴⁷, suggests metabolic capabilities similar to *Bacillus pasteurii*.

Reactors R3 and R3* also had a measurable cell density in the surface layer (Figure 4.2C). This indicates that some urea-degrading microbes survived, and were able to grow

after the autoclaving process, demonstrating the persistence and resilience of the native microbes. Nevertheless, measured cell densities in R3 and R3* were lower relative to R1, R1*, R2, and R2*, consistent with the longer lag period observed based on the effluent pH (Figure 4.1C).

4.3 Specific Gravity Measurements

If MICP occurred in the syringe bioreactors, calcium carbonate precipitation should be evident. One way this was demonstrated was by changes in the specific gravity of the tailings. The untreated iron mine tailings have a specific gravity of 2.9-3.1, while calcite has a specific gravity of 2.71. Thus, an observed decrease in specific gravity is consistent with calcium carbonate formation. Correspondingly, the specific gravity decreased towards the upper soil layers in all of the reactors (Figure 4.3), indicating calcium carbonate formation was more prevalent near the surface of the bioreactors and decreased with depth in the soil horizon. The corresponding CaCO₃ content based on the method calibration curve are presented in Table 4.1.

Table 4.1: Percent by weight of calcium carbonate in syringe barrel layers.

		% by wt. CaCO ₃					
Layer	Depth (cm)	R1	R1*	R2	R2*	R3	R3*
T	0.9	15.2	12.1	11.2	11.9	10.9	13.4
1	1.8	6.1	5.5	6.0	7.7	6.4	6.5
2	2.7	4.6	6.5	4.5	6.2	5.9	5.6
3	4.5	2.5	3.4	3.4	6.2	3.4	3.9

These results are consistent with the cell count data (Figure 4.2), which were also greater in the upper soil layers, suggesting a correlation between the numbers of microbes present and the calcium carbonate precipitation. Interestingly, the specific gravity data also indicate that calcium carbonate precipitation occurred in the deeper soil horizons, although not to the same degree as observed in the surface layer. In general, the reactors and duplicates had similar patterns in the data trends. It appears that specific gravity changes measurements are most prevalent and dramatic near the surface of the bioreactors.

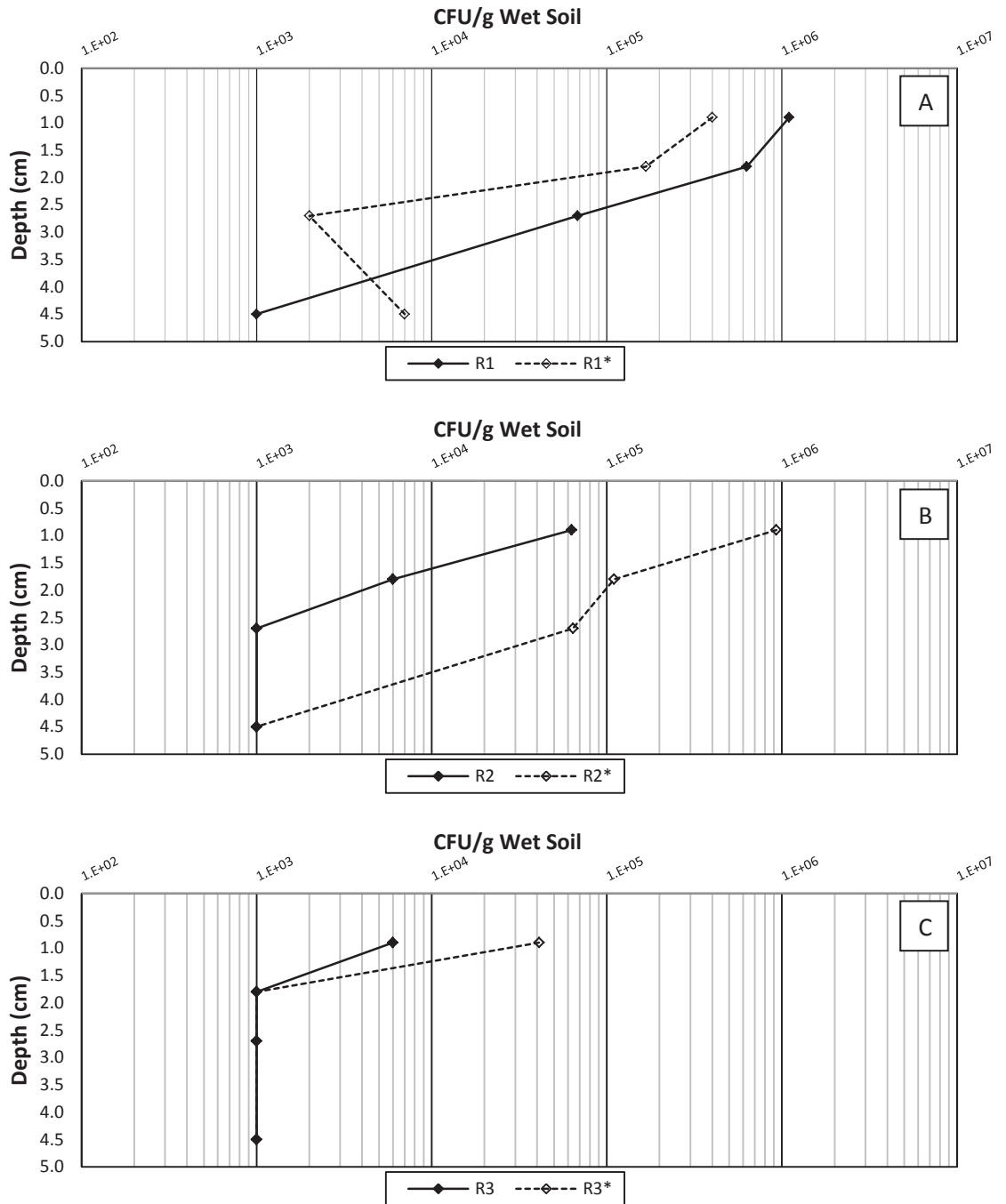


Figure 4.2: Viable cell plate counts (CFU/g wet soil) in the syringe bioreactors, (A) inoculated with *S. pasteurii*, (B) with native microorganisms, and (C) using autoclaved iron mine tailings. For samples that did not produce any countable plates (30-300 CFU), the result is reported as the lower detection limit, 10^3 CFU/g wet soil.

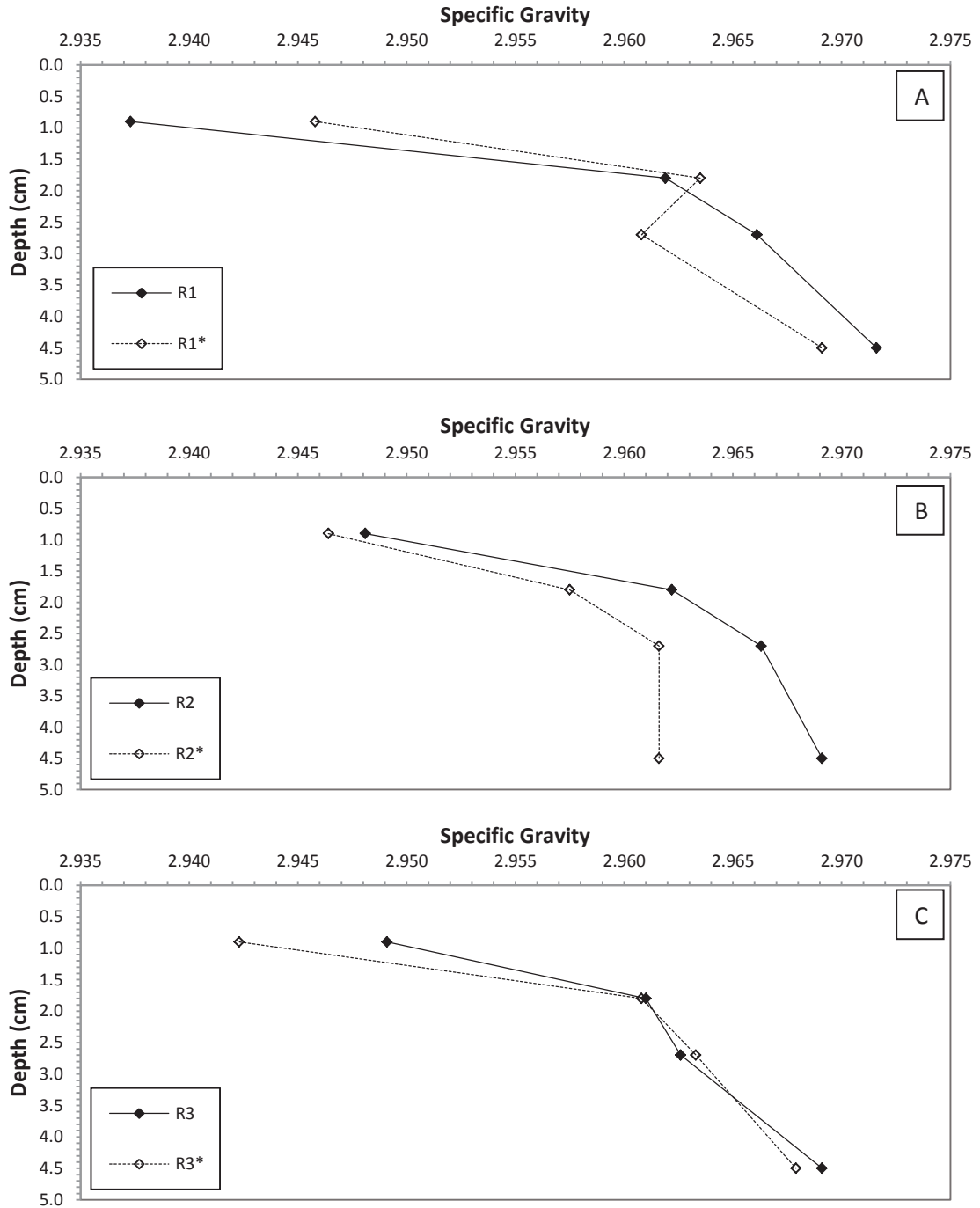


Figure 4.3: Specific gravity measurements in the syringe bioreactors, (A) inoculated with *S. pasteurii*, (B) native microorganisms, and (C) using autoclaved iron mine tailings.

4.4 Calcium Carbonate Measurements

Calcium carbonate precipitation was also measured using the pressure-calculator apparatus. Pressure is expected to be generated from the dissolution of the calcium carbonate in the sample, with higher calcium carbonate contents resulting in higher measureable pressures. However, the measured pressure trends in the syringe bioreactors were not consistent with the other data trends indicating greater microbial activity and MICP near the surface of the reactors. As shown in Figure 4.4, most of the reactors actually had decreasing pressures towards the upper soil layers, which is contrary to the expected pressure trend. In general, the pressure measurements were all near the pressure generated by the background carbonate minerals in the tailings (approximately 3.2 psi). This background level was due to the dissolution of carbonates already present in the iron mine tailings which was measured and noted during the construction of the pressure-calculator calibration curve.

The lack of conclusive trends in the pressure-calculator results may be related to the method used for preparing the soil samples. For this method, each soil layer was crushed and homogenized to reduce the bias potentially associated with grab sampling before placing a 1 gram subsample of the homogenized material into the pressure vessel. However, when the white surface crust was homogenized with the underlying iron mine tailings, the amount of microbially-induced carbonates available for reaction with the hydrochloric acid was reduced, and thereby the pressure generated was reduced. In comparison, previous trials (data not shown), in which the solid white precipitate alone was used in the pressure calculator resulted in a pressure increase using this method. These results indicate that the pressure-calculator method is very sensitive to the soil sample being analyzed, and that sample selection plays a key role in obtaining results that are easily differentiated from the background carbonates.

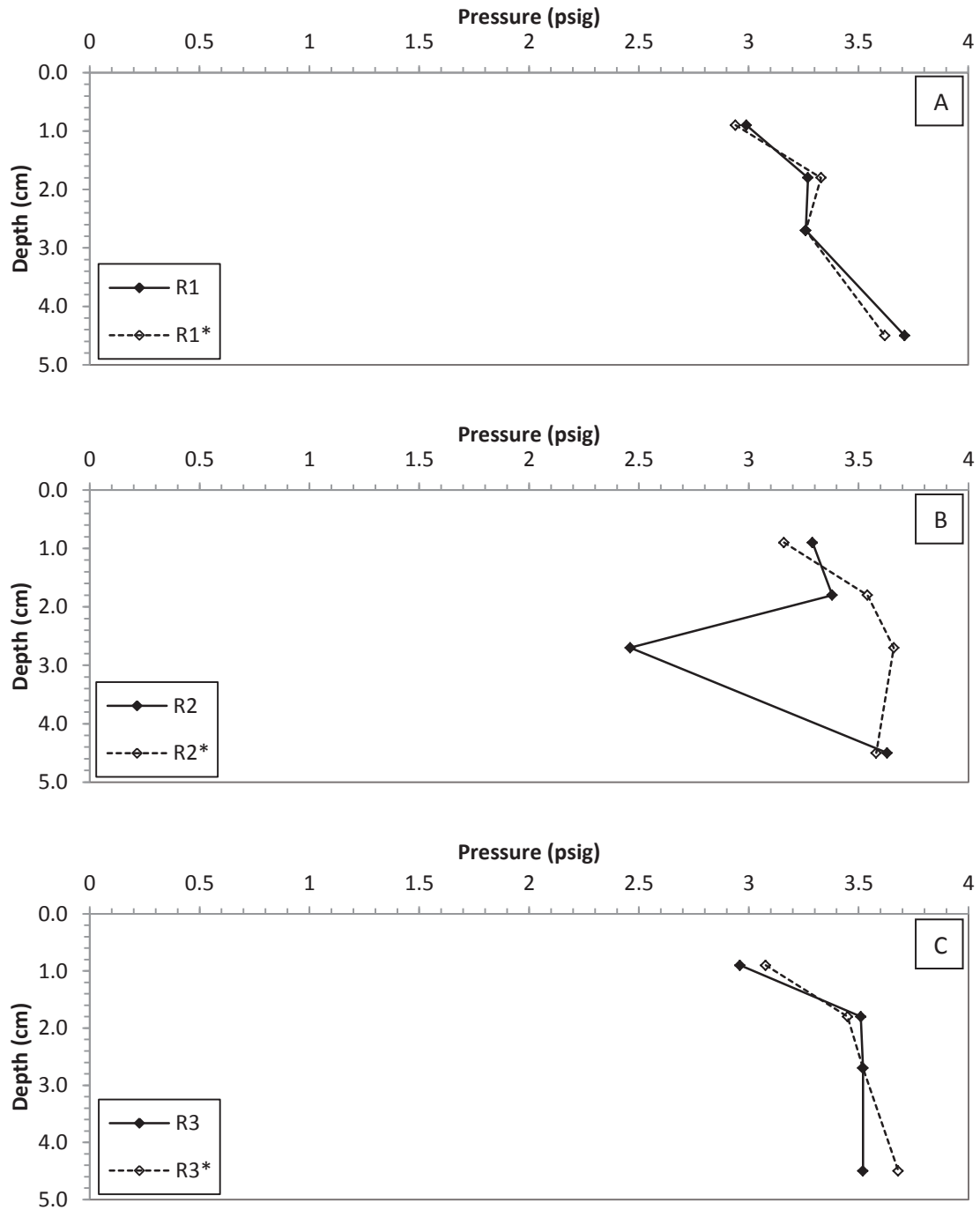


Figure 4.4: Calcium carbonate content based on the measured pressure in the syringe bioreactors, (A) inoculated with *S. pasteurii*, (B) native microorganisms, and (C) using autoclaved iron mine tailings.

4.5 ESEM Analysis

The surface crust of R1, R2, and R3 were also observed using the ESEM at the same time the EDS analysis was performed. During these visual observations, features of interest were noted such as evidence of bacteria, the types of crystal structures present, and bridging of particles (Table 4.2). Rod-shaped pitting in calcium carbonate structures provided evidence of bacteria, as well as visible rod-shaped bacteria. No bacteria or pitting were visible in the SEM imaging for R1 (Figure 4.5), suggesting complete encapsulation due to a relatively high rate of calcium carbonate formation. Pitting in the calcium carbonate structures is prevalent in both R2 (Figure 4.6) and R3 (Figure 4.7), indicating a slower rate of calcium carbonate formation. Different combinations of crystalline structures were observed in the surface crust layer of each reactor. Based on previous observations indicating that different excreted biomolecules can affect calcium carbonate crystalline formation⁶³, these results suggest that different microbial populations may have been present in each bioreactor. Taken together, these results provide more evidence that native bacterial communities were involved in the precipitation of the calcium carbonate structures.

Table 4.2: Summary of crystal formation morphology in biologically treated iron mine tailings assessed during ESEM imaging. The tailings powder is iron mine tailings directly beneath the surface crust.

Soil Specimen		Surface Crust			Tailings Powder		
Reactor		R1	R2	R3	R1	R2	R3
<i>Bacteria Evidence</i>			•				•
Crystal Type	<i>Amorphous</i>	•	•	•			
	<i>Cubic</i>	•	•				•
	<i>Conglomeration</i>	•	•	•			•
	<i>Angular</i>		•	•			•
	<i>Rod</i>		•				•
	<i>Flake</i>		•		•	•	•

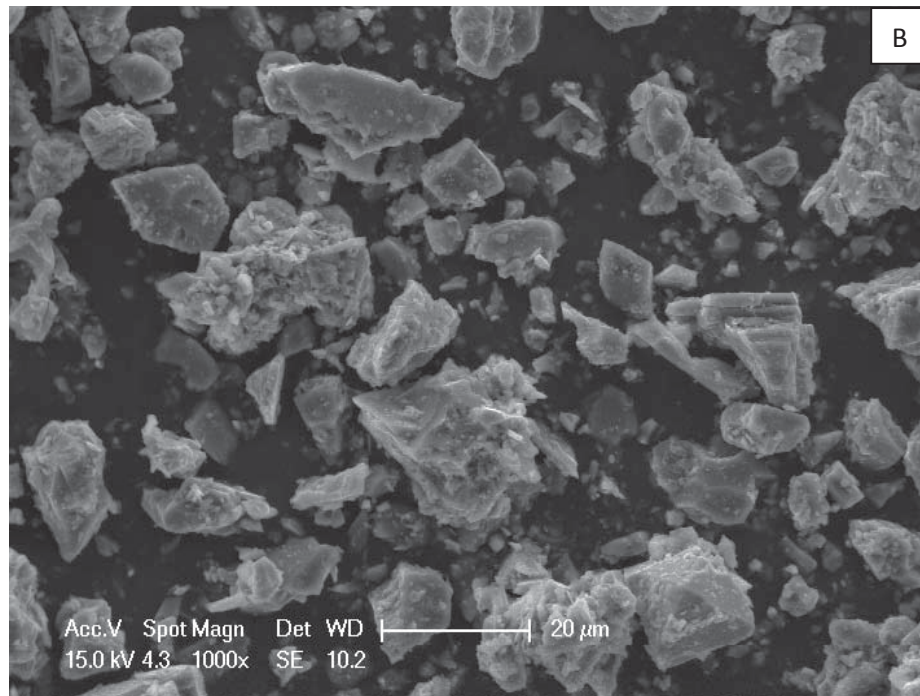
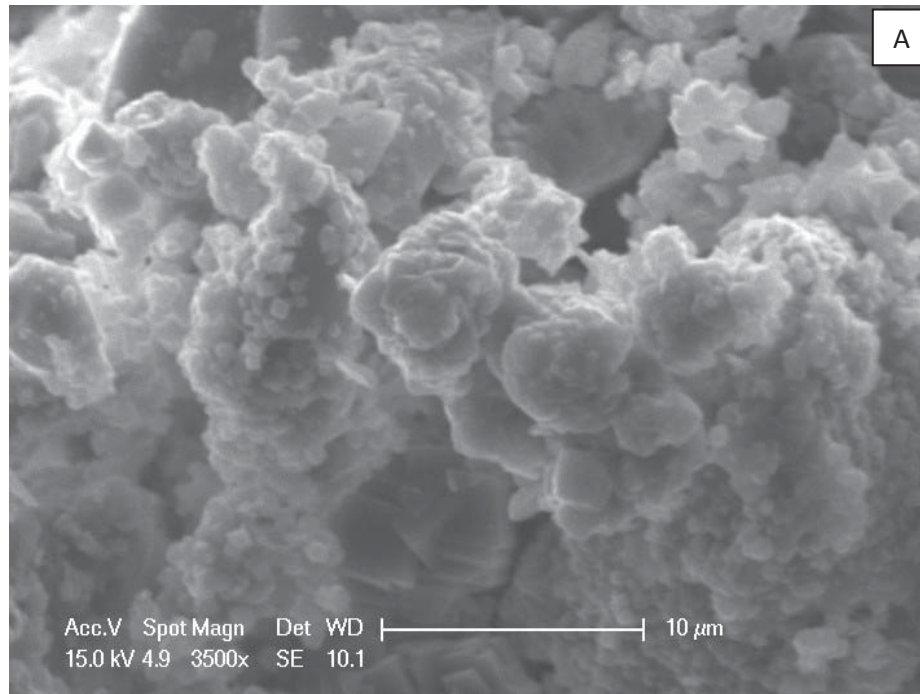


Figure 4.5: Surface crust layer at 3500x magnification in R1 (A), and crust layer with iron mine tailings in R1 crushed into powder at 1000x magnification (B).

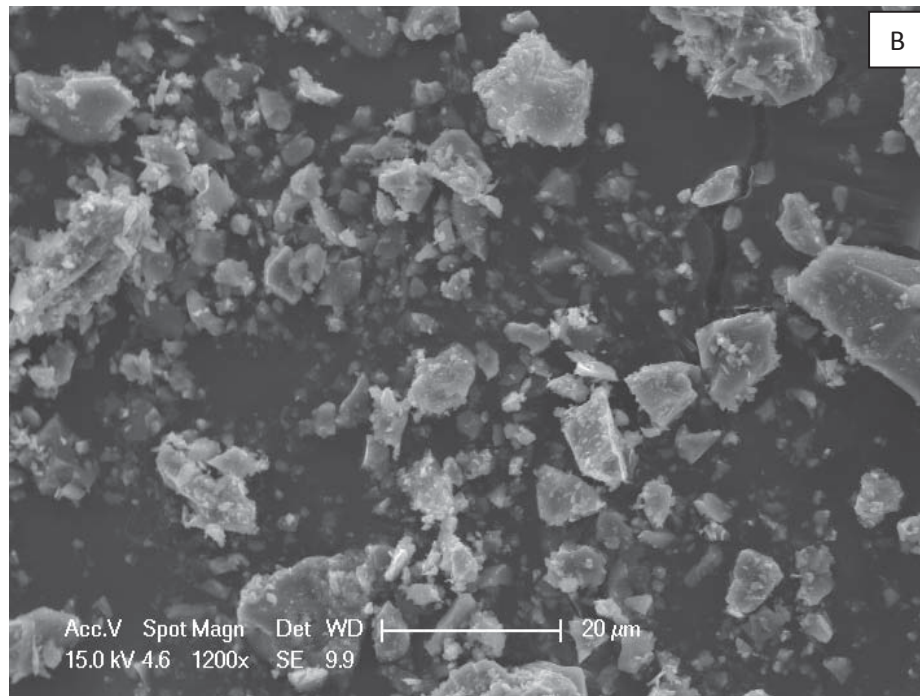
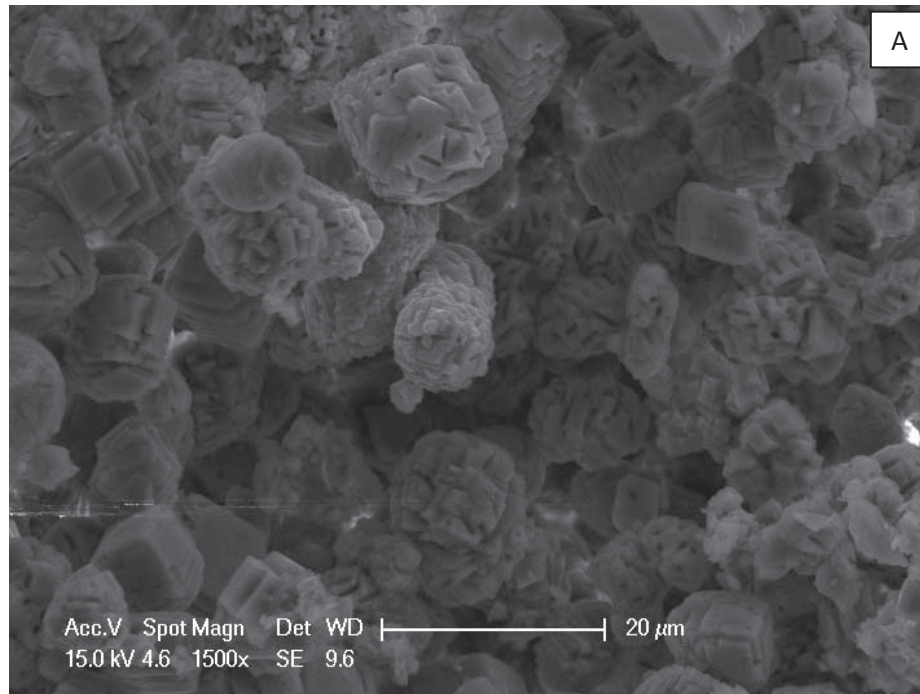


Figure 4.6: Surface crust layer at 1500x magnification of R2 (A). Crust layer with iron mine tailings in R2 crushed into powder at 1200x magnification (B).

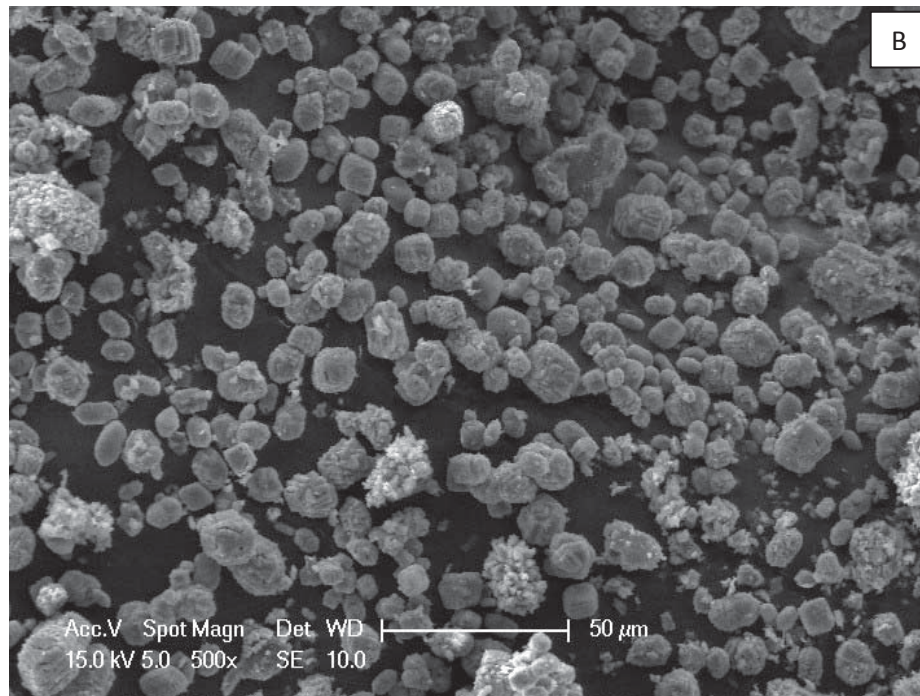
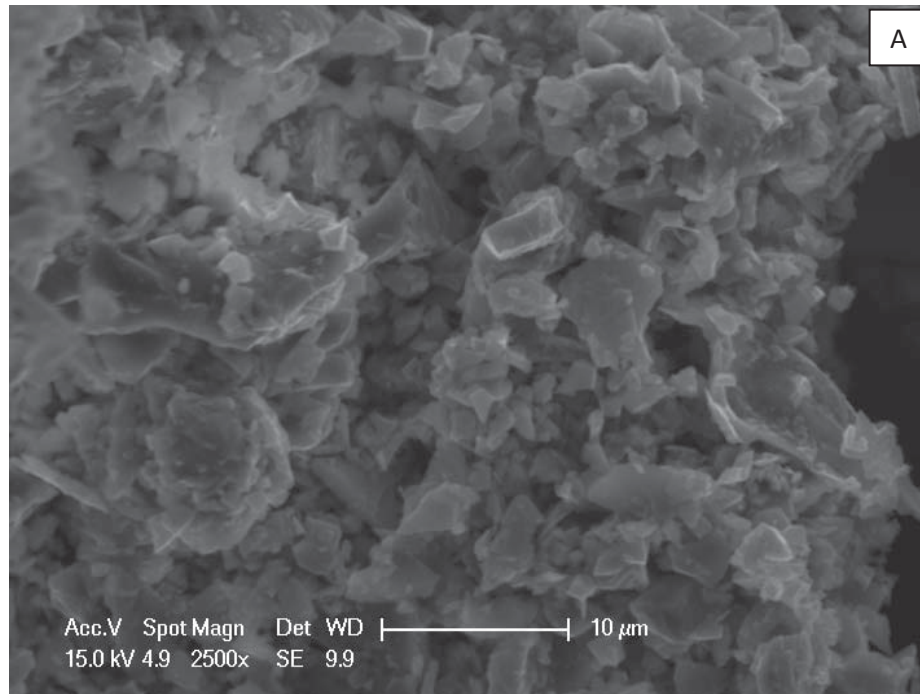


Figure 4.7: Surface crust layer at 2500x magnification of R3 (A) and crust layer with iron mine tailings in R3 crushed into powder at 500x magnification (B).

4.6 EDS Analysis

To evaluate the content of the white precipitate formed, the relative elemental analysis was obtained using EDS and samples of the solid white surface precipitate, and the iron mine tailings directly under the surface crust. As summarized in Table 4.3, in general, high percentages of carbon, oxygen, silicon, and iron were observed in the layers. The latter is expected in iron mine tailings. R1 and R2 also showed high relative percentages of calcium (22.77%, and 41.34% respectively) in the crust sample, consistent with the other data indicating the occurrence of MICP. However, the iron mine tailing powder layers in R1 and R2 showed very little percentage of calcium, indicating that MICP is primarily occurring at the air-soil interface. In comparison, R3 had only moderate amounts of calcium present (7.38% in the crust, 11.79% in the powder), indicating MICP is occurring, but less effectively than in the other reactors. Nevertheless, these results provide additional evidence that native microorganisms in the mine tailings are capable of MICP.

Table 4.3: EDS analysis of syringe barrel soil surface crust layer for R1, R2, and R3. Some elements present at less than 1% (by wt.) were not included in this table. A complete assessment is located in Appendix A. The crust sample refers to the white surface crust; the powder sample refers to the mine tailings directly under the white crust.

Reactor	Type	EDS Analysis (Percent by wt.)							
		C	O	Mg	Al	Si	Cl	Ca	Fe
R1	<i>Crust</i>	-	51.92	0.88	0.68	12.81	0.54	22.77	10.09
	<i>Powder</i>	-	46.71	1.71	1.43	24.05	0.78	2.06	21.24
R2	<i>Crust</i>	10.71	44.46	-	0.07	0.99	0.25	41.34	0.95
	<i>Powder</i>	21.35	40.51	1.30	1.12	16.71	0.24	1.22	16.09
R3	<i>Crust</i>	13.23	42.18	0.91	0.87	16.11	0.55	7.38	17.14
	<i>Powder</i>	24.49	42.81	0.75	0.61	9.56	0.18	11.79	9.10

4.7 Summary and Conclusions

A series of proof-of-concept experiments were performed using syringe barrel reactors to evaluate the potential for stimulating MICP on the surface of iron mine tailings. The trends in pressure calcimeter data were inconclusive, but the trends observed with pH, cell plate counts, specific gravity, EDS/ESEM were consistent with successful biocementation of the iron mine tailings. Although the changes in soil composition and properties were not of a large magnitude, they did indicate that measurable amounts of calcium carbonate were generated. Thus, the data obtained using the syringe barrel bioreactors successfully demonstrated that MICP is a viable option for use in fine grained iron mine tailings.

Chapter 5 – Soil Box Bioreactors Results and Discussion

The syringe barrel experiments provided a successful preliminary demonstration of the potential for stimulating MICP in fine-grained materials. Therefore, the experimental system was scaled up to larger soil box reactors to more conclusively evaluate the potential for, and the result of, stimulating MICP in the iron mine tailings. Based on a visual assessment of the soil boxes at the conclusion of the test, treatment of each bioreactor, with the exception of R2*, resulted in a significant white surface crust, as seen in Figure 5.1. A close up of the crust formed in R1 is presented in Figure 5.2. When compared to the syringe barrel reactors, this observation suggests that the extended treatment duration of the soil box experiments (23 days compared to 10 days), coupled with a larger surface area, significantly impacted the extent of calcium carbonate precipitation. As reviewed in Chap. 2, the development of a calcium carbonate crust via stimulation of MICP is expected to also result in an increase in the system pH, clogging of the pore space due to the accumulation of calcium carbonate precipitation, and increased numbers of urea-degrading bacteria. To examine these trends, the pH of the fluid draining from the syringe barrel reactors, and the percolation rate through the tailings, were monitored during the treatment phase. After the treatment phase, the overall extent of MICP was evaluated from a combination of analytical methods including microbiological measurements (urea agar slants, cell plate counts), measurements of the extent of calcium carbonate precipitation (specific gravity change, CO₂ pressure measurements), SEM techniques (ESEM and EDS), and measurement of the strength of the surface of the treated tailings (obtained through the ball bearing test). The results from these analytical tests in the soil boxes had more defined trends than the syringe barrel experiment, and provided stronger evidence that MICP is possible, measurable, and effective in fine grained iron mine tailings. Additionally, the results confirm the presence of native urea-degraders in the iron tailings, and demonstrate their effectiveness in inducing the precipitation of calcium carbonate.



Figure 5.1: Surfaces of bioreactors after the conclusion of the treatment phase for R1 (A), R1* (B), R2 (C), R2* (D), R3 (E), and R3* (F).



Figure 5.2: Solid white precipitate crust from R1. Note the iron mine tailings directly beneath the crust.

5.1 pH of Effluent

During the treatment phase, the biological activity in the soil boxes was monitored by measuring the pH of the effluent twice daily (Figure 5.3). In all of the reactors, the pH ultimately converged to a value of approximately 9, which is consistent with the theoretical equilibrium pH of the growth medium with urea hydrolysis⁶² and similar to what has been observed by other researchers in systems promoting ureolysis with the same medium^{8,14}. Reactors R1 and R1* initially showed a decrease in pH for the first three days of treatment (Figure 5.3A). However, after day three, the pH steadily rose until day 9, at which point the pH plateaued at approximately pH 9, with fluctuations of ± 0.2 pH units for the rest of the treatment phase. Based on these data, ureolysis and the MICP process began in the inoculated reactors R1 and R1* after a short lag period of about 4 days.

The pattern in the effluent pH varied in the two uninoculated soil boxes, with only the native microbes (Figure 5.3B). Similar to reactors R1 and R1*, reactor R2 initially had a steady decrease in pH, but in this case it lasted until about day 7, after which the pH began to increase, reaching a value of approximately pH 9 by day 9. The increase in pH is consistent with the occurrence of ureolysis, and the syringe barrel experimental results, which indicates that native urea-degraders were present in the iron mine tailings. In comparison, the pH of the effluent from R2* held steady at approximately pH 8.6 for the duration of the experiment. These data suggest there may not have been a significant population of urea-degraders in the tailings of R2*, which is consistent with the fact that R2* had the least surface precipitate after the treatment phase (Figure 5.1D).

Reactor R3 also had a steady decrease in effluent pH until about day 6 (Figure 5.3C). Subsequently, the pH steadily rose until day 9, ultimately converging on a pH of approximately 9, which indicates that ureolysis was occurring. Similarly, the pH of R3* steadily decreased until day 11, after which the pH increased to approximately pH 9. These results indicate that the microbial community in R3* had a longer lag phase than the other reactors, whereas the pH trend of R3 is more similar to the trend observed in R2. The observed ultimate pH of approximately 9 is significant because it indicates that

the native urea-degrading microorganisms were not completely destroyed during the autoclaving process, and were able to survive and grow.

5.2 Percolation

The cell growth and MICP expected to accompany the ureolysis suggested by the effluent pH trends should result in clogging of the porous media, leading to increased head loss, decreased hydraulic conductivity, and decreased flow rate^{7,64}. However, for the soil box reactors, the trends in the measured percolation flow through each reactor was generally inconclusive (Figure 5.4). With the exception of R1* and R2, no discernable decrease in flow was observed over the treatment duration. Flows ranged widely from approximately 0.5 mL/hour (R2*) to approximately 2.5 mL/hour (R3). The low flow rate of R2* may have been due to the filter paper rupturing and the outlet clogging with sand particles (see Figure 3.5). A decrease in flow rate indicated more plugging of the pore spaces in the reactor. Given the lack of a significant decrease in flow rate, the percolation rate was not a useful parameter for assessing the extent of MICP in this experimental system

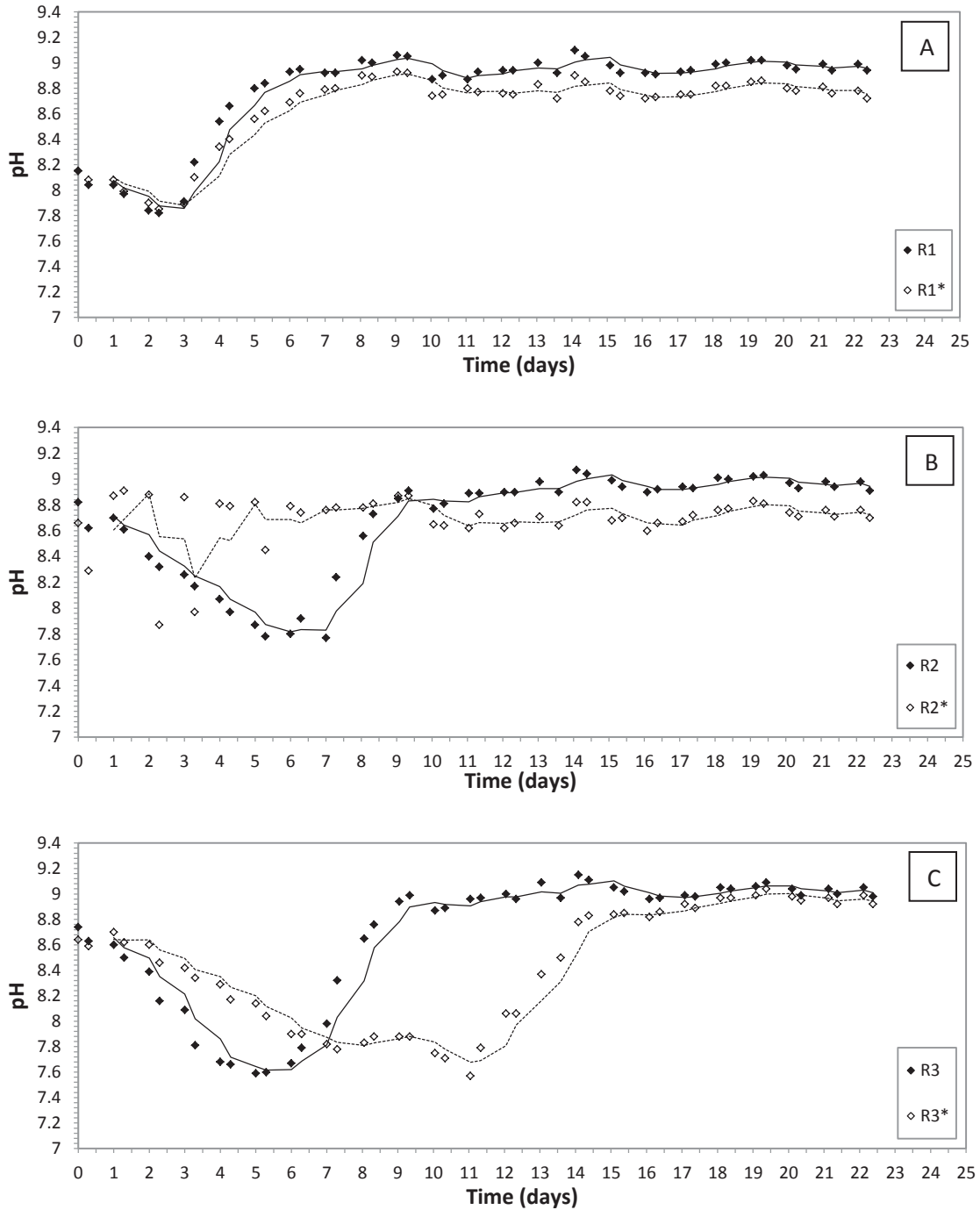


Figure 5.3: pH of the effluent from the soil box bioreactors, (A) inoculated with *S. pasteurii*, (B) with native microorganisms, and (C) using autoclaved iron mine tailings. Symbols represent individual sample measurements, and lines represent the three day moving average of the experimental data.

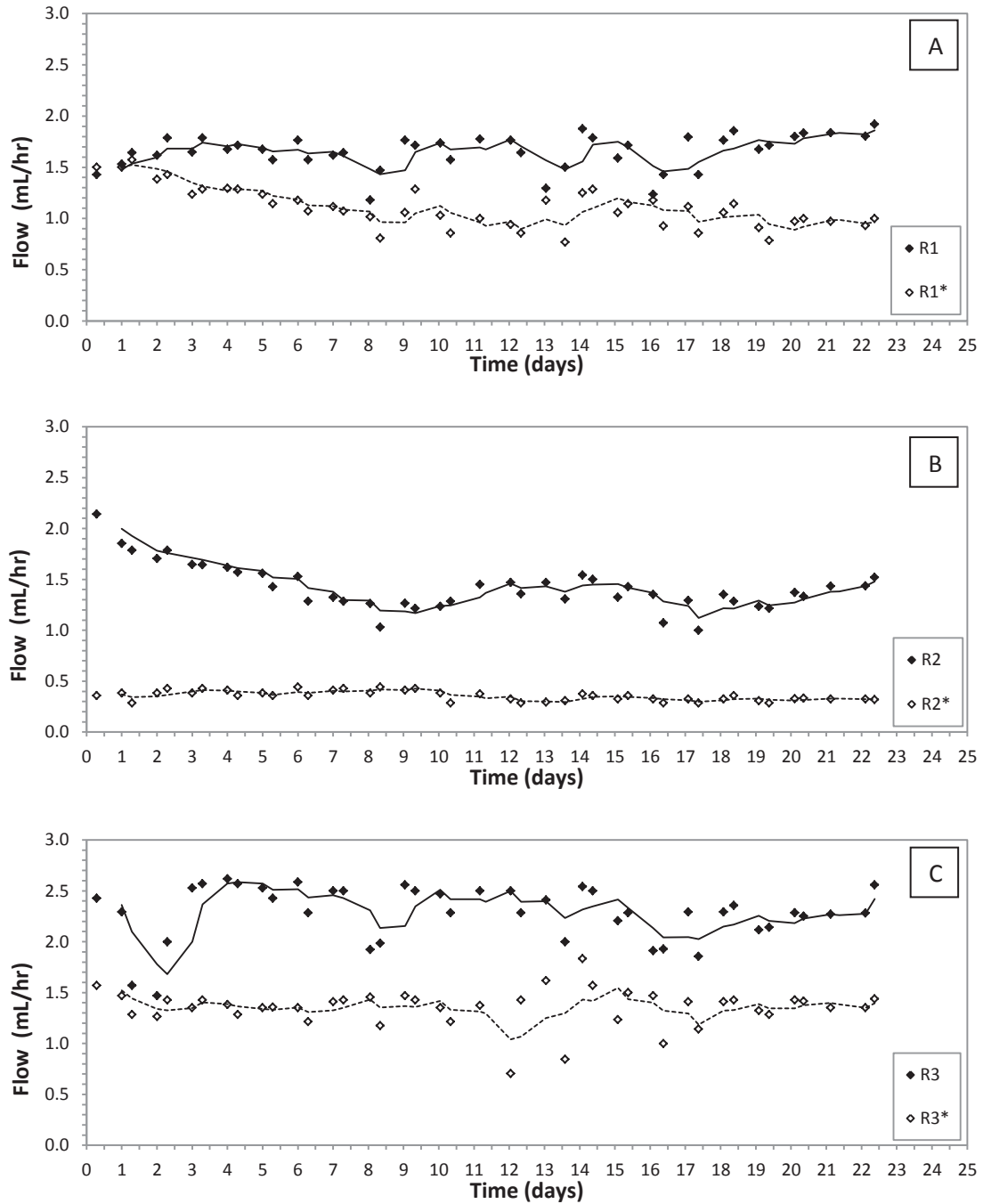


Figure 5.4: The percolation effluent flow rate through the soil box bioreactors, (A) inoculated with *S. pasteurii*, (B) with native microorganisms, and (C) using autoclaved iron mine tailings. Symbols represent individual measurements, and lines represent the three day moving average of the experimental data.

5.3 Urea Agar Slants

To confirm the presence of urea degraders in the soil box reactors, as suggested by the pH data, especially the reactors that were not inoculated (i.e., R2/R2*, and R3/R3*), urea agar slants were conducted by heavily streaking the slants with material from the upper most crust layer in each reactor (Figure 5.5). No pink color change indicative of the pH change associated with ureolysis was observed within the first 6 hours in reactor R2*, although, the expected color change was observed in the other reactors. However, after 12 hours, the slants inoculated from all reactors were pink to the butt of the agar slant, with the exception of R2*, where the pink color did not extend into the butt of the slant. After 24 hours, all agar slants were pink throughout. Based on these results, urea degraders were considered present in all bioreactors, whether they were inoculated with *S. pasteurii* or not. Therefore, urea degrading microbes appear to have been present in the native microbial community of the tailings.

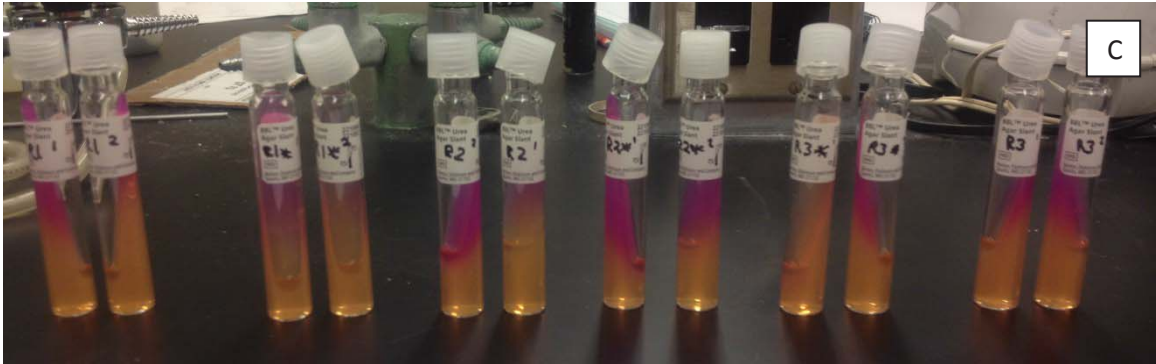
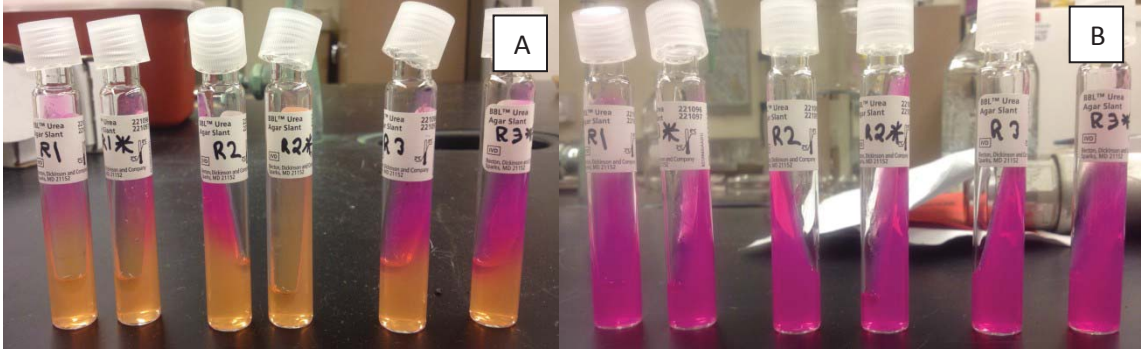


Figure 5.5: Urea - Agar slants after 6 hours of incubation time (A and C) and after 24 hours of incubation time (B and D). All reactors tested positive for urea-degraders. From left to right (in duplicates), R1,R1*, R2,R2*,R3,R3*.

5.4 Cell Counts

Because urea-CaCl₂ growth medium was applied to the soil boxes, it was expected that the cell density would increase in the reactors. As illustrated in Figure 5.6, all of the reactors had a high cellular density near the surface of the reactors, with very low cell counts (below or near the detection limit) observed at depths greater than 2.5 cm below the soil surface. This trend was expected in R1 and R1*, because the inoculum was applied to the surface of the soil, and it is likely that the iron mine tailings acted as a filter to prevent the *S. pasteurii* cells added during the inoculation period from being able to penetrate deeper than 2.5 cm. The physical straining (i.e., filtration) of cells by a porous medium, in which the movement of bacteria is blocked by pores smaller than the cells, is proportional to bacterial size. In general, straining is an important mechanism when the limiting dimension of the bacteria is greater than 5% of the mean diameter of the media particles⁶⁵. For the dry tailings, the d₅₀ is approximately 26 μm, for which 5% is 1.3 μm. Given the typical size of *S. pasteurii* (average of 2.8 μm⁶⁶), it is very likely that the limiting dimension might be ≥ 1.3 μm, and straining is likely.

In the bioreactors, it might be expected that the microorganisms with ureolytic capacity may be present in the deeper soil horizons, but low cell counts were observed with depth in R2, R2*, R3, and R3* as well. This could be attributed to a lack of sufficient substrates (e.g., carbon and energy source, oxygen) to sustain bacterial growth at depth because the oxygen and/or nutrients were probably utilized by the bacteria near the surface, (and in the case of R1 and R1*, where they were applied). However, it was found that urease activity was not negatively impacted by anoxic or anaerobic conditions⁶², so oxygen supply may not be the key factor in ureolytic activity, but instead impacts cellular growth¹⁹.

Interestingly, although a high cell density was expected in both R1 and R1*, the final measured cellular density was also similarly high in the reactors containing native microorganisms (R2, R2*) and autoclaved iron mine tailings (R3, R3*). This indicates that some subset of the native microbial community in the tailings is able to grow on the ATCC 1376 Tris-YE medium agar plates, which is the suggested growth medium for *S.*

*pasteurii*⁴⁷. This in turn suggests that these native microbes have metabolic capabilities similar to *S. pasteurii*. The fact that relatively dense cell populations were observed in R3 and R3* indicates that the microbial communities were not completely destroyed during the autoclaving process, and eventually rebounded.

Although the cell plate counts were similar, the colony morphologies on the agar plates differed in each set of soil conditions after the 36 hour incubation period (Figure 5.7). R1 and R1* resulted in medium sized colonies that were approximately the same size as the other colonies present on the Tris-YE plate, indicating that *S. pasteurii* was the dominant bacteria present. Additionally, the colonies were smooth and circular, consistent with the colony description from ATCC for *S. pasteurii* grown on this media⁴⁷. R2 and R2* had two dominant colony sizes (large and small) which indicated that two types of bacteria were dominant in the reactors. The larger colonies did not have sharp edges. Additionally, very faint, small colonies were observed, but it was not apparent that they would grow, and could not be counted during the cell plate counts. However, this indicated that another type of bacteria was also present in those reactors. R3 and R3* had small, medium, and large colonies. These bacteria originated from the autoclaved iron mine tailings, which indicates that possibly a different bacterial community was able to survive and persist compared to what was observed in R2 and R2*. Long, rod shaped bacteria (which composed the large colonies), and short, rod shaped bacteria (which composed the small colonies) were observed with wet mounts prepared for R2, R2*, R3, and R3*. *S. pasteurii* is also a rod shaped bacterium.

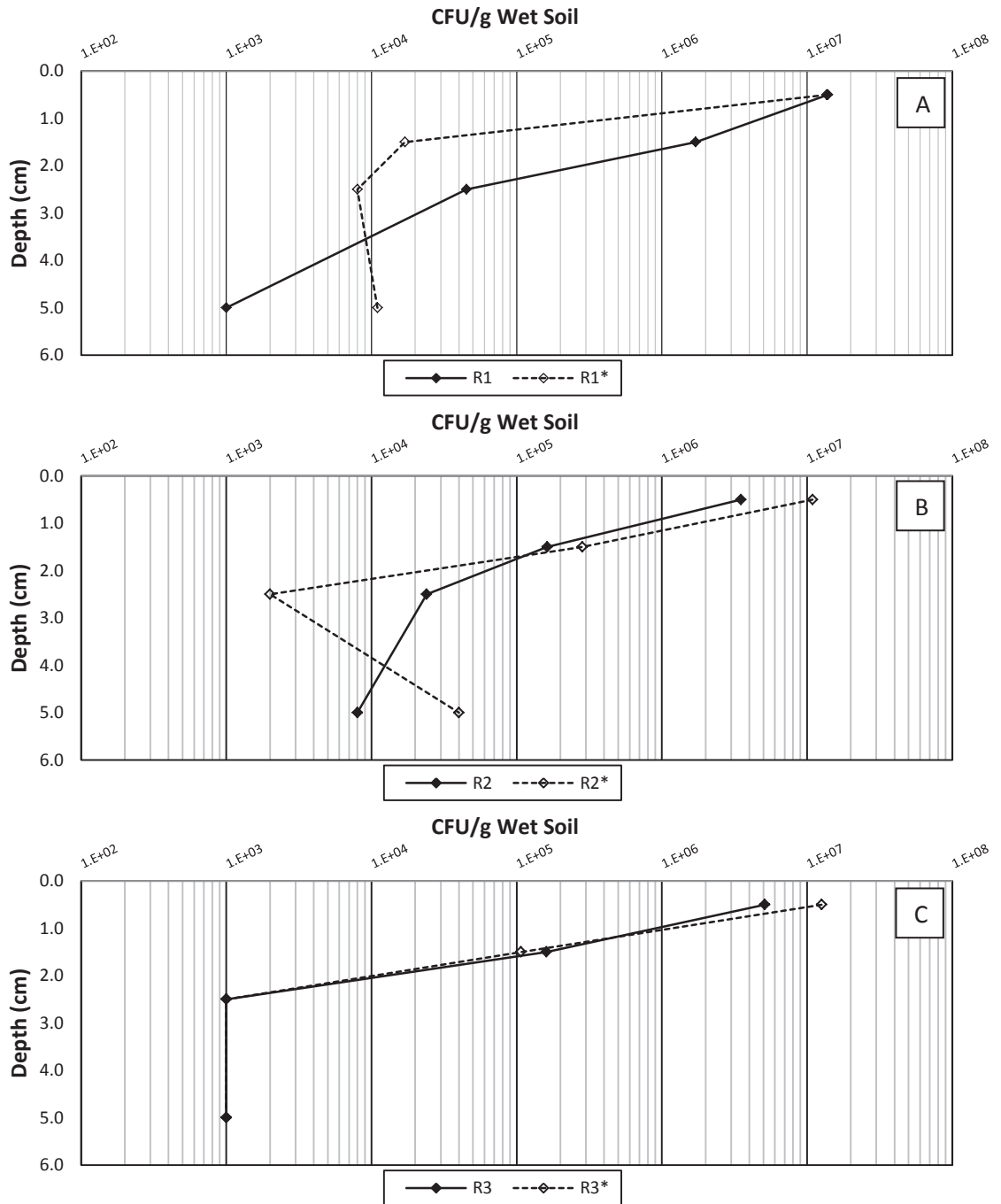


Figure 5.6: Viable cell plate counts (CFU/g wet soil) with depth in the soil box bioreactors, (A) inoculated with *S. pasteurii*, (B) with native microorganisms, and (C) using autoclaved mine tailings. For samples that did not produce countable plate counts (30-300 CFU), the result is reported as the lower detection limit, 10^3 CFU/g wet soil.

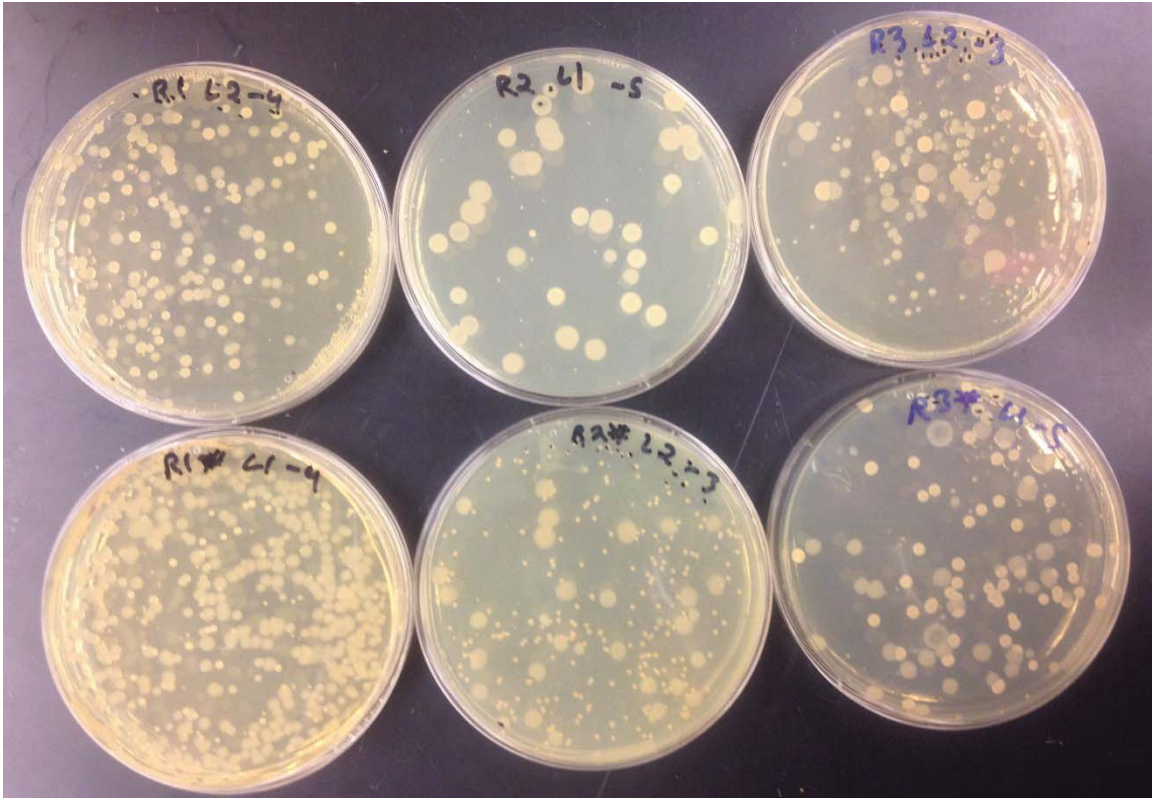


Figure 5.7: Bacterial colony morphology for (Left) R1,R1*, (Middle) R2,R2*, (Right) R3,R3*.

5.5 Specific Gravity

If MICP occurred in the soil box bioreactors, as suggested by the effluent pH and microbiological measurements, then calcium carbonate precipitation should be evident. One way the accumulation of calcium carbonate precipitation was demonstrated was by changes in the specific gravity (SG) of the tailings, because the untreated iron mine tailings have a specific gravity of 2.9-3.1, while calcite has a specific gravity of 2.71. In fact, the specific gravity was observed to decrease significantly near the surface of each bioreactor, as illustrated in Figure 5.8, with very similar trends in the duplicates of each treatment. The greatest decrease in specific gravity occurred in the reactors that were inoculated with *S. pasteurii*, with R1 reaching SG = 2.59, and R1* reaching SG = 2.55 at the surface. Because the reactors bioaugmented with *S. pasteurii* attained a specific gravity of the surface crust that was below 2.71, it is hypothesized that a different calcium carbonate mineral was formed other than calcite. For example, vaterite has a specific gravity of 2.54⁶⁷ and spherical structures that are a typical form for vaterite were observed with the ESEM, as discussed below.

Specific gravity estimates were greater in the deeper soil horizons for all of the reactors, indicating less MICP. As discussed above, it is assumed fewer added cells were able to penetrate to the deeper soil horizons, and/or the inoculated or native cells were less likely be stimulated in the deeper in the soil horizons, due to the added substrate being consumed in the upper soil layers where biological activity is highest. This is expected as the effectiveness of MICP depends on the soil being sufficiently permeable to allow the adequate flow of injected chemicals to the bacteria, and the number of particle contacts available within the soil matrix, because the more particle contacts, the greater the impact of precipitation on the soil matrix⁶⁸. Dense, well graded soils, like the iron tailings should have a higher number of particle contacts per unit volume compared to loose, poorly graded soils⁶²; however, the transport of cells and amendments is limited. For example, Mortensen *et al.* (2011) found that coarser and well graded sands had a faster

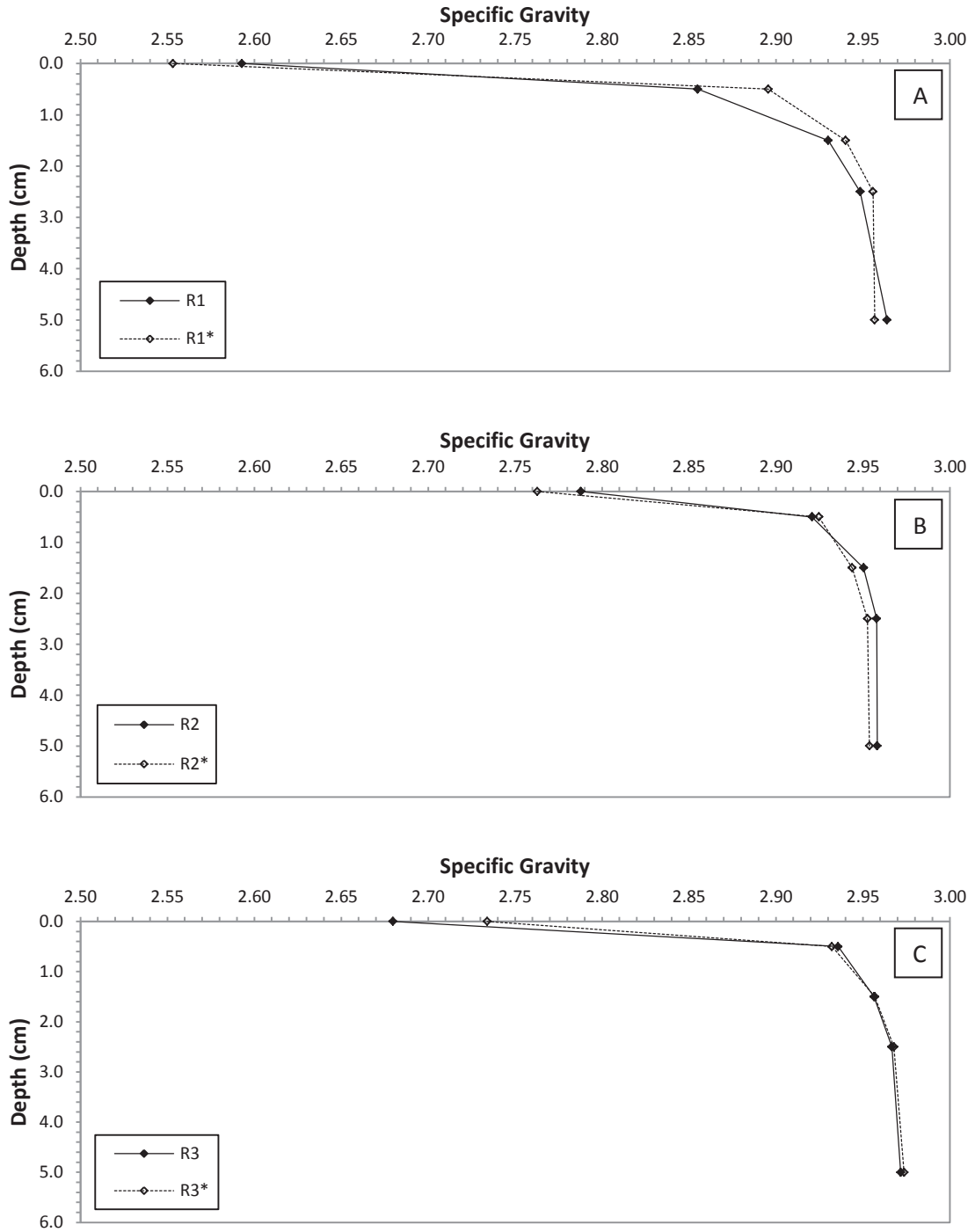


Figure 5.8: Specific gravity measurements in the soil box bioreactors, (A) inoculated with *S. pasteurii*, (B) with native microorganisms, and (C) using autoclaved iron mine tailings.

rate of precipitation that finer and more poorly graded soils. Very coarse soils (e.g., pea gravel with $D_{50} = 4.9$ mm), and very fine soils (e.g., silica flour with $D_{50} = 0.01$ mm), had the very slowest rates of precipitation.

Given that the bacterial cells are mediating the changes in the chemistry that promote the calcium carbonate precipitation, and cell numbers were greatest where the greatest change in specific gravity occurred, it is hypothesized that there should be a correlation between specific gravity and the cell numbers. This relationship is evaluated in Figure 5.9, which demonstrates the strong correlation between the specific gravity of the sample layer and the cell density. The data in Figure 5.9 also indicate that inoculation with *S. pasteurii* (i.e., reactors R1 and R1*) resulted in greater specific gravity change per cell density compared to the equivalent cell density of the native microorganisms (e.g., reactors R2/R2* and R3/R3*). This observation suggests that treatment with *S. pasteurii* is more effective at MICP than stimulation of the native microorganisms for the given treatment duration and inoculum concentration.

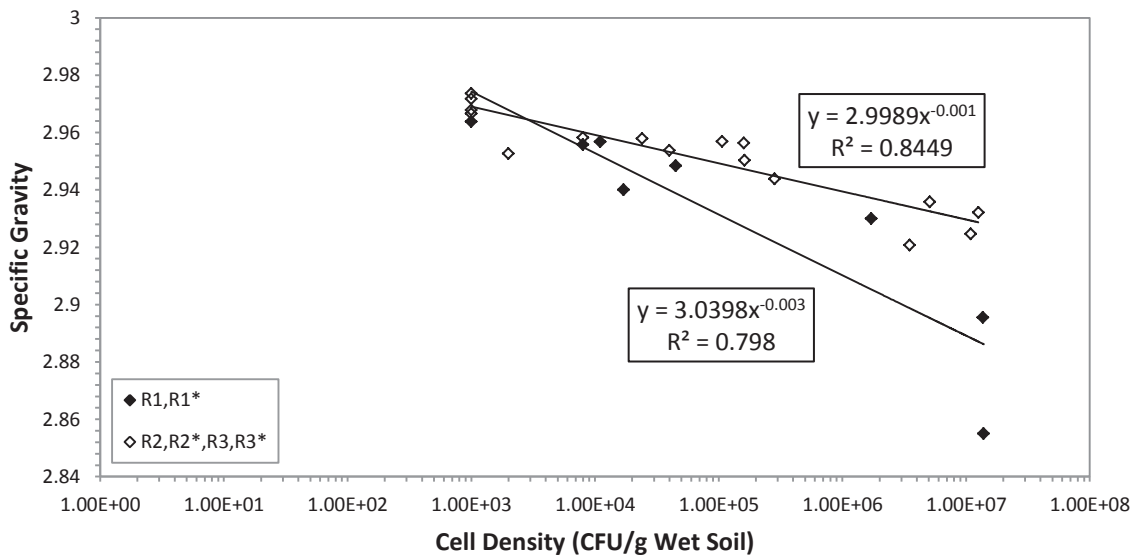


Figure 5.9: Cell density plotted against specific gravity demonstrating a general correlation between cellular density and specific gravity changes.

5.6 Calcium Carbonate

Calcium carbonate precipitation was also measured using the pressure-calculator apparatus. Pressure is expected to be generated from the dissolution of the calcium carbonate in the sample, with higher calcium carbonate contents resulting in higher measureable pressures. As shown in Figure 5.10, the measured pressures from the dissolution of carbonates in the soil box bioreactors more clearly demonstrate the impact of MICP than the results from the syringe bioreactors. Samples from the top layer of all the soil box bioreactors (consisting of the white surface crust) resulted in significantly higher pressures compared to the lower layers (0.5-5 cm depth). Pressures recorded for the samples from the lower layers were generally above the background pressure of 3.2 psi, but did not exhibit any discernable trends.

The greatest pressures recorded were for the surface crust samples from reactors R1 and R3, at 14.84 and 15.09 psi, respectively. Surface crust samples from R1* and R2 produced the second highest pressures at 10.94 and 9.8 psi, respectively, while the surface crust samples from R2* and R3* resulted in the lowest pressure recordings of 7.01 and 9.73 psi, respectively. These pressures indicate significant calcium carbonate precipitate in the surface layer of each bioreactor. Specifically, based on the calibration curve in Chapter 3, these pressures correspond to 17.3 to 61.1 % calcium carbonate by weight in the surface crusts. These values are much higher than the calcium carbonate contents observed in some experiments with sand columns. For example, in sand column experiments using a treatment medium similar to the Stocks-Fischer (1999) recipe used in this experiment, but with a higher NH_4Cl level, it was observed the percent calcite by mass values ranging from about 2 to 3 % near the medium injection point⁶². This is much lower than the values observed in this work with the iron tailings, but those high values were only observed at the surface.

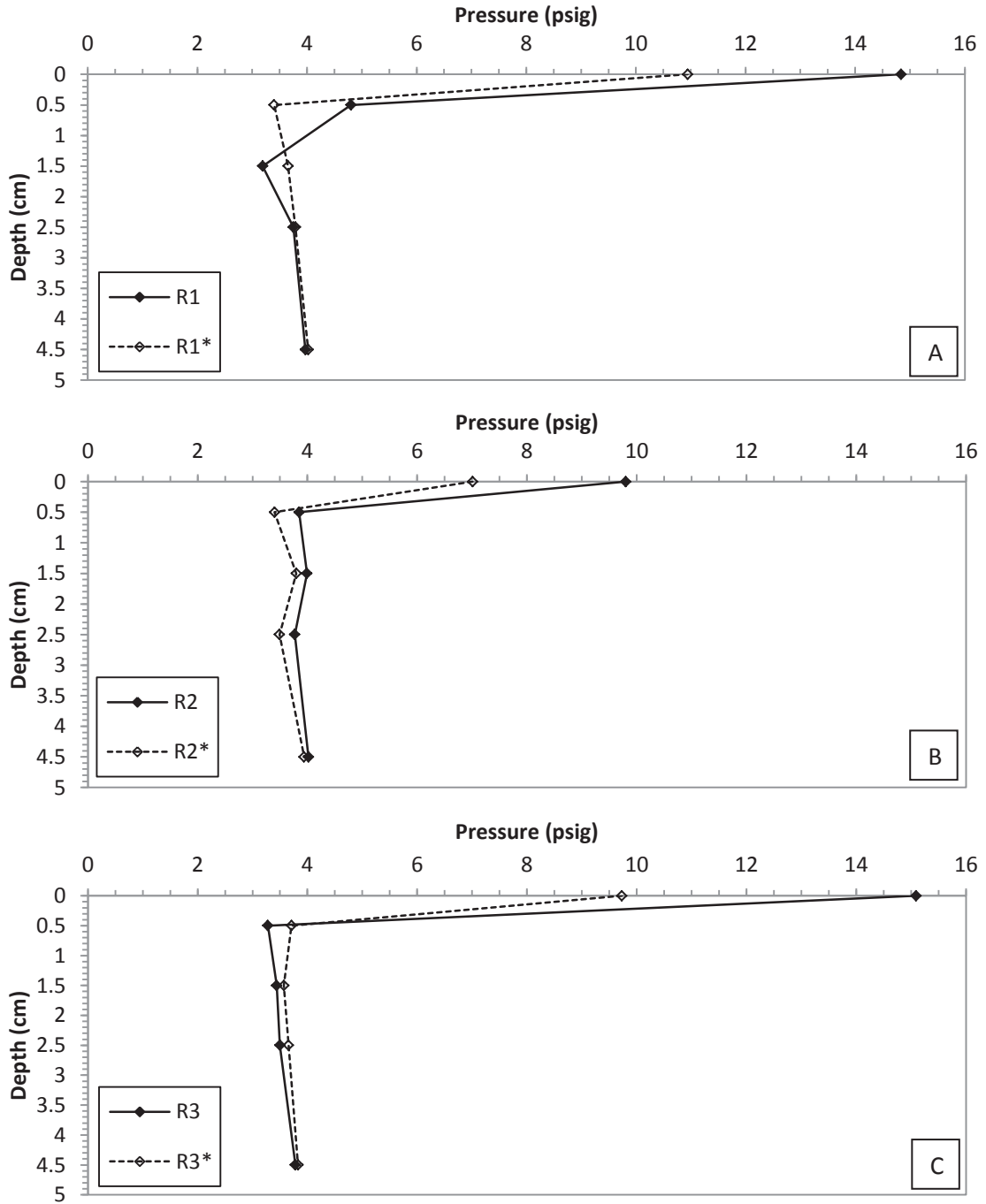


Figure 5.10: Calcium carbonate content (based on the pressure calcimeter) in soil box bioreactors, (A) inoculated with *S. pasteurii*, (B) with native microorganisms, and (C) using autoclaved iron mine tailings.

Given that the specific gravity estimates and the measurements with the pressure calcimeter are both representative of the mass of calcium carbonate precipitate formed, it is interesting to compare the two measurements. As demonstrated by the data shown in Figure 5.11, there is a relatively strong linear correlation between the two values. Although there is some bias in the best-fit linear regression due to the large number of data points at or near the background levels, it is important to note that all of the measured pressures that are above the background pressure level correspond to measured specific gravities that were below the background specific gravity of the untreated tailings.

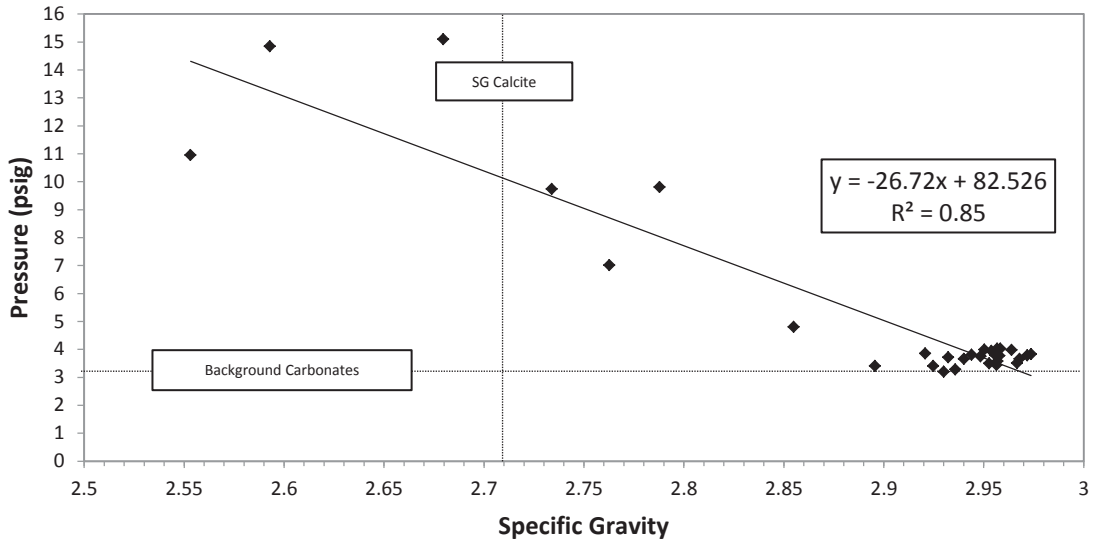


Figure 5.11: Pressure measurements plotted against measured specific gravity for all layers of all bioreactors. The specific gravity of calcite (2.71) is plotted along with the background pressure due to naturally present carbonates in the iron mine tailings).

5.7 ESEM Results

The surface crust of R1, R2, and R3 were also observed using the ESEM. Interestingly, different crystalline structures were observed in the soil box treated surface crusts (Table 5.1) than were observed with the syringe barrel reactors (Table 4.2). Whereas the precipitates observed in the syringe barrel crusts exhibited a variety of form (e.g., amorphous, cubic, conglomeration, angular, rod, flake), the dominant crystal morphologies in the soil box bioreactor crusts consisted of amorphous solids and small cubic conglomerations, with very little of the other crystalline morphologies found in the syringe barrel reactors present. This suggests that the extended treatment duration of the soil box reactors provided better conditions for formation of amorphous solids precipitates. In addition to the amorphous solids and conglomerations, spherical structures were observed in the crust layers of R1 (Figure 5.12A), R2 (Figure 5.13A), and R3 (Figure 5.14A). Some literature suggests that the spherical morphologies are vaterite⁶⁹, and could be a result of certain biomolecules serving as a nucleation site for calcium carbonate crystal formation⁶³.

Significant bacterial pitting was also noted in areas of the crust layers of R1 (Figure 5.12A), R2 (Figure 5.13A), and R3 (Figure 5.14A) consisting of amorphous precipitates. However, less pitting was noted in other calcium carbonate structures, suggesting that there may have been complete encapsulation of the bacteria associated with those crystalline structures.

Inter-particle bridging between iron mine tailings particles by calcium carbonate precipitate was not readily apparent. However, small cubic crystals paired with amorphous solids on the angular iron mine tailings were observed in the tailing samples of R1 (Figure 5.12B), R2 (Figure 5.13B), and R3 (Figure 5.14B), providing evidence that those particles were indeed cemented together.

Table 5.1: Summary of crystal formation morphology in biologically treated iron mine tailings. The tailings powder is iron mine tailings directly beneath the surface crust.

Soil Specimen		Surface Crust			Tailing Powder		
Reactor		R1	R2	R3	R1	R2	R3
<i>Bacteria Evidence</i>		•	•	•			
Crystal Type	<i>Amorphous</i>	•	•	•			
	<i>Cubic</i>	•				•	•
	<i>Conglomeration</i>	•	•	•	•	•	•
	<i>Angular</i>		•				
	<i>Rod</i>		•				
	<i>Flake</i>		•		•	•	•
	<i>Spherical</i>	•	•	•			

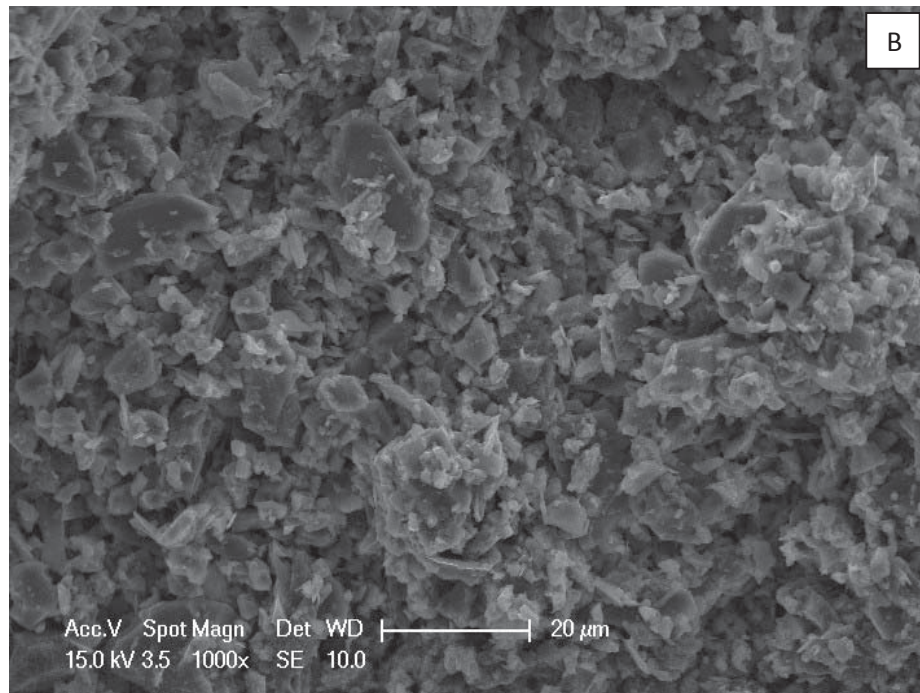
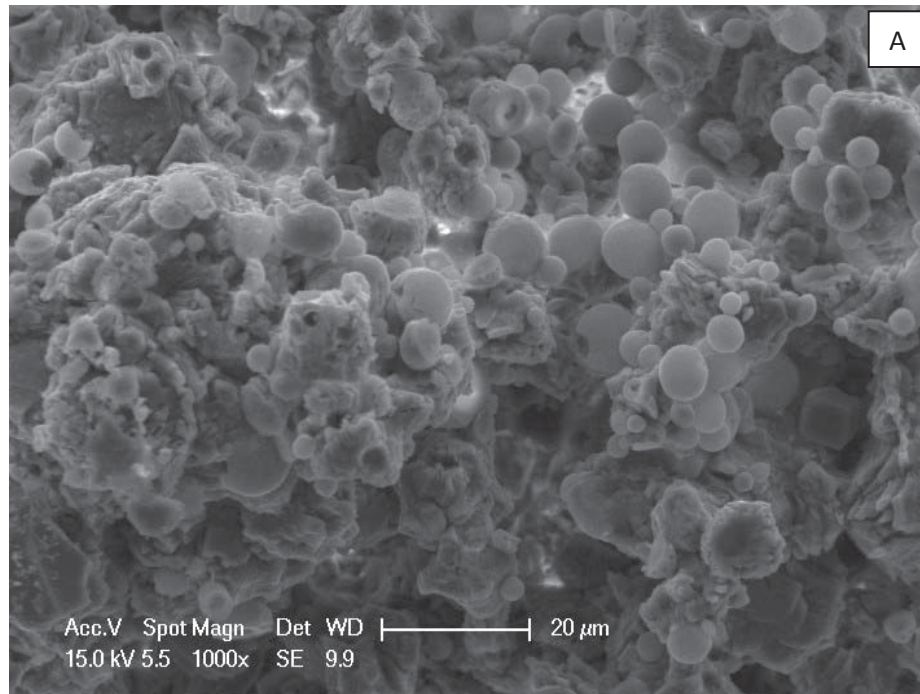


Figure 5.12: Surface crust layer in R1 at 1000x magnification (A), and iron mine tailings underneath the surface crust in R1 at 1000x magnification (B).

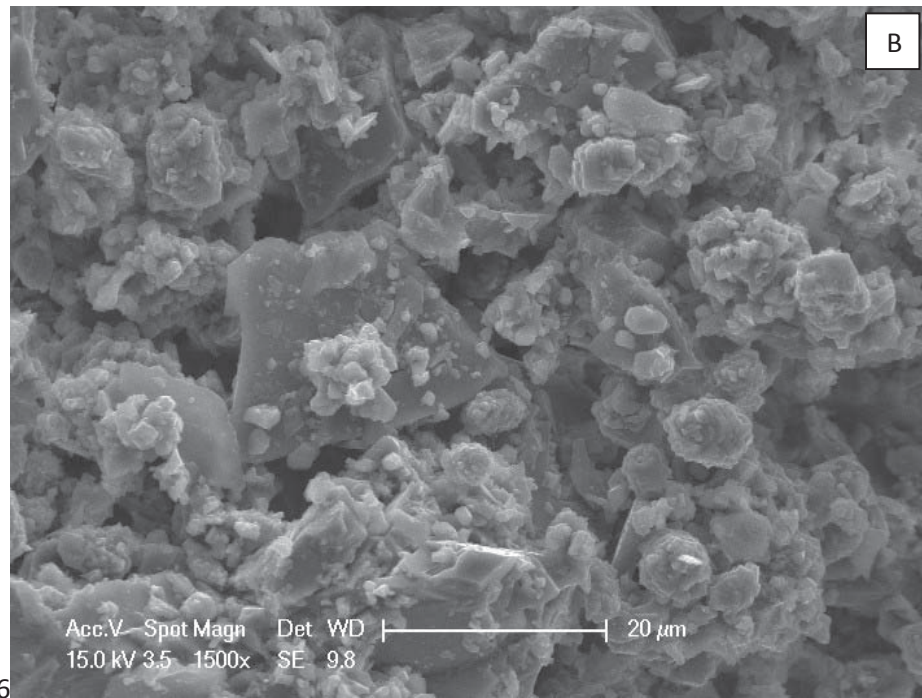
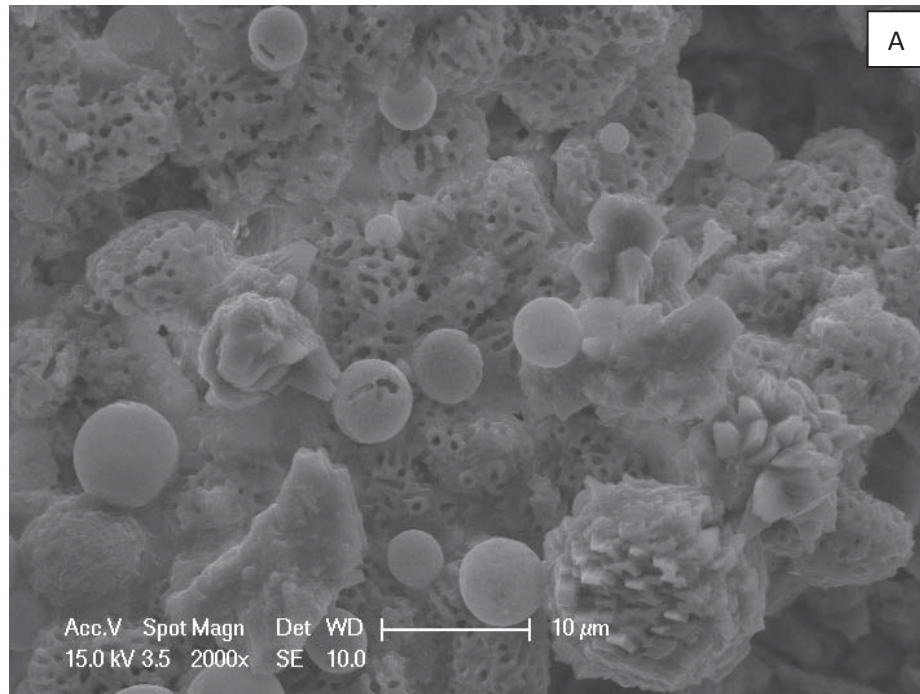


Figure 5.13: Surface crust layer in R2 at 2000x magnification (A), and iron mine tailings underneath the surface crust in R2 at 1500x magnification (B).

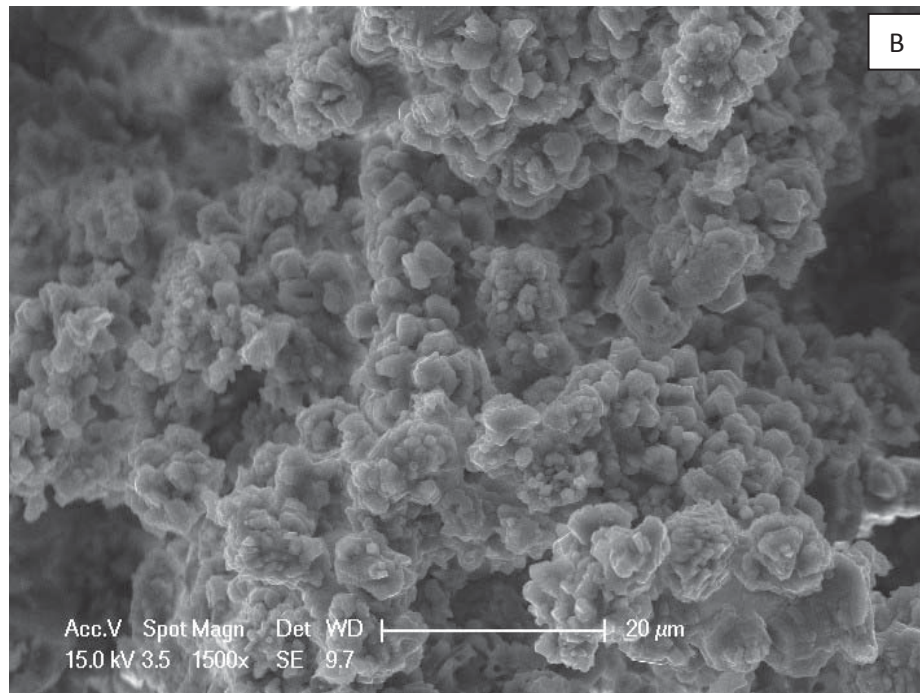
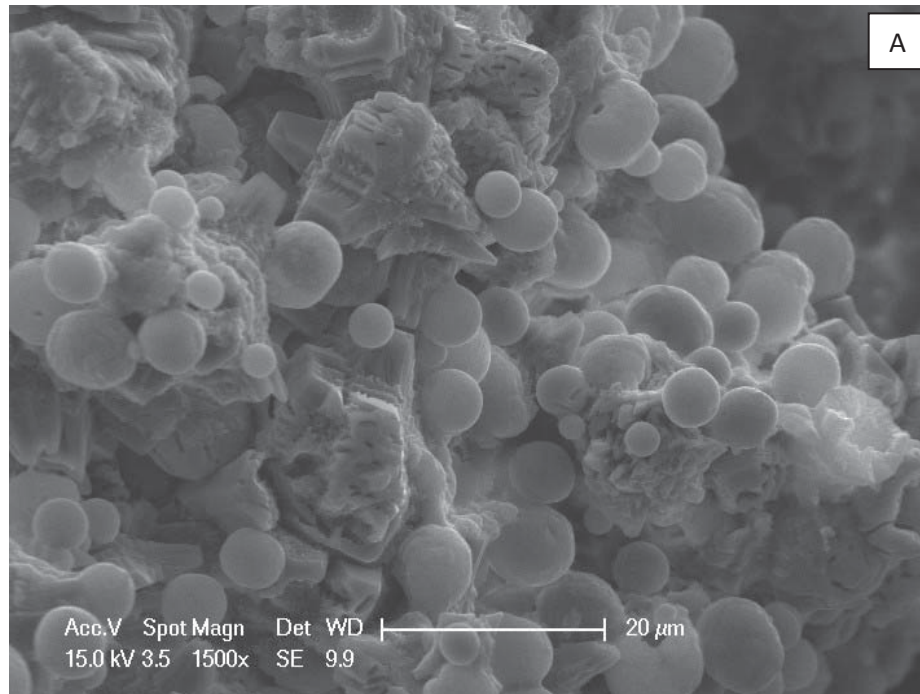


Figure 5.14: Surface crust layer in R3 at 1500x magnification (A), and iron mine tailings underneath surface crust in R3 at 1500x magnification (B).

5.8 EDS Analysis

The surface crusts of R1, R2, and R3, were also analyzed using EDS at the same time the ESEM observations were made. As summarized in Table 5.2, all of the reactors had a high percentage of calcium in the crust samples, which correlates with the other analytical measurements (e.g., specific gravity, pressure calcimeter) indicating a very high percentage of calcium carbonate in the surface crust. Consistent with the pressure calcimeter results, R1 and R2 had the highest relative percentage of calcium in the crust layer at 64% and 49.5%, followed by R3 at 44%. The iron tailings directly under the surface crust had lower percentages of calcium present, and a higher relative percentage of iron. Although reduced relative to the surface crust, the percentages of calcium in the iron mine tailings layers of R2 (24.8%) and R3 (32.0%) were still relatively high. This may be due to the occurrence of MICP in those layers, or it may be that the mine tailing sample used for the EDS analysis included some of the white surface crust.

Table 5.2: EDS Analysis of surface crust layer from the soil box bioreactor experiment. The crust sample refers to the white surface crust; the powder sample refers to the mine tailings directly under the white crust.

Reactor	Type	EDS Analysis (Percent by wt.)					
		C	O	Si	Cl	Ca	Fe
R1	<i>Crust</i>	6.32	27.24	0.25	0.65	64.63	0.90
	<i>Powder</i>	10.74	45.82	23.89	1.69	1.41	16.45
R2	<i>Crust</i>	-	48.93	0.78	0.24	49.52	0.54
	<i>Powder</i>	-	42.11	11.88	1.03	24.79	20.19
R3	<i>Crust</i>	-	54.69	0.09	1.06	43.94	0.23
	<i>Powder</i>	-	52.42	9.18	0.52	32.03	5.85

5.9 Ball Bearing Drop Test

The final analysis performed was the ball drop test, which was used to evaluate whether the surface crust formed via MICP resulted in an increase of the surface strength of the treated iron mine tailings compared to an untreated control at the same moisture content. The untreated control consisted of fine grained iron mine tailings packed into a larger soil box (6" x 6" surface area). Specimens were tested at different moisture contents because each bioreactor was drying at different rates after the treatment phase was concluded. As illustrated in Figure 5.15, all surfaces of the bioreactors resulted in a reduction in the diameter of the impact crater at the tested moisture content when compared to the crater in the corresponding untreated tailings specimen. These results indicate that the strength of the treated surfaces observed in each bioreactor increased due to the calcium carbonate precipitation resulting from the stimulated biological activity. These results also suggest that the ball bearing drop test is a potentially useful technique for evaluating the strength of engineered and natural biological surface crusts. Previous studies have used the needle penetrometer test to evaluate the surface strength of biological soil crusts⁷⁰, but in preliminary tests performed during this research, the needle penetrometer was inconclusive in determining increases in surface strength generated by MICP on the iron tailings. Additionally, the method of penetrometer for surface crust characterization is inherently different than that of a saltating particle⁷⁰; the needle penetrometer measures the maximum force required for penetration, whereas in-situ wind erosion events would result in the gradual exposure of saltating particles onto the surface crust from an oblique angle. Thus, the needle penetrometer was not considered the best option for strength characterization on biological crusts.

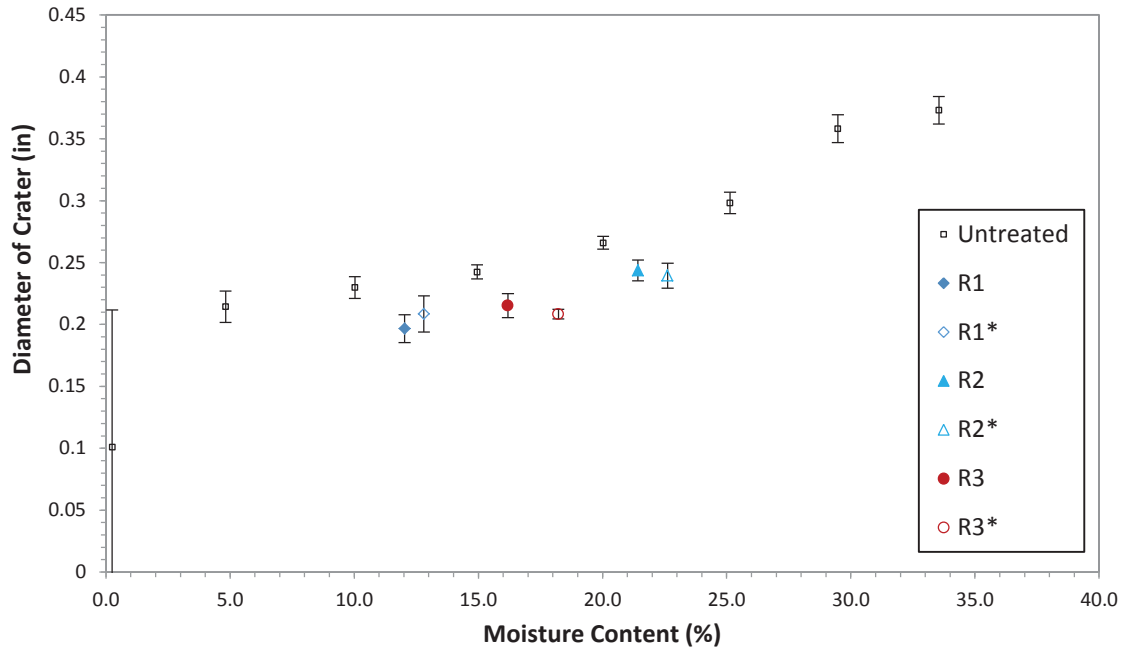


Figure 5.15: Results for the crater diameter from the ball drop test on biotreated and untreated iron tailings, as a function of the sample moisture content. Each symbol represents the average of 5 measurements, and the error bars represent \pm one standard deviation. Note that a high standard deviation was calculated at a moisture content of 0%, due to some ball drops not creating a crater.

5.10 Summary and Conclusions

Scaled-up experiments were performed using soil box bioreactors to more carefully evaluate the potential for stimulating MICP on the surface of iron mine tailings. In general, analysis of the test results indicates that all bioreactors behaved as expected with the stimulation of ureolysis and MICP: a visible surface crust was formed, the effluent pH increased, cell numbers increased, urea degradation was demonstrated, and calcium carbonate precipitation was demonstrated via changes in specific gravity and pressure calcimeter measurements. This was true in the reactors that were inoculated with *S. pasteurii* and those with only native microorganisms present, although the bioaugmented reactors R1 and R1* demonstrated greater calcium carbonate precipitation throughout the soil horizons. Nevertheless, the observation that microbes already present in the tailings were capable of MICP with urea addition is an important finding with implications for the potential application of this technique in the field. Finally, the MICP also resulted in an increase in the surface strength of the iron tailings, which provides further evidence that MICP has potential as a dust hazard mitigation biotechnology.

Chapter 6 – Summary and Conclusions

Mining operations result in the production of massive volumes of tailings, which are deposited in large-scale permanent impoundments. One of the key environmental hazards associated with these impoundments is the generation of fugitive dust storms. A variety of conventional approaches are available for control of the dusting hazard associated with mine tailing impoundments, however, each of these methods has its limitations and potential negative side effects. One potentially innovative approach for modifying the surface properties of the mine tailings, and thereby providing dust mitigation is to apply bioengineering methods. In particular, the overall goal of this project was to evaluate the potential for biocementation as a permanent solution for minimizing fugitive dust emissions.

The first objective of this research was to perform a bench-scale feasibility study of the potential for stimulating MICP in fine-grained iron mine tailings. Initially a variety of challenges were encountered working with the iron mine tailings, as the fine particle size presented difficulties in applying the biotreatment process. However, those challenges were eventually overcome, and syringe barrel bioreactors were used to successfully demonstrate that inoculated *S. pasteurii* was able to stimulate MICP on the surface of the fine grained material. The occurrence of MICP on the surface of the treated iron mine tailings in the syringe barrel reactors was demonstrated through a variety of analyses including changes in the effluent pH, specific gravity, cell counts, pressure calcimeter measurements, ESEM, and EDS.

Importantly, the presence of natural urea-degraders in the iron tailings was discovered during the treatment phase of the experiment. These native microbes also resulted in measurable differences in the composition and properties of the surface crust on the iron mine tailings that were similar in magnitude to the changes observed in the reactors bioaugmented with *S. pasteurii*. This discovery opens the possibility that MICP could potentially be applied to iron mine tailings by biostimulating the native microorganisms,

rather than inoculating the tailings with non-native urea-degrading microorganisms, and then applying stimulatory amendments.

The second objective of this research was to scale up the bioreactor size from the syringe barrels to soil boxes. The larger soil boxes created a better environment for evaluating the potential for MICP in the iron tailings, and for evaluating the resulting improvement in the surface strength of the tailings samples via calcium carbonate precipitation. The longer treatment duration of the soil box experiments, paired with the larger surface area, resulted in more dramatic MICP-dependent changes in soil composition and properties, which were evaluated using the effluent pH and percolation rate during treatment, and microbiological measurements (i.e., via cell plate counts and urea degrader slants) and calcium carbonate measurements (i.e., via specific gravity, and pressure calcimeter), as well as ESEM and EDS, after treatment. In addition, the surface strength of the tailings specimens post treatment was tested using the ball bearing drop test. This test, which was developed as part of this research project, demonstrated a strength increase due to the surface crust soil layer for all of the treated bioreactors, and with further development may be a tool with broader utility for testing the surface strength of biological soil crusts.

In summary, the evidence obtained throughout this study indicates significant calcium carbonate precipitation occurred on the surface of iron mine tailings as a result of biological processes mediated not only by bioaugmented *S. pasteurii*, but also by the native microorganisms. The results demonstrate that MICP is indeed achievable in the surface layers of fine grained materials such as the iron tailings. These preliminary results will further progress the use of MICP for geotechnical applications, such as dust mitigation, and better define the difficulties associated with bioengineering fine grained soil material.

Chapter 7 – Recommendations for Further Research

In the process of performing this research, many iterations and trials were conducted before ultimately developing consistent, repeatable protocols. Nevertheless, further improvements could be made to better characterize the effectiveness of MICP in iron mine tailings. For example, the experimental conditions used could be varied to evaluate the potential for optimizing the process. The treatment duration necessary for producing measurable and reproducible replicate data, and maximizing MICP should be evaluated. Such information would result in better laboratory data, and further the potential application of the results of this research for field scale biotreatment processes. Additionally, other factors that could be modified in an effort to optimize application of MICP for reducing dust emission include the void ratio and moisture content.

Other methods of inoculation should also be tested to better reflect how bioaugmentation might be accomplished in possible large scale application. In this work, the percolation method of inoculation worked well for developing a surface crust, but in-situ field application may involve tilling or mixing of an *S. pasteurii* inoculum into the surface soil. Thus, those methods should be adapted and tested on a laboratory scale to better assess inoculation effectiveness and differences. For applications attempting to stimulate the native urea degraders in mine tailings, the specific amendments and concentrations required for biostimulating MICP in the field should also be evaluated, with a goal of maximizing the MICP and minimizing the environmental impact.

Some of the analytical methods applied in this research also could benefit from further evaluation and development. Changes in specific gravity and the pressure calcimeter provided useful evidence of calcium carbonate precipitation. The methods appear to be correlated as expected, but the correlation would benefit from further evaluation. In addition, the ball bearing drop test appears to have potential for use in testing the surface strength of biological soil crusts. Nevertheless, the current test protocol is crude and could be optimized to improve the application of the test, and the quality of the data collected.

A cost analysis for application of MICP to improve the surface strength of mine tailings is also recommended. Such an analysis would allow for comparison of the capital and OEM costs of biomodification of the mine tailings with other established methods. Furthermore, a short term and long term cost analysis paired with a life cycle assessment would allow this biotechnology to become more seriously considered as a fugitive dust hazard mitigation technology by the operators of tailings impoundments.

Finally, it is recommended that the biologically treated iron mine tailings be characterized with other strength tests, to better understand the strength increase produced via MICP. This recommendation could be achieved through further testing with a wind tunnel, penetrometer, and a triaxial cell test. Additionally, the results of strength tests such as those with MICP could be compared with other established dust suppressant methods to better understand the effectiveness of MICP compared to other methods.

Bibliography

- 1 USEPA. Design and Evaluation of Tailings Dams. 63 (USEPA, 1994).
- 2 USEPA. Dust Control and Stabilization. (USEPA, Washington D.C., 2003).
- 3 USAF. Dust Control for Roads, Airfields, and Adjacent Areas. Report No. TM 5-830-3/AFM 88-17, 42 (1987).
- 4 USEPA. Potential Environmental Impacts of Dust Suppressants: "Avoiding Another Times Beach". 97 (USEPA, 2002).
- 5 Seagren, E. A. & Aydilek, A. in *Environmental Microbiology* Vol. 2 (2009).
- 6 Chou, C., Seagren, E. A., Aydilek, A. & Maugel, T. *Bacterially-Induced Calcite Precipitation via Ureolysis*, 2008).
- 7 Stabnikov, V., Naeimi, M., Ivanov, V. & Chu, J. Formation of water-impermeable crust on sand surface using biocement. *Cement and Concrete Research* **41**, 1143-1149, doi:10.1016/j.cemconres.2011.06.017 (2011).
- 8 Stocks-Fisher, S., Galinat, J. K. & Bang, S. Microbiological precipitation of CaCO₃. *Soil Biology and Biochemistry* **31**, 1563-1571 (1999).
- 9 *Bergey's Manual of Systematic Bacteriology*. 2 edn, (Springer, 2005).
- 10 Madigan, M. T., Martinko, J. M. & Parker, J. *Brock Biology of Microorganisms*. 10 edn, (Prentice Hall, 2003).
- 11 Nielsen, T. H., Bone, T. A. & Sorensen, J. Significance of microbial urea turnover in N cycling of three Danish agricultural soil. *FEMS Microbiology Ecology* **25**, 147-157 (1998).
- 12 Jahns, T. Ammonium Urea-Dependent Generation of a Proton Electrochemical. *Journal of Bacteriology* **178**, 403-409 (1996).
- 13 Bang, S., Min, S. & Bang, S. Application of Microbiologically Induced Soil Stabilization Technique for dust suppression. *International Journal of Geo-Engineering*, 27-37 (2011).
- 14 Dejong, J. T., Fritzges, M. B. & Nusslein, K. Microbially Induced Cementation to Control Sand Response to Undrained Shear. *Journal of Geotechnical and Geoenvironmental Engineering* **132**, 1381-1392, doi:10.1061//asce/1090-0241/2006/132:11/1381 (2006).
- 15 Bang, S., Galinat, J. K. & Ramakrishnan, V. Calcite precipitation induced by polyurethane-immobilized *Bacillus pasteurii*. *Enzyme and Microbial Technology* **28**, 404-409 (2001).
- 16 Ramachandran, S. K., Ramakrishnan, V. & Bang, S. S. Remediation of concrete using microorganisms. *ACI Materials Journal* (2001).
- 17 Whiffin, V. S., van Paassen, L. A. & Harkes, M. P. Microbial Carbonate Precipitation as a Soil Improvement Technique. *Geomicrobiology Journal* **24**, 417-423, doi:10.1080/01490450701436505 (2007).
- 18 Chu, J., Stabnikov, V. & Ivanov, V. Microbially Induced Calcium Carbonate Precipitation on Surface or in the Bulk of Soil. *Geomicrobiology Journal* **29**, 544-549, doi:10.1080/01490451.2011.592929 (2012).
- 19 Martin, D., Dodds, K., Ngwenya, B. T., Butler, I. B. & Elphick, S. C. Inhibition of *Sporosarcina pasteurii* under anoxic conditions: implications for subsurface

- carbonate precipitation and remediation via ureolysis. *Environmental Science and Technology* **46**, 8351-8355, doi:10.1021/es3015875 (2012).
- 20 Krajewska, B. Ureases I. Functional, catalytic and kinetic properties: A review. *Journal of Molecular Catalysis B: Enzymatic* **59**, 9-21, doi:10.1016/j.molcatb.2009.01.003 (2009).
- 21 Benini, S. *et al.* The crystal structure of *Sporosarcina pasteurii* urease in a complex with citrate provides new hints for inhibitor design. *Journal of biological inorganic chemistry : JBIC : a publication of the Society of Biological Inorganic Chemistry* **18**, 391-399, doi:10.1007/s00775-013-0983-7 (2013).
- 22 Karplus, A. P., Pearson, M. A. & Hausinger, R. P. 70 Years of crystalline urease: what have we learned? *Accounts of Chemical Research* **30**, 330 (1997).
- 23 Benini, S. *et al.* A new proposal for urease mechanism based on the crystal structures of the native and inhibited enzyme from *Bacillus pasteurii*: why urea hydrolysis costs two nickels. *Structure* **7**, 205-216, doi:10.1016/s0969-2126(99)80026-4 (1999).
- 24 Gianfreda, L., De Cristofaro, A., Rao, M. A. & Violante, A. Kinetic Behavior of Synthetic Organo- and Organo-Mineral-Urease Complexes. *Soil Sci. Soc. Am. J.* **59**, 811-815, doi:10.2136/sssaj1995.03615995005900030025x (1995).
- 25 Pettit, N. M., Smith, A. R. J., Freedman, R. B. & Burns, R. G. Soil urease: Activity, stability and kinetic properties. *Soil Biology and Biochemistry* **8**, 479-484, doi:http://dx.doi.org/10.1016/0038-0717(76)90089-4 (1976).
- 26 Bachmeier, K. L., Williams, A. E., Warmington, J. R. & Bang, S. Urease activity in microbiologically-induced calcite precipitation. *Journal of Biotechnology* **93**, 171-181 (2002).
- 27 Krajewska, B. Ureases. II. Properties and their customizing by enzyme immobilizations: A review. *Journal of Molecular Catalysis B: Enzymatic* **59**, 22-40, doi:10.1016/j.molcatb.2009.01.004 (2009).
- 28 Hutchinson, G. L. & Viets Jr., F. G. Nitrogen enrichment of surface water by adsorption of ammonia volatilized from cattle feedlots. *American Association for the Advancement of Science* **166**, 514-515 (1969).
- 29 Mobley, H., Cortesia, M., Rosenthal, L. & Jones, B. Characterization of Urease from *Campylobacter pylori*. *Journal of Clinical Microbiology* **26**, 831-836 (1988).
- 30 Goodman, B. E. Transport of small molecules across cell membranes: water channels and urea transporters. **26**, 146-157, doi:10.1152/advan.00027.2002 (2002).
- 31 Sawada, K. Mechanisms of crystal growth of ionic crystals in solution. Formation, transformation, and growth inhibition of calcium carbonates. *Crystallization Processes*, 39-68 (1998).
- 32 Schultz-Lam, S., Fortin, D., Davis, B. S. & Beveridge, T. J. Minerization of Bacterial Surfaces. *Chemical Geology* **132**, 171-181 (1996).
- 33 Chou, C.-W., Seagren, E. A., Aydilek, A. H. & Lai, M. Biocalcification of Sand through Ureolysis. *Journal of Geotechnical and Geoenvironmental Engineering* **137**, 1179-1189, doi:10.1061/(asce)gt.1943-5606.0000532 (2011).

- 34 Ariyanti, D., Handayani, N. A. & Hadiyanto. An Overview of Biocement Production from Microalgae. *International Journal of Science and Engineering* **2**, 30-33 (2011).
- 35 Hammes, F. & Verstraete, W. Key roles of pH and calcium metabolism in microbial carbonate precipitation. *Reviews in Environmental Science and Biotechnology* **1**, 3-7 (2002).
- 36 Whiffin, V. S. *Microbial CaCO₃ precipitation for the production of biocement* Doctor of Philosophy thesis, Murdoch University, (2004).
- 37 Kile, D., Eberl, D., Hoch, A. & Reddy, M. An assessment of calcite crystal growth mechanisms based on crystal size distributions. *Geochimica et Cosmochimica Acta* **64**, 2937-2950 (1999).
- 38 Castanier, S., Le Metayer-Levrel, G. & Perthuisot, J. P. Ca-carbonates precipitation and limestone genesis - the microbiogeologist point of view. *Sedimentary Geology* **126**, 9-23 (1999).
- 39 Villar, J. V. & Dawe, G. A. The Tilden Mine - A New Processing Technique for Iron Ore. 26 (The Cleveland-Cliffs Iron Company).
- 40 Robinson, G. W. & LaBerge, G. L. *Minerals of the Lake Superior Iron Ranges*. 58 (A. E. Seaman Mineral Museum, 2013).
- 41 Cannon, W. F. *The lake superior iron ranges: geology and mining*, (2011).
- 42 USEPA. *Fine Particle (PM_{2.5}) Designations, Frequent Questions*, (2014).
- 43 Chen, R., Lee, I. & Zhang, L. Biopolymer Stabilization of Mine Tailings for Dust Control. *Journal of Geotechnical and Geoenvironmental Engineering* **141**, 04014100, doi:10.1061/(asce)gt.1943-5606.0001240 (2015).
- 44 USEPA. *EPA Bans PCB Manufacture; Phases out Uses*, (1979).
- 45 ASTM. Standard Test Method for pH of Soils. Report No. ASTM D4972-01, (American Society for Testing and Materials).
- 46 ASTM. Standard Test Method for Particle-Size Analysis of Soils. Report No. ASTM D422 - 63(2007)e2, (American Society for Testing and Materials, 2007).
- 47 Collection, A. T. C. *Sporosarcina pasteurii* (ATCC® 11859™)
<http://www.atcc.org/products/all/11859.aspx>.
- 48 Collection, A. T. C. *ATCC medium: 1376 Bacillus pasteurii NH4-YE medium*.
<http://www.atcc.org/~media/C332DC4BBD4A4414AF07C38863C1822B.ashx>
- 49 Al Qabany, A., Soga, K. & Santamarina, C. Factors Affecting Efficiency of Microbially Induced Calcite Precipitation. *Journal of Geotechnical and Geoenvironmental Engineering* **138**, 992-1001, doi:10.1061/(asce)gt.1943-5606.0000666 (2012).
- 50 Chou, C. *Biomodification of geotechnical properties of sand* Master of Science thesis, University of Maryland, (2007).
- 51 *Standard Methods for the Examination of Water and Wastewater*. 17 edn, (1989).
- 52 ASTM. Standard Test Methods for Laboratory Determination of Water (Moisture) Content of Soil and Rock by Mass. Report No. ASTM D2216 - 10, (2010).
- 53 DeGregorio, V. B. Loading Systems, Sample Preparation, and Liquefaction. *Journal of Geotechnical Engineering* **116** (1990).

- 54 Gerhardt, P. *Methods for General and Molecular Bacteriology*. (American Society for Microbiology, 1994).
- 55 Lindahl, V. & Bakken, L. R. Evaluation of methods for extraction of bacteria for soil. *FEMS Microbiology Ecology* **16** (1995).
- 56 Gagliardi, J. V. & Karns, J. S. Leaching of Escherichia coli O157:H7 in Diverse Soils under Various Agricultural Management Practices. *Applied and Environmental Microbiology* **66**, 877-883, doi:10.1128/aem.66.3.877-883.2000 (2000).
- 57 Brink, B. *Urease Test Protocol*, American Society for Microbiology, 2010.
- 58 Roberts, W. L., Campbell, T. J. & Rapp, G. R. *Encyclopedia of Minerals (Second Edition)*. 2 edn, 979 (Van Nostrand Reinhold, 1990).
- 59 Zanko, L. M., Niles, H. B. & Oreskovich, J. A. Mineralogical and microscopic evaluation of coarse taconite tailings from Minnesota taconite operations. *Regulatory toxicology and pharmacology : RTP* **52**, S51-65, doi:10.1016/j.yrtph.2007.09.016 (2008).
- 60 Sherrod, L. A., Dunn, G., Peterson, G. A. & Kolberg, R. L. Inorganic Carbon Analysis by Modified Pressure-Calcimeter Method. *Soil Science Society of America Journal* **66**, 7 (2002).
- 61 Fonnesbeck, B. B., Boettinger, J. L. & Lawley, J. R. Improving a Simple Pressure-Calcimeter Method for Inorganic Carbon Analysis. *Soil Science Society of America Journal* **77**, 1553, doi:10.2136/sssaj2012.0381 (2013).
- 62 Mortensen, B. M., Haber, M. J., DeJong, J. T., Caslake, L. F. & Nelson, D. C. Effects of environmental factors on microbial induced calcium carbonate precipitation. *J Appl Microbiol* **111**, 338-349, doi:10.1111/j.1365-2672.2011.05065.x (2011).
- 63 Tark Han, J., Xu, X. & Cho, K. Sequential formation of calcium carbonate superstructure: From solid/hollow spheres to sponge-like/solid films. *Journal of Crystal Growth* **308**, 110-116, doi:10.1016/j.jcrysgro.2007.07.050 (2007).
- 64 Burbank, M. *et al.* Geotechnical Tests of Sands Following Bioinduced Calcite Precipitation Catalyzed by Indigenous Bacteria. *Journal of Geotechnical and Geoenvironmental Engineering* **139**, 928-936, doi:10.1061/(asce)gt.1943-5606.0000781 (2013).
- 65 Herzig, J. P., Leclerc, D. M. & Goff, P. L. Flow Suspensions through Porous Media - Application to Deep Filtration. *Industrial and Engineering Chemistry* **62** (1970).
- 66 Tobler, D. J., Cuthbert, M. O. & Phoenix, V. R. Transport of Sporosarcina pasteurii in sandstone and its significance for subsurface engineering technologies. *Applied Geochemistry* **42**, 38-44, doi:10.1016/j.apgeochem.2014.01.004 (2014).
- 67 Anthony, J. W., Bideaux, R. A., Bladh, K. W. & Nichols, M. C. *Handbook of Mineralogy*. (2003).
- 68 Mitchell, J. K. & Santamarina, J. C. Biological Considerations in Geotechnical Engineering. *Journal of Geotechnical and Geoenvironmental Engineering* **131**, 1222-1233, doi:10.1061//asce/1090-0241/2005/131:10/1222 (2005).

- 69 Shen, Q. *et al.* Properties of Amorphous Calcium Carbonate and the Template Action of Vaterite Spheres. *Journal of Physical Chemical B* **110**, 2994-3000 (2006).
- 70 Rice, M. A. & McEwan, I. K. Crust strength: a wind tunnel study of the effect of impact by saltating particles on cohesive soil surfaces. *Earth Surface Processes and Landforms* **26**, 721-733, doi:10.1002/esp.217 (2001).

Acknowledgements

I would like to thank my advisor, Dr. Eric A. Seagren for giving me the opportunity to conduct the culmination of this research. Additionally, this work would not have been completed without the support from Dr. Stanley Vitton, and Dr. Thomas Oommen. Their knowledge and expertise have been invaluable to this research. I would also like to extend my gratitude to Rob Fritz and Kiko de Melo e Silva for providing essential resources and skills to build and test equipment that was necessary to complete various studies. Furthermore, I would like to thank Bonnie Zwissler for her knowledge and assistance for the duration of my research, and thank the undergraduate assistants who have been a great asset. Additionally, this project was funded by National Science Foundation grant number 1234126. Everyone has been helpful in guiding this research along, and has proved invaluable for the success of this project. Thank you.

APPENDIX A - Syringe Barrel Bioreactors

Table A.8.1: pH of syringe barrel bioreactor effluent.

Hours	Days	R1	R1*	R2	R2*	R3	R3*
0	0	8	8	8	8.1	8	7.5
17	0.7	8.25	8.25	7.75	7.75	7.25	7.25
21	0.9	8.75	8.75	8.25	8.25	7.75	7.75
38	1.6	8.75	8.75	7.75	7.75	7.25	7.75
45	1.9	8.57	8.58	8.67	8.64	8.3	8.31
62	2.6	8.75	8.75	7.75	7.75	7.25	7.25
69	2.9	8.3	8.4	8.48	8.5	8.11	8.22
86	3.6	8.5	8.5	6.95	6.95	6.95	6.95
93	3.9	8.48	8.4	7.98	7.88	7.98	7.84
110	4.6	8.85	8.3	6.95	7.25	6.65	6.65
117	4.9	9.05	8.9	7.61	7.67	7.98	7.53
134	5.6	9	9	7.9	8.2	8	8.3
141	5.9	9.03	8.95	8.33	8.54	8.5	8.54
158	6.6	9.25	9	8	8.85	8.2	8.4
165	6.9	8.82	8.85	9.25	8.8	8.62	8.78
182	7.6	8.85	9	9.25	9.25	8.85	9
189	7.9	8.87	8.88	8.85	8.87	8.85	8.89
206	8.6	8.85	8.85	9	8.85	9	9
213	8.9	8.87	8.84	8.93	8.86	8.82	8.91
230	9.6	8.7	8.7	8.85	8.85	9	9

Table A.8.2: Raw data for viable plate counts in the syringe barrel bioreactors. “TMC” denotes “Too Many to Counts”.

Reactor 1 - Inoculated, Urea-CaCl2				
	L0	L1	L2	L3
10^{-3}	TMC	403	68	0
10^{-4}	110	63	9	0
10^{-5}	15	5	0	0
10^{-6}	3	0	1	0
10^{-7}	0	0	0	0
<i>Mass in Blender</i>	1.007	1.01	1.007	1.01

Reactor 1* - Inoculated, Urea-CaCl2				
	L0	L1	L2	L3
10^{-3}	331	167	2	7
10^{-4}	40	17	0	0
10^{-5}	5	0	1	0
10^{-6}	1	0	0	0
10^{-7}	0	0	0	0
<i>Mass in Blender</i>	1.007	1.009	1.004	1.002

Reactor 2 - Native, Urea-CaCl2				
	L0	L1	L2	L3
10^{-3}	63	6	0	0
10^{-4}	32	0	0	0
10^{-5}	1	0	0	0
10^{-6}	0	0	0	0
10^{-7}	0	0	0	0
<i>Mass in Blender</i>	1.007	1.005	1.003	1.001

Reactor 2* - Native, Urea-CaCl2				
	L0	L1	L2	L3
10^{-3}	TMC	110	64	0
10^{-4}	93	10	2	0
10^{-5}	5	0	1	0
10^{-6}	0	0	0	0
10^{-7}	0	0	0	0
<i>Mass in Blender</i>	1.001	1.009	1.005	1.007

Reactor 3 - Autoclaved, Urea-CaCl2				
	L0	L1	L2	L3
10^{-3}	6	0	0	0
10^{-4}	0	0	0	0
10^{-5}	0	0	0	0
10^{-6}	0	0	0	0
10^{-7}	0	0	0	TMC
<i>Mass in Blender</i>	1.018	1.007	1.019	1.011

Reactor 3* - Autoclaved, Urea-CaCl2				
	L0	L1	L2	L3
10^{-3}	41	22	0	0
10^{-4}	7	0	0	0
10^{-5}	0	1	0	0
10^{-6}	0	0	0	0
10^{-7}	0	0	0	0
<i>Mass in Blender</i>	1.005	1.009	1.003	1.002

Table A.8.3: Raw data for specific gravity measurements of the syringe barrel bioreactors R2*, R3, and R3*. Grayed data indicates a non-composite sample.

Reactor 1					Reactor 1*					Reactor 2				
Tin #	Layer	Weight Cup	Weight Cup + Soil	Mass Soil	Tin #	Layer	Weight Cup	Weight Cup + Soil	Mass Soil	Tin #	Layer	Weight Cup	Weight Cup + Soil	Mass Soil
	0	2.08826	12.0996	10.01134		0	2.08822	12.13604	10.04782		0	2.08829	12.19144	10.1032
1	1	2.09035	12.02965	9.93934	4	1	2.08986	12.40874	10.31888	7	1	2.08801	2.46394	0.37593
2	2	2.08985	13.14751	11.05766	5	2	2.08994	12.45185	10.36191	8	2	2.09018	12.42731	10.3371
3	3	2.0881	12.12827	10.04017	6	3	2.08815	12.14896	10.06081	9	3	2.0882	12.10044	10.0122

Bin	Run	Specific Gravity	Deviation		Bin	Run	Specific Gravity	Deviation		Bin	Run	Specific Gravity	Deviation	
L0	1	2.9471	0.0071		L0	1	2.9583	0.0077		L0	1	2.9613	0.0077	
	2	2.9415	0.0014			2	2.952	0.0034			2	2.957	0.0034	
	3	2.9375	-0.0026			3	2.949	-0.0014			3	2.9522	-0.0014	
	4	2.937	-0.0031			4	2.9464	-0.0042			4	2.9494	-0.0042	
	5	2.9373	-0.0028			5	2.9458	-0.0055			5	2.9481	-0.0055	
L1	1	2.9722	0.0065		L1	1	2.9705	0.0047		L1	1	2.977	0.0094	
	2	2.9668	0.0012			2	2.9673	0.0015			2	2.9697	0.0021	
	3	2.9644	0.0012			3	2.9637	-0.0021			3	2.9653	-0.0023	
	4	2.9629	0.0027			4	2.9641	-0.0017			4	2.9637	-0.0039	
	5	2.9619	0.0038			5	2.9635	-0.0023			5	2.9622	-0.0054	
L2	1	2.9823	0.0101		L2	1	2.9737	0.007		L2	1	2.9812	0.0093	
	2	2.9751	0.0029			2	2.9673	0.0006			2	2.9741	0.0022	
	3	2.9699	0.0023			3	2.965	0.0017			3	2.97	-0.0019	
	4	2.9676	0.0046			4	2.9667	0.001			4	2.9681	-0.0038	
	5	2.9661	0.0061			5	2.9608	0.0059			5	2.9663	-0.0056	
L3	1	2.9948	0.0159		L3	1	2.9884	0.0127		L3	1	2.9957	0.0166	
	2	2.9811	0.0022			2	2.9781	0.0025			2	2.9882	0.0091	
	3	2.9748	-0.0041			3	2.9731	-0.0026			3	2.9734	-0.0057	
	4	2.9723	-0.0066			4	2.9697	-0.006			4	2.9691	-0.01	
	5	2.9716	-0.0073			5	2.9691	-0.0066			5	2.9691	-0.01	

Table A.8.4: Raw data for specific gravity measurements of the syringe barrel bioreactors R2*, R3, and R3*.

Reactor 2*				
Tin #	Layer	Weight Cup	Weight Cup + Soil	Mass Soil
	0	2.08865	12.1456	10.05695
	1	2.08885	12.22908	10.14023
	2	2.08885	12.09985	10.011
	3	2.08878	12.16054	10.07176

Reactor 3				
Tin #	Layer	Weight Cup	Weight Cup + Soil	Mass Soil
	0	2.08895	12.21902	10.13007
	1	2.008872	12.2191	10.21023
	2	2.08873	12.62886	10.54013
	3	2.08869	12.01904	9.93035

Reactor 3*				
Tin #	Layer	Weight Cup	Weight Cup + Soil	Mass Soil
	Top	2.0887	12.19261	10.10391
	1	2.08849	12.29757	10.20908
	2	2.08896	12.09437	10.00541
	3	2.0889	12.12603	10.03713

Bin	Run	Specific Gravity	Deviation	
L0	1	2.9608	0.0095	
	2	2.9534	0.0021	
	3	2.949	-0.0024	
	4	2.9472	-0.0042	
	5	2.9464	-0.005	
L1	1	2.9715	0.009	
	2	2.9647	0.0022	
	3	2.9605	-0.0021	
	4	2.9583	-0.0042	
	5	2.9575	-0.005	
L2	1	2.9768	0.0097	
	2	2.9696	0.0025	
	3	2.9648	-0.0023	
	4	2.9626	-0.0045	
	5	2.9616	-0.0055	
L3	1	2.9634	0.0009	
	2	2.9625	0	
	3	2.9627	0.0001	
	4	2.9626	0	
	5	2.9616	-0.001	

Bin	Run	Specific Gravity	Deviation	
L0	1	2.9611	0.0077	
	2	2.9552	0.0019	
	3	2.9514	-0.0019	
	4	2.9499	-0.0034	
	5	2.9491	-0.0043	
L1	1	2.9723	0.0076	
	2	2.9662	0.0015	
	3	2.9634	-0.0014	
	4	2.9609	-0.0038	
	5	2.961	-0.0038	
L2	1	2.9725	0.0063	
	2	2.9673	0.0011	
	3	2.9650	-0.0012	
	4	2.9637	-0.0025	
	5	2.9626	-0.0036	
L3	1	2.9848	0.0105	
	2	2.9772	0.0029	
	3	2.9715	-0.0029	
	4	2.9691	-0.0052	
	5	2.9691	-0.0052	

Bin	Run	Specific Gravity	Deviation	
L0	1	2.9534	0.0072	
	2	2.9476	0.0014	
	3	2.9446	-0.0015	
	4	2.9431	-0.0031	
	5	2.9423	-0.0039	
L1	1	2.9759	0.01	
	2	2.9673	0.0013	
	3	2.9636	-0.0024	
	4	2.9621	-0.0039	
	5	2.9608	-0.0051	
L2	1	2.9709	0.0048	
	2	2.9667	0.0008	
	3	2.9648	-0.0011	
	4	2.9639	-0.002	
	5	2.9633	-0.0026	
L3	1	2.9861	0.0119	
	2	2.977	0.0027	
	3	2.9716	-0.0027	
	4	2.9689	-0.0054	
	5	2.9679	-0.0064	

Table A.8.5: Raw data for the pressure-calculator method in the syringe barrel bioreactors.

Syringe 1					
Layer	Mass Soil in Bottle	6-Hour Pressure	2	3	Average
0	1.004	2.99	2.99	2.99	2.99
1	1.009	3.27	3.27	3.27	3.27
2	1.002	3.26	3.26	3.26	3.26
3	1.002	3.71	3.71	3.71	3.71

Syringe 1*					
Layer	Mass Soil in Bottle	6-Hour Pressure	2	3	Average
0	1.001	2.94	2.94	2.94	2.94
1	1.006	3.33	3.33	3.33	3.33
2	1.004	3.26	3.26	3.26	3.26
3	1.002	3.62	3.62	3.62	3.62

Syringe 2					
Layer	Mass Soil in Bottle	6-Hour Pressure	2	3	Average
0	1	3.29	3.29	3.29	3.29
1	1.001	3.38	3.38	3.38	3.38
2	1.007	2.46	2.46	2.46	2.46
3	1.002	3.63	3.63	3.63	3.63

Syringe 2*					
Layer	Mass Soil in Bottle	6-Hour Pressure	2	3	Average
0	1.003	3.16	3.16	3.16	3.16
1	1.004	3.54	3.54	3.54	3.54
2	1	3.66	3.66	3.66	3.66
3	1.002	3.58	3.58	3.58	3.58

Syringe 3					
Layer	Mass Soil in Bottle	6-Hour Pressure	2	3	Average
0	1.001	2.96	2.96	2.96	2.96
1	1	3.51	3.51	3.51	3.51
2	1.003	3.52	3.52	3.52	3.52
3	1.004	3.52	3.52	3.52	3.52

Syringe 3*					
Layer	Mass Soil in Bottle	6-Hour Pressure	2	3	Average
0	1.004	3.07	3.08	3.08	3.077
1	1	3.45	3.45	3.45	3.45
2	1.002	3.52	3.52	3.52	3.52
3	1.001	3.68	3.68	3.68	3.68

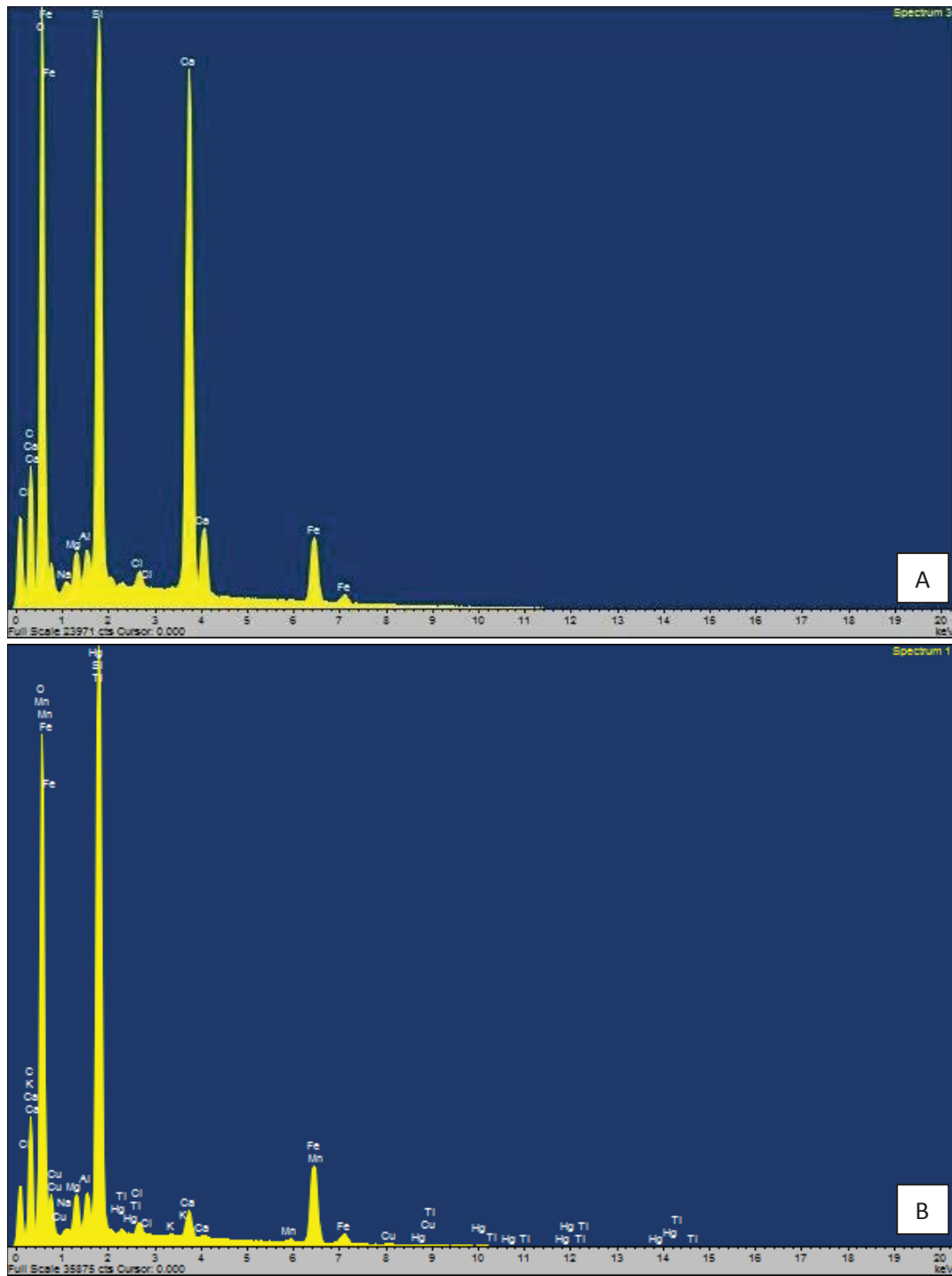


Figure A.1: EDS Spectra of R1 for the white surface crust precipitate (Plot A) and surface mine tailing powder (Plot B)

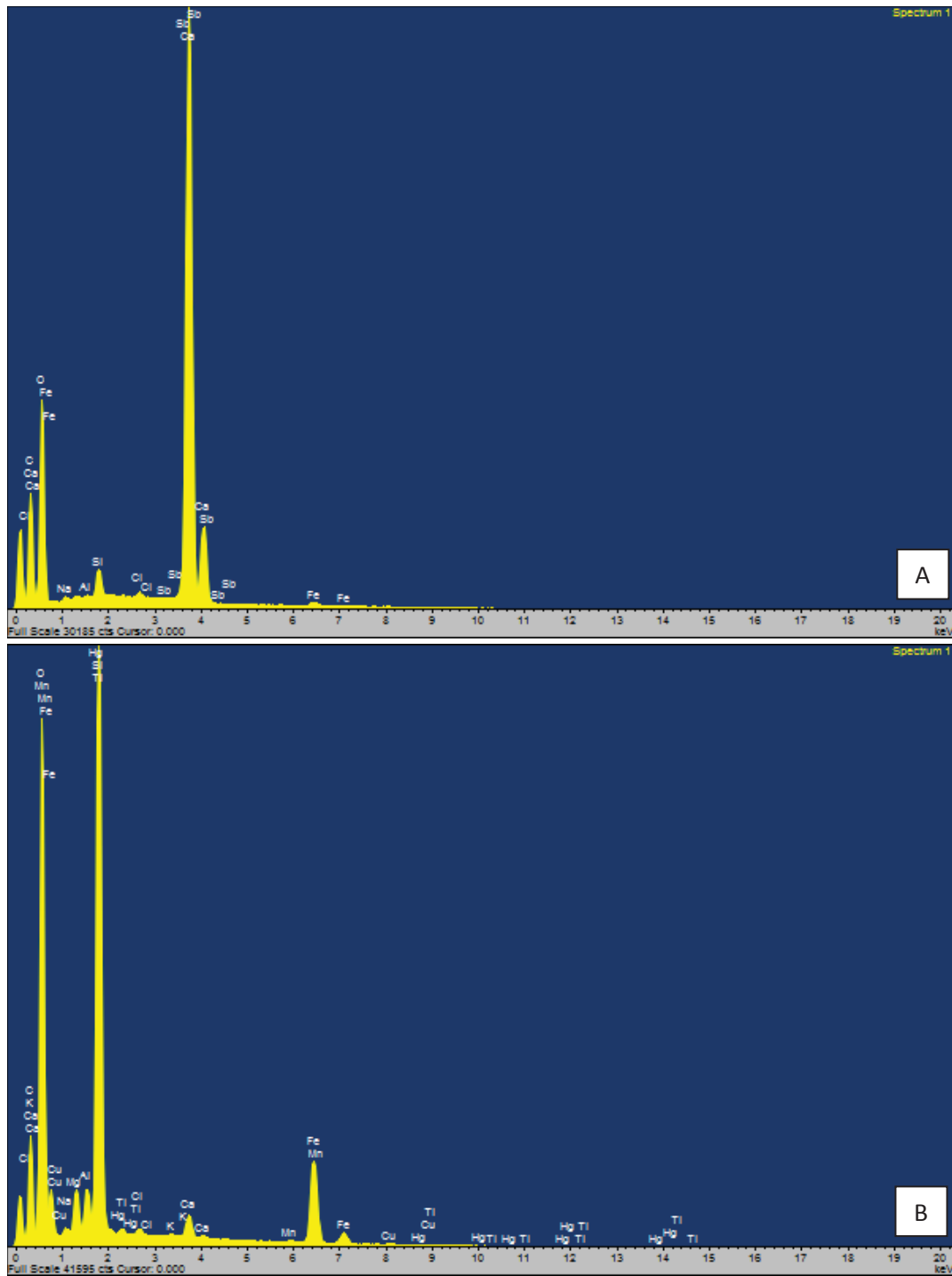


Figure A.2: EDS Spectra of R2 for the white surface crust precipitate (Plot A) and surface mine tailing powder (Plot B)

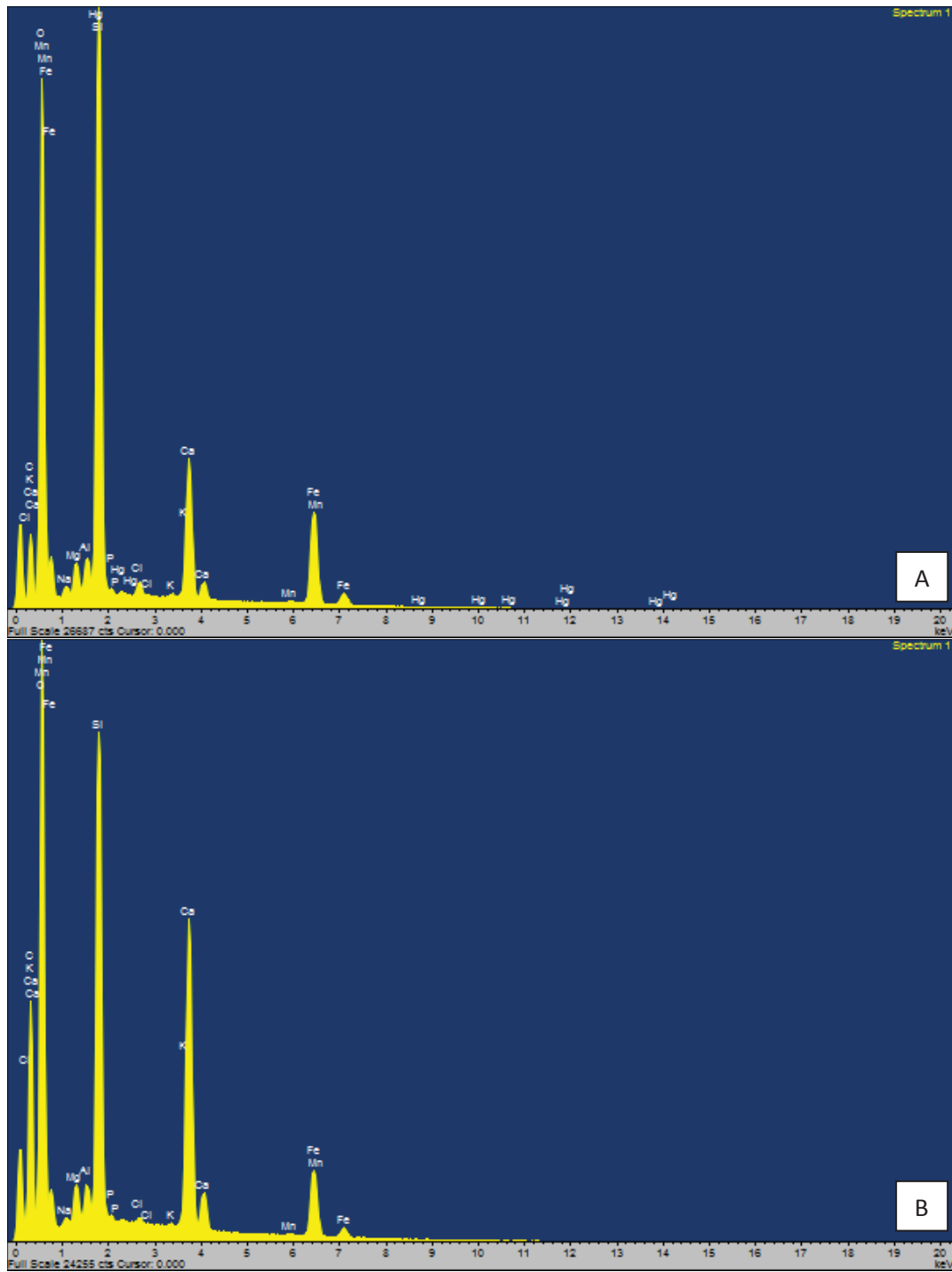


Figure A.3: EDS Spectra of R3 for the white surface crust precipitate (Plot A) and surface mine tailing powder (Plot B)

Table A.8.6: Complete EDS analysis of syringe barrel surface crust layers for R1, R2, and R3.

Reactor	Type	EDS Analysis (Percent by wt.)															
		C	O	Na	Mg	Al	Si	P	Cl	K	Ca	Mn	Fe	Cu	Hg	Ti	Sb
R1	<i>Crust</i>	-	51.92	0.31	0.88	0.68	12.81	-	0.54	-	22.77	-	10.09	-	-	-	-
	<i>Powder</i>	-	46.71	0.35	1.71	1.43	24.05	-	0.78	0.13	2.06	0.54	21.24	0.03	0.52	0.45	-
R2	<i>Crust</i>	10.71	44.46	0.18	-	0.07	0.99	-	0.25	-	41.34	-	0.95	-	-	-	1.05
	<i>Powder</i>	21.35	40.51	0.25	1.30	1.12	16.71	-	0.24	0.08	1.22	0.38	16.09	-0.04	0.44	0.34	-
R3	<i>Crust</i>	13.23	42.18	0.42	0.91	0.87	16.11	0.27	0.55	0.14	7.38	0.34	17.14	-	0.47	-	-
	<i>Powder</i>	24.49	42.81	0.20	0.75	0.61	9.56	0.14	0.18	0.10	11.79	0.27	9.10	-	-	-	-

APPENDIX B - Soil Box Bioreactors

Table B.1: pH of bioreactor effluent in the soil box bioreactors. Day 6, R1* is an interpolated value.

Hours	Days	R1	R1*	R2	R2*	R3	R3*
0	0	8.15	8.15	8.82	8.66	8.74	8.64
7	0.3	8.04	8.08	8.62	8.29	8.63	8.59
24	1	8.04	8.08	8.7	8.87	8.6	8.7
31	1.3	7.97	7.99	8.61	8.91	8.5	8.62
48	2	7.84	7.9	8.4	8.88	8.39	8.6
55	2.3	7.82	7.85	8.32	7.87	8.16	8.46
72	3	7.91	7.89	8.26	8.86	8.09	8.42
79	3.3	8.22	8.1	8.17	7.97	7.81	8.34
96	4	8.54	8.34	8.07	8.81	7.68	8.29
103	4.3	8.66	8.4	7.97	8.79	7.66	8.17
120	5	8.8	8.56	7.87	8.82	7.59	8.14
127	5.3	8.84	8.62	7.78	8.45	7.6	8.04
144	6	8.93	8.69	7.8	8.79	7.67	7.9
151	6.3	8.95	8.76	7.92	8.74	7.79	7.9
168	7	8.92	8.79	7.77	8.76	7.98	7.82
175	7.3	8.92	8.8	8.24	8.78	8.32	7.78
193.2	8.1	9.02	8.9	8.56	8.78	8.65	7.83
200	8.3	9	8.89	8.73	8.81	8.76	7.88
217	9.0	9.06	8.93	8.85	8.87	8.94	7.88
224	9.3	9.05	8.92	8.91	8.87	8.99	7.88
241	10.0	8.87	8.74	8.77	8.65	8.87	7.75
248	10.3	8.9	8.75	8.81	8.64	8.89	7.71
265	11.0	8.87	8.8	8.89	8.62	8.96	7.57
272	11.3	8.93	8.77	8.89	8.73	8.97	7.79
289	12.0	8.94	8.76	8.9	8.62	9	8.06
296	12.3	8.94	8.75	8.9	8.66	8.96	8.06
313	13.0	9	8.83	8.98	8.71	9.09	8.37
326	13.6	8.92	8.72	8.9	8.64	8.97	8.5
338	14.1	9.1	8.9	9.07	8.82	9.15	8.78
345	14.4	9.05	8.85	9.04	8.82	9.11	8.83
362	15.1	8.98	8.78	8.99	8.68	9.05	8.84
369	15.4	8.92	8.74	8.94	8.7	9.02	8.85
386	16.1	8.92	8.72	8.9	8.6	8.96	8.82
393	16.4	8.91	8.73	8.92	8.66	8.97	8.86
410	17.1	8.93	8.75	8.94	8.67	8.99	8.92
417	17.4	8.94	8.75	8.93	8.72	8.98	8.89
434	18.1	8.99	8.82	9.01	8.76	9.05	8.97
441	18.4	9	8.82	9	8.77	9.04	8.97
458	19.1	9.02	8.85	9.02	8.83	9.06	8.99
465	19.4	9.02	8.86	9.03	8.81	9.09	9.04
482.5	20.1	8.98	8.8	8.97	8.74	9.04	8.98
488.5	20.4	8.95	8.78	8.93	8.71	8.99	8.95
507	21.1	8.99	8.81	8.98	8.76	9.04	8.97
513	21.4	8.94	8.76	8.94	8.71	9	8.92
530.75	22.1	8.99	8.78	8.98	8.76	9.05	8.99
537	22.4	8.94	8.72	8.91	8.7	8.98	8.92

Table B.2: Percolation and flow data for soil box bioreactors.

Time			Volume in Graduated Cylinder						Flow (mL/hour)					
Hours	Days	Hours	R1	R1*	R2	R2*	R3	R3*	R1	R1*	R2	R2*	R3	R3*
0	0	-	19	23	33	6	38	26.5	-	-	-	-	-	-
7	0.3	7.0	10	10.5	15	2.5	17	11	1.4	1.5	2.1	0.4	2.4	1.6
24	1	17.0	26	25.5	31.5	6.5	39	25	1.5	1.5	1.9	0.4	2.3	1.5
31	1.3	7.0	11.5	11	12.5	2	11	9	1.6	1.6	1.8	0.3	1.6	1.3
48	2	17.0	27.5	23.5	29	6.5	25	21.5	1.6	1.4	1.7	0.4	1.5	1.3
55	2.3	7.0	12.5	10	12.5	3	14	10	1.8	1.4	1.8	0.4	2.0	1.4
72	3	17.0	28	21	28	6.5	43	23	1.6	1.2	1.6	0.4	2.5	1.4
79	3.3	7.0	12.5	9	11.5	3	18	10	1.8	1.3	1.6	0.4	2.6	1.4
96	4	17.0	28.5	22	27.5	7	44.5	23.5	1.7	1.3	1.6	0.4	2.6	1.4
103	4.3	7.0	12	9	11	2.5	18	9	1.7	1.3	1.6	0.4	2.6	1.3
120	5	17.0	28.5	21	26.5	6.5	43	23	1.7	1.2	1.6	0.4	2.5	1.4
127	5.3	7.0	11	8	10	2.5	17	9.5	1.6	1.1	1.4	0.4	2.4	1.4
144	6	17.0	30	20	26	7.5	44	23	1.8	1.2	1.5	0.4	2.6	1.4
151	6.3	7.0	11	7.5	9	2.5	16	8.5	1.6	1.1	1.3	0.4	2.3	1.2
168	7	17.0	27.5	19	22.5	7	42.5	24	1.6	1.1	1.3	0.4	2.5	1.4
175	7.3	7.0	11.5	7.5	9	3	17.5	10	1.6	1.1	1.3	0.4	2.5	1.4
193.2	8.1	18.2	21.5	18.5	23	7	35	26.5	1.2	1.0	1.3	0.4	1.9	1.5
200	8.3	6.8	10	5.5	7	3	13.5	8	1.5	0.8	1.0	0.4	2.0	1.2
217	9.0	17.0	30	18	21.5	7	43.5	25	1.8	1.1	1.3	0.4	2.6	1.5
224	9.3	7.0	12	9	8.5	3	17.5	10	1.7	1.3	1.2	0.4	2.5	1.4
241	10.0	17.0	29.5	17.5	21	6.5	42	23	1.7	1.0	1.2	0.4	2.5	1.4
248	10.3	7.0	11	6	9	2	16	8.5	1.6	0.9	1.3	0.3	2.3	1.2
268	11.2	20.0	35.5	20	29	7.5	50	27.5	1.8	1.0	1.5	0.4	2.5	1.4
272	11.3	4.0	-	-	-	-	-	-	-	-	-	-	-	-
289	12.0	17.0	30	16	25	5.5	42.5	12	1.8	0.9	1.5	0.3	2.5	0.7
296	12.3	7.0	11.5	6	9.5	2	16	10	1.6	0.9	1.4	0.3	2.3	1.4
313	13.0	17.0	22	20	25	5	41	27.5	1.3	1.2	1.5	0.3	2.4	1.6
326	13.6	13.0	19.5	10	17	4	26	11	1.5	0.8	1.3	0.3	2.0	0.8
338	14.1	12.0	22.5	15	18.5	4.5	30.5	22	1.9	1.3	1.5	0.4	2.5	1.8
345	14.4	7.0	12.5	9	10.5	2.5	17.5	11	1.8	1.3	1.5	0.4	2.5	1.6
362	15.1	17.0	27	18	22.5	5.5	37.5	21	1.6	1.1	1.3	0.3	2.2	1.2
369	15.4	7.0	12	8	10	2.5	16	10.5	1.7	1.1	1.4	0.4	2.3	1.5
386	16.1	17.0	21	20	23	5.5	32.5	25	1.2	1.2	1.4	0.3	1.9	1.5
393	16.4	7.0	10	6.5	7.5	2	13.5	7	1.4	0.9	1.1	0.3	1.9	1.0
410	17.1	17.0	30.5	19	22	5.5	39	24	1.8	1.1	1.3	0.3	2.3	1.4
417	17.4	7.0	10	6	7	2	13	8	1.4	0.9	1.0	0.3	1.9	1.1
434	18.1	17.0	30	18	23	5.5	39	24	1.8	1.1	1.4	0.3	2.3	1.4
441	18.4	7.0	13	8	9	2.5	16.5	10	1.9	1.1	1.3	0.4	2.4	1.4
458	19.1	17.0	28.5	15.5	21	5.25	36	22.5	1.7	0.9	1.2	0.3	2.1	1.3
465	19.4	7.0	12	5.5	8.5	2	15	9	1.7	0.8	1.2	0.3	2.1	1.3
482.5	20.1	17.5	31.5	17	24	5.75	40	25	1.8	1.0	1.4	0.3	2.3	1.4
488.5	20.4	6.0	11	6	8	2	13.5	8.5	1.8	1.0	1.3	0.3	2.3	1.4
507	21.1	18.5	34	18	26.5	6	42	25	1.8	1.0	1.4	0.3	2.3	1.4
513	21.4	6.0	-	-	-	-	-	-	-	-	-	-	-	-
530.75	22.1	17.8	32	16.5	25.5	5.75	40.5	24	1.8	0.9	1.4	0.3	2.3	1.4
537	22.4	6.3	12	6.25	9.5	2	16	9	1.9	1.0	1.5	0.3	2.6	1.4

Table B.3: Raw data for viable plate counts in the soil box bioreactors. “TMC” denotes “Too Many to Count”.

Reactor 1 - Inoculated, Urea-CaCl2				
	L1	L2	L3	L4
10^{-3}	TMC	TMC	11	0
10^{-4}	TMC	171	4	0
10^{-5}	139	33	0	0
10^{-6}	15	3	0	0
10^{-7}	4	0	0	0
<i>Mass in Blender</i>	1.002	1.002	1.001	1.002

Reactor 1* - Inoculated, Urea-CaCl2				
	L1	L2	L3	L4
10^{-3}	TMC	17	8	11
10^{-4}	TMC	0	1	2
10^{-5}	137	3	0	0
10^{-6}	14	0	10	1
10^{-7}	2	1	0	0
<i>Mass in Blender</i>	1.007	1.002	1	1.006

Reactor 2 - Native, Urea-CaCl2				
	L1	L2	L3	L4
10^{-3}	TMC	162	24	8
10^{-4}	TMC	12	0	3
10^{-5}	35	0	0	0
10^{-6}	10	0	0	0
10^{-7}	3	0	0	0
<i>Mass in Blender</i>	1.002		1.005	1.002

Reactor 2* - Native, Urea-CaCl2				
	L1	L2	L3	L4
10^{-3}	TMC	283	2	40
10^{-4}	TMC	47	2	3
10^{-5}	109	2	1	4
10^{-6}	18	0	3	1
10^{-7}	2	2	2	0
<i>Mass in Blender</i>		1.003	1.003	1.003

Reactor 3 - Autoclaved, Urea-CaCl2				
	L1	L2	L3	L4
10^{-3}	TMC	160	0	0
10^{-4}	TMC	10	0	0
10^{-5}	51	1	0	0
10^{-6}	11	0	0	0
10^{-7}	0	0	0	0
<i>Mass in Blender</i>	1.004	1	1.009	1.004

Reactor 3* - Autoclaved, Urea-CaCl2				
	L1	L2	L3	L4
10^{-3}	TMC	107	1	0
10^{-4}	TMC	9	0	0
10^{-5}	126	0	0	0
10^{-6}	12	0	0	2
10^{-7}	1	0	0	0
<i>Mass in Blender</i>	1.004	1.003	1.006	1.008

Table B.4: Raw data for specific gravity measurements of the soil box bioreactors R1, R1*, and R2.

Reactor 1					Reactor 1*					Reactor 2				
Tin #	Layer	Weight Cup	Weight Cup + Soil	Mass Soil	Tin #	Layer	Weight Cup	Weight Cup + Soil	Mass Soil	Tin #	Layer	Weight Cup	Weight Cup + Soil	Mass Soil
	0	2.08808	4.49566	2.40758		0	2.08736	4.16465	2.07729		0	2.08707	4.59285	2.50578
	1	2.08745	3.58882	1.50137		1	2.08786	7.07552	4.98766		1	2.08769	7.96047	5.87278
	2	2.08792	6.34632	4.2584		2	2.08751	8.88216	6.79465		2	2.08787	12.03501	9.94714
	3	2.08776	10.34288	8.25512		3	2.08743	10.4907	8.40327		3	2.08786	10.26587	8.17801
	4	2.08821	12.50601	10.4178		4	2.08764	12.10046	10.01282		4	2.0878	13.69744	11.6096

Bin	Run	Specific Gravity	Deviation		Bin	Run	Specific Gravity	Deviation		Bin	Run	Specific Gravity	Deviation	
L0	1	2.5997	0.0022		L0	1	2.5521	0.0014		L0	1	2.7924	0.0033	
	2	2.6003	0.0029			2	2.5475	-0.0032			2	2.7897	0.0007	
	3	2.5987	0.0012			3	2.5523	0.0015			3	2.7886	-0.004	
	4	2.5955	-0.0019			4	2.5486	-0.0022			4	2.7868	-0.0023	
	5	2.5929	-0.0045			5	2.5532	-0.0025			5	2.7878	-0.0013	
L1	1	2.8616	0.0044		L1	1	2.9007	0.0031		L1	1	2.9319	0.0055	
	2	2.8565	-0.0006			2	2.8995	0.0019			2	2.9298	0.0034	
	3	2.859	0.0018			3	2.8967	-0.001			3	2.9249	-0.0015	
	4	2.8537	-0.0035			4	2.8957	-0.0019			4	2.9246	-0.0018	
	5	2.855	-0.0021			5	2.8956	-0.002			5	2.9208	-0.0056	
L2	1	2.9357	0.0065		L2	1	2.957	0.0107		L2	1	2.9649	0.0089	
	2	2.993	0.0039			2	2.9474	0.0011			2	2.9586	0.0027	
	3	2.9144	-0.0147			3	2.9452	-0.0012			3	2.9542	-0.0018	
	4	2.9324	0.0033			4	2.942	-0.0044			4	2.9516	-0.0043	
	5	2.9301	0.001			5	2.9401	-0.0063			5	2.9504	-0.0055	
L3	1	2.9657	0.0108		L3	1	2.9732	0.011		L3	1	2.9734	0.0097	
	2	2.9571	0.0022			2	2.9656	0.0034			2	2.9669	0.0032	
	3	2.9528	-0.0021			3	2.9587	-0.0034			3	2.962	-0.0017	
	4	2.9505	-0.0044			4	2.9575	-0.0047			4	2.9582	-0.0055	
	5	2.9485	-0.0064			5	2.9558	-0.0063			5	2.9579	-0.0058	
L4	1	2.9889	0.0155		L4	1	2.9751	0.0101		L4	1	2.9734	0.0094	
	2	2.9776	0.0041			2	2.966	0.0031			2	2.9661	0.0021	
	3	2.9601	-0.0034			3	2.961	-0.002			3	2.9623	-0.0017	
	4	2.9668	-0.0066			4	2.9581	-0.0049			4	2.9598	-0.0042	
	5	2.9639	-0.0095			5	2.9568	-0.0062			5	2.9583	-0.0057	

Table B.5: Raw data for specific gravity measurements of the soil box bioreactors R2*, R3, and R3*.

Reactor 2*					Reactor 3					Reactor 3*				
Tin #	Layer	Weight Cup	Weight Cup + Soil	Mass Soil	Tin #	Layer	Weight Cup	Weight Cup + Soil	Mass Soil	Tin #	Layer	Weight Cup	Weight Cup + Soil	Mass Soil
	0	2.0869	3.78324	1.69634		0	2.08682	4.58188	2.49506		0	2.08695	4.184	2.09705
	1	2.08763	6.13128	4.04365		1	2.0875	5.84137	3.75387		1	2.08768	6.02608	3.9384
	2	2.08739	11.45334	9.36595		2	2.0883	10.15792	8.06962		2	2.08773	10.3736	8.28587
	3	2.08753	10.17018	8.08265		3	2.0883	11.07922	8.990921		3	2.0881	11.24897	9.16087
	4	2.0872	12.44617	10.35897		4	2.0883	14.01141	11.92311		4	2.008831	12.87373	10.8649

Bin	Run	Specific Gravity	Deviation		Bin	Run	Specific Gravity	Deviation		Bin	Run	Specific Gravity	Deviation	
L0	1	2.765	0.001		L0	1	2.6777	-0.0007		L0	1	2.7403	0.0045	
	2	2.7618	-0.0021			2	2.679	0.0005			2	2.736	0.0002	
	3	2.765	0.001			3	2.6804	0.002			3	2.735	-0.0008	
	4	2.7653	0.0014			4	2.6754	-0.003			4	2.7339	-0.0019	
	5	2.7627	-0.0013			5	2.6797	0.0012			5	2.7339	-0.0019	
L1	1	2.9347	0.0049		L1	1	2.9442	0.0034		L1	1	2.9469	0.011	
	2	2.9313	0.0015			2	2.944	0.0032			2	2.9361	0.0002	
	3	2.9292	-0.0006			3	2.9415	0.0007			3	2.9624	-0.0035	
	4	2.929	-0.0008			4	2.9383	-0.0025			4	2.9321	-0.0038	
	5	2.9247	-0.0051			5	2.9358	-0.0049			5	2.9322	-0.0038	
L2	1	2.9564	0.0076		L2	1	2.9706	0.0084		L2	1	2.9695	0.0083	
	2	2.9506	0.0018			2	2.9636	0.0015			2	2.9629	0.0017	
	3	2.9476	-0.0012			3	2.9614	-0.0007			3	2.9598	-0.0014	
	4	2.9454	-0.0034			4	2.9586	-0.0035			4	2.9569	-0.0043	
	5	2.9439	-0.0049			5	2.9564	-0.0058			5	2.9569	-0.0043	
L3	1	2.9659	0.0083		L3	1	2.9813	0.0097		L3	1	2.9823	0.0094	
	2	2.9598	0.0022			2	2.9734	0.0018			2	2.9745	0.0016	
	3	2.9557	-0.0019			3	2.9696	-0.002			3	2.9709	-0.002	
	4	2.9539	-0.0037			4	2.9669	-0.0047			4	2.9689	-0.004	
	5	2.9527	-0.0049			5	2.9667	-0.0049			5	2.9679	-0.005	
L4	1	2.9709	0.0093		L4	1	2.9875	0.01		L4	1	2.9936	0.0128	
	2	2.9634	0.0018			2	2.9803	0.0028			2	2.9836	0.0028	
	3	2.9593	-0.0022			3	2.9753	-0.0022			3	2.9778	-0.003	
	4	2.9575	-0.0041			4	2.9725	-0.0049			4	2.9752	-0.0056	
	5	2.9538	-0.0048			5	2.9718	-0.0057			5	2.9737	-0.0071	

Table B.6: Raw data for the pressure-calculator method in the soil box bioreactors.

Bioreactor 1					
Layer	Mass Soil in Bottle	6-Hour Pressure	2	3	Average
0	1.001	14.84	14.84	14.83	14.84
1	1.003	4.8	4.8	4.8	4.8
2	1.005	3.19	3.19	3.19	3.19
3	1.004	3.75	3.75	3.75	3.75
4	1.004	3.97	3.97	3.97	3.97

Bioreactor 1*					
Layer	Mass Soil in Bottle	6-Hour Pressure	2	3	Average
0	1.002	10.95	10.94	10.94	10.94
1	1.003	3.4	3.4	3.4	3.4
2	1.001	3.65	3.66	3.65	3.65
3	1.003	3.79	3.79	3.79	3.79
4	1.004	4.02	4.02	4.02	4.02

Bioreactor 2					
Layer	Mass Soil in Bottle	6-Hour Pressure	2	3	Average
0	1	9.8	9.8	9.8	9.8
1	1.002	3.85	3.85	3.85	3.85
2	1.003	3.99	3.99	3.99	3.99
3	1.004	3.77	3.77	3.77	3.77
4	1	4.02	4.02	4.02	4.02

Bioreactor 2*					
Layer	Mass Soil in Bottle	6-Hour Pressure	2	3	Average
0	1.001	7.01	7.01	7.01	7.01
1	1.002	3.4	3.4	3.4	3.4
2	1.003	3.79	3.8	3.8	3.80
3	1.001	3.49	3.49	3.49	3.49
4	1.002	3.94	3.94	3.94	3.94

Bioreactor 3					
Layer	Mass Soil in Bottle	6-Hour Pressure	2	3	Average
0	1.001	15.09	15.09	15.09	15.09
1	1.001	3.28	3.28	3.28	3.28
2	1.005	3.44	3.44	3.44	3.44
3	1.004	3.5	3.5	3.5	3.50
4	1	3.78	3.78	3.78	3.78

Bioreactor 3*					
Layer	Mass Soil in Bottle	6-Hour Pressure	2	3	Average
0	1	9.73	9.73	9.73	9.73
1	1.004	3.71	3.71	3.71	3.710
2	1	3.57	3.57	3.57	3.57
3	1.003	3.65	3.66	3.66	3.66
4	1.004	3.83	3.83	3.83	3.83

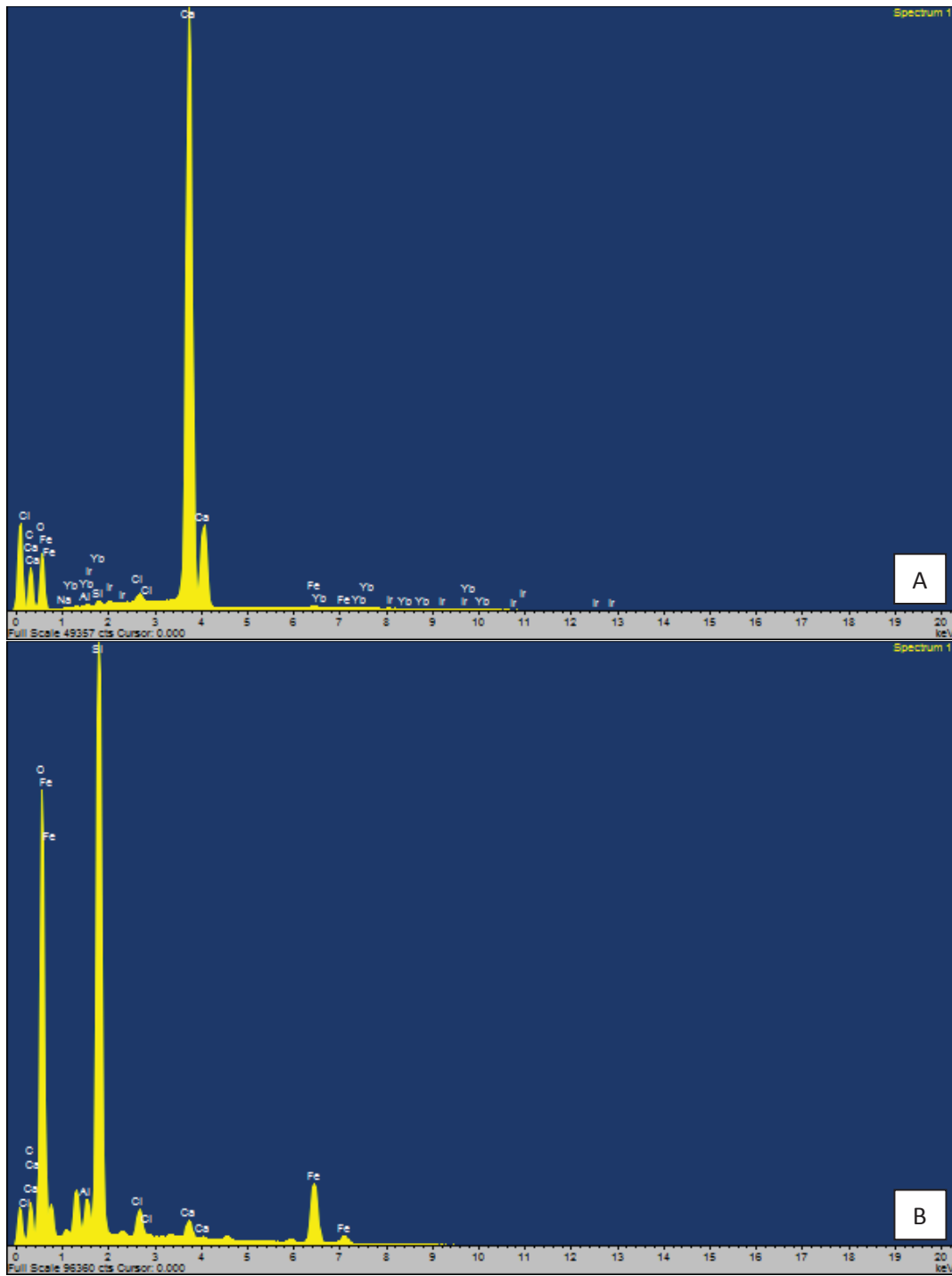


Figure B.1: EDS Spectra of R1 for the white surface crust precipitate (Plot A) and surface tailings powder (Plot B).

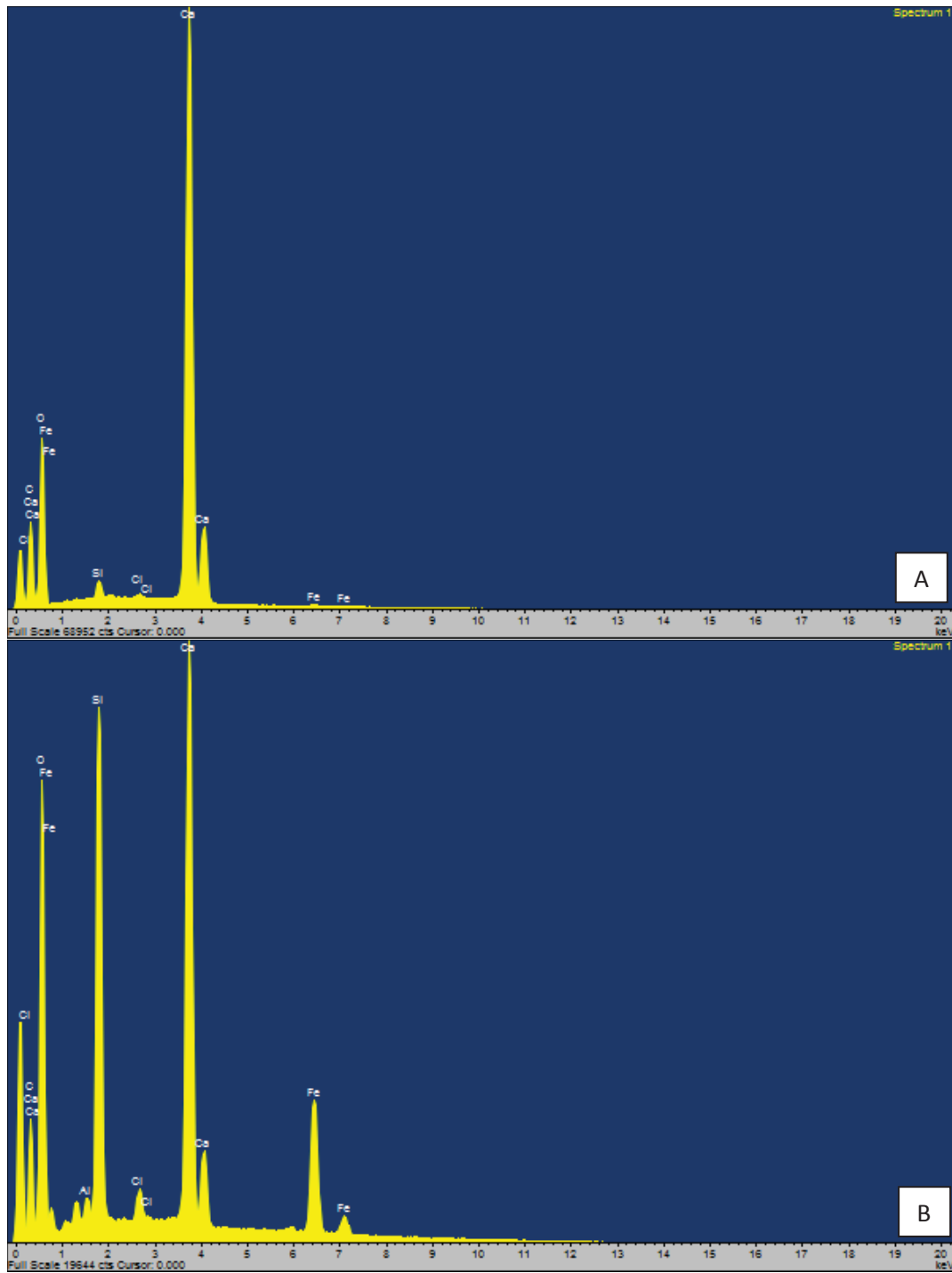


Figure B.2: EDS Spectra of R2 for the white surface crust precipitate (Plot A) and surface tailings powder (Plot B).

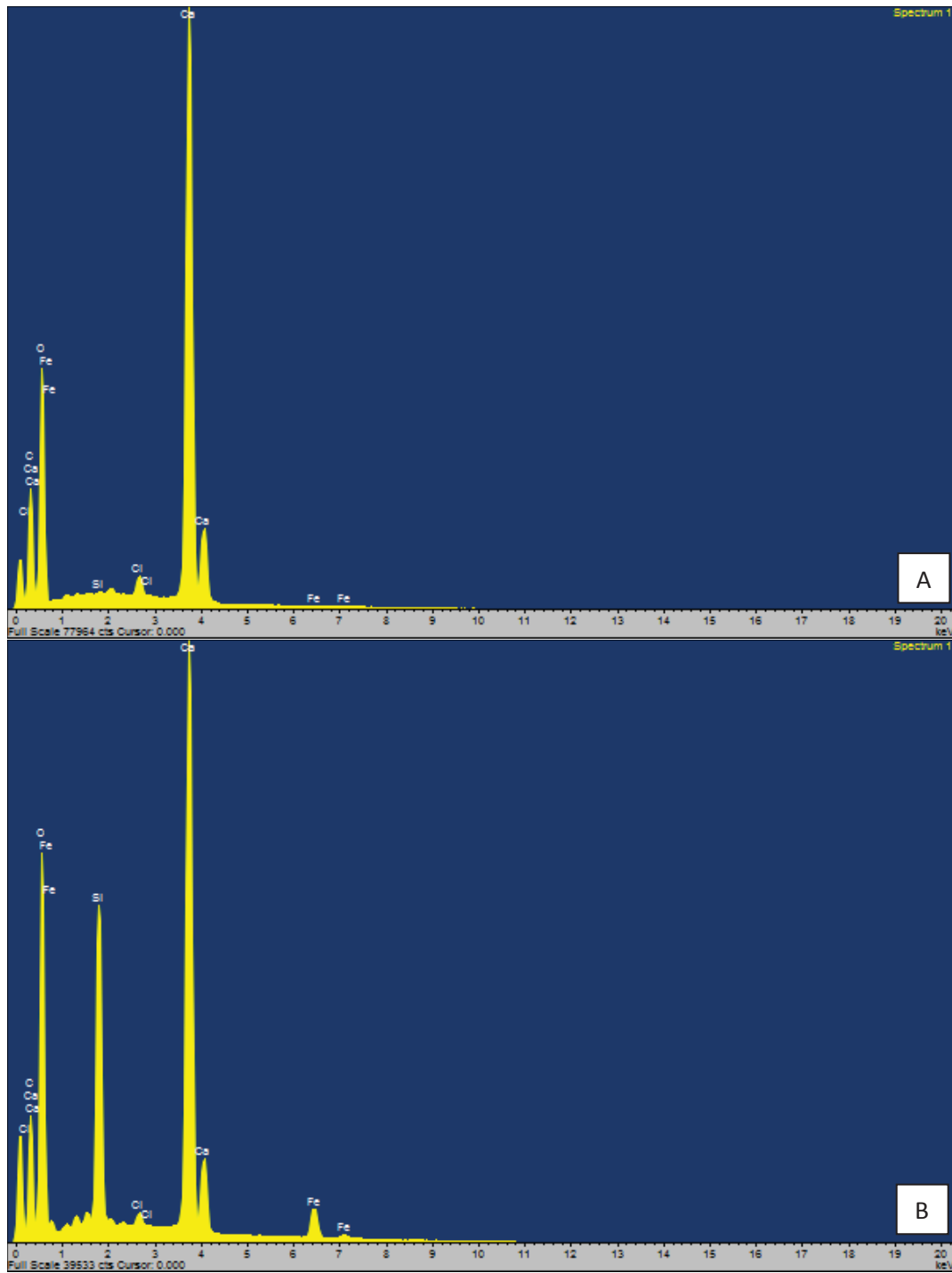


Figure B.3: EDS Spectra of R3 for the white surface crust precipitate (Plot A) and surface tailings powder (Plot B).

Table B.7: Raw data for the ball drop strength test.

Reactor	Moisture Content (%)	Diameter X (in.)	Diameter Y (in.)	Average	Average	STDEV.P
R1	12.0	0.2095	0.201	0.205	0.197	0.011232
	12.0	0.1935	0.2035	0.199		
	12.0	0.1755	0.2085	0.192		
	12.0	0.2005	0.1545	0.178		
	12.0	0.2075	0.2115	0.210		
R1*	12.8	0.1975	0.251	0.224	0.208	0.014555
	12.8	0.185	0.208	0.197		
	12.8	0.1765	0.1965	0.187		
	12.8	0.206	0.2355	0.221		
	12.8	0.207	0.2215	0.214		
R2	21.4	0.234	0.2585	0.246	0.244	0.008387
	21.4	0.244	0.2415	0.243		
	21.4	0.278	0.2375	0.258		
	21.4	0.2215	0.244	0.233		
	21.4	0.2375	0.2395	0.239		
R2*	22.6	0.229	0.2285	0.229	0.239	0.010109
	22.6	0.264	0.24	0.252		
	22.6	0.249	0.2185	0.234		
	22.6	0.263	0.2395	0.251		
	22.6	0.244	0.2185	0.231		
R3	16.2	0.1835	0.232	0.208	0.215	0.009636
	16.2	0.2405	0.225	0.233		
	16.2	0.2125	0.204	0.208		
	16.2	0.2125	0.205	0.209		
	16.2	0.207	0.23	0.219		
R3*	18.2	0.209	0.2145	0.212	0.208	0.003971
	18.2	0.2045	0.2145	0.210		
	18.2	0.1845	0.221	0.203		
	18.2	0.2025	0.207	0.205		
	18.2	0.225	0.201	0.213		

APPENDIX C - Calibration Curves

Table C.1: Raw data for the acid treated and non-acid treated pycnometer calibration curve.

Pycnometer Calibration Curve - Acid Treated						
<i>Tube Label</i>	<i>Mass Test Tube (g)</i>	<i>Mass Mag in Test Tube (g)</i>	<i>Mass CaCO₃ (g)</i>	<i>Total Mass</i>	<i>% CaCO₃</i>	<i>Specific Gravity</i>
1	2.092	0.000	5.058	5.058	100.0	2.722
2	7.613	0.601	2.400	3.001	80.0	2.752
3	7.560	1.995	1.858	3.853	48.2	2.783
4	7.649	1.798	1.255	3.053	41.1	2.823
5	7.637	2.408	0.620	3.028	20.5	2.859
6	2.091	4.995	0.000	4.995	0.0	2.904

Pycnometer Calibration Curve - Non - Acid Treated						
Original Bin	Bin	Weight Cup	Weight Cup + Soil	Weight Soil	% CaCO₃	Final SG
CaCO3 3	1	2.09118	5.07429	2.98311	100.0	2.715
-	2	2.09098	5.08629	2.99531	79.9	2.759
-	3	2.09133	5.09795	3.00662	60.1	2.812
-	4	2.09119	5.09244	3.00125	40.2	2.866
-	5	2.09116	5.08098	2.98982	20.0	2.921
Mag 5	6	2.09097	5.07597	2.985	0.0	2.985

Table C.2: Raw data for the mine tailing and calcium carbonate calibration curve.

Bin	%CaCO₃	Specific Gravity	Mass in Serum Bottle	Pressure			Average
				1	2	3	
-	%	-	g	1	2	3	
1	100	2.72066	1.0009	<i>OVERLOAD</i>			
2	80	2.71717	1.0011	<i>OVERLOAD</i>			
3	60	2.7608	1.0018	14.24	14.24	14.24	14.24
4	40	2.81408	1.0069	10.62	10.62	10.61	10.62
5	20	2.86757	1.0071	7.19	7.18	7.18	7.18
6	0	3.02475	1.0071	3	3.07	3.07	3.05